Thesis for the degree of Doctor of Philosophy

Exploration of Metal Composites and Carbon Nanotubes for Thermal Interfaces

Josef Hansson

Electronics Materials and Systems Laboratory
Department of Microtechnology and Nanoscience – MC2
Chalmers University of Technology
Göteborg, Sweden 2020

Exploration of Metal Composites and Carbon Nanotubes for Thermal Interfaces

Josef Hansson

Göteborg, April 2020

ISBN 978-91-7905-278-2

Doktorsavhandlingar vid Chalmers tekniska högskola
Ny serie nr 4630
ISSN 0346-718X

Electronics Materials and Systems Laboratory
Department of Microtechnology and Nanoscience – MC2
Chalmers University of Technology
SE-412 96 Göteborg
Sweden
Telephone: +46 (0)31-772 1000

Printed by Chalmers Reproservice, Chalmers University of Technology
Göteborg, Sweden, April 2020

Exploration of Metal Composites and Carbon Nanotubes for Thermal Interfaces

Josef Hansson
Electronics Materials and Systems Laboratory
Department of Microtechnology and Nanoscience – MC2
Chalmers University of Technology, SE-412 96 Göteborg, Sweden

Abstract

Modern microelectronics are perpetually pushing against limitations caused by inadequate heat dissipation. One of the critical bottlenecks is at the interfaces between different materials and components. Thermal interface materials (TIM) are used to improve the heat transfer at these interfaces, and to improve TIMs is one of the critical research areas in order to reduce the total thermal resistance for electronics systems.

A TIM requires both high thermal conductivity, ability to conform to mating surfaces, and the ability to absorb stress from thermal expansion mismatch during thermal cycling. Solder based TIMs utilize solder to form a strong connection between the mating surfaces with high thermal conductivity, but their stiffness prevents adequate absorption of thermal expansion mismatch. In this thesis, the solder is combined with a fiber network phase, which modifies the mechanical properties, while maintaining the continuous heat paths within the solder. This solder matrix fiber network composite TIM allows for the tailoring of the mechanical properties of solder based TIM while retaining thermal performance.

Another promising TIM candidate is based on arrays of vertically aligned CNTs. CNT arrays can achieve good thermal performance, but the reliability had not previously been investigated experimentally. A thorough investigation of the reliability of CNT array TIM revealed that reliability is not guaranteed, but requires careful matching between CNT array height, bonding method and substrate configuration.

Furthermore, we developed a new joule self-heating chemical vapor deposition (CVD) method for the synthesis of double-sided CNT arrays on thin foils, which can be used both as TIM or as supercapacitor electrodes. Double-sided arrays are challenging with conventional CNT array synthesis methods, but the Joule heating CVD method allows for rapid, scalable and uniform synthesis of large area double-sided arrays. Finally, this method was used to study the effect of heat treatment of CNT arrays on graphite. The heat treatment serves to simultaneously improve the CNT crystallinity, eliminate catalyst residues, and form a seamless connection between CNT arrays and graphite.

Keywords: Thermal interface materials, Solder, Carbon nanotubes

List of Papers

This thesis is based on the following appended papers:

[I] **Josef Hansson**, Torbjörn MJ Nilsson, Lilei Ye and Johan Liu, "Novel nanostructured thermal interface materials: a review", *International Materials Reviews*, Vol. 63, no. 1, pp. 22-45, 2017

[II] **Josef Hansson**, Lilei Ye and Johan Liu, "Fabrication and Characterization of a Carbon Fiber Solder Composite Thermal Interface Material", *Proceedings of IMAPS Nordic Conference on Microelectronics Packaging (NordPac)*, 2017

[III] **Josef Hansson**, Torbjörn MJ Nilsson, Lilei Ye and Johan Liu, "Effect of fiber concentration on mechanical and thermal properties of a solder matrix fiber composite thermal interface material", *IEEE Transactions on Components, Packaging and Manufacturing Technology*, vol. 9, no. 6, pp. 1045-1053, 2019

[IV] **Josef Hansson**, Majid Kabiri Samani, Andreas Nylander, Lilei Ye, Nan Wang, Torbjörn MJ Nilsson and Johan Liu, "Synthesis of a Graphene Carbon Nanotube Hybrid Film by Joule Self-heating CVD for Thermal Applications", *Proceedings of IEEE 68th Electronic Components and Technology Conference*, 2018

[V] Andreas Nylander, **Josef Hansson**, Majid Kabiri Samani, Christian Chandra Darmawan, Ana Borta Boyon, Laurent Divay, Lilei Ye, Yifeng Fu, Afshin Ziaei and Johan Liu, "Reliability Investigation of a Carbon Nanotube Array Thermal Interface Material", *Energies*, vol. 12, no. 11, paper no. 2080, 2019

[VI] **Josef Hansson***, Qi Li*, Anderson Smith, Isaac Zakaria, Torbjörn MJ Nilsson, Andreas Nylander, Lilei Ye, Per Lundgren, Johan Liu and Peter Enoksson, "Bipolar Electrochemical Capacitors using Double-sided Carbon Nanotubes on Graphite Electrodes", *Journal of Power Sources*, Vol. 451, 2277652019, 2020

[VII] **Josef Hansson**, Andreas Nylander, Mattias Flygare, Krister Svensson, Lilei Ye, Torbjörn MJ Nilsson, Yifeng Fu and Johan Liu, "Effects of high temperature treatment of carbon nanotube arrays on graphite: increased crystallinity, anchoring and inter-tube bonding", Under review by *Nanotechnology*

[VIII] Andreas Nylander*, **Josef Hansson***, Torbjörn MJ Nilsson, Lilei Ye, Yifeng Fu and Johan Liu, "Degradation of Carbon Nanotube Array Thermal Interface Materials Through Thermal Aging: Effects of Bonding, Array Height and Catalyst Oxidation", In manuscript

Related publications by the author not included in the thesis:

[A] Wei Mu, **Josef Hansson**, Shuangxi Sun, Michael Edwards, Yifeng Fu, Kjell Jeppson and Johan Liu, "Double-Densified Vertically Aligned Carbon Nanotube Bundles for Application and Integration in 3D High Aspect Ratio TSV Interconnects", *Proceedings of IEEE 66th Electronic Components and Technology Conference*, 2016.

[B] **Josef Hansson**, Lilei Ye, Henric Rhedin and Johan Liu, "A Review of Recent Progress of Thermal Interface Materials: From Research to Industrial Applications", *Proceedings of the 2016 IMAPS Nordic Conference on Microelectronics Packaging*, 2016

[C] **Josef Hansson**, Carl Zandén, Lilei Ye, Johan Liu, "Review of current progress of thermal interface materials for electronics thermal management applications", *Proceedings of IEEE 16th International Conference on Nanotechnology (IEEE-NANO)*, 2016

[D] Maulik Satwara, **Josef Hansson**, Lilei Ye, Henric Rhedin and Johan Liu, "Finite element analysis of bond line thickness and fiber distribution in solder based thermal interface materials", *Proceedings of the 2017 IMAPS Nordic Conference on Microelectronics Packaging (NordPac)*, 2017

[E] Yifeng Fu, **Josef Hansson**, Ya Liu, Shujing Chen, Abdelhafid Zehri, Majid Kabiri Samani, Nan Wang, Yuxiang Ni, Yan Zhang, Zhi-Bin Zhang, Qianlong Wang, Mengxiong, Li, Hongbin Lu, Marianna, Sledzinska, Clivia M Sotomayor Torres, Sebastian Volz, Alexander A Balandin, Xiangfan Xu and Johan Liu, "Graphene related materials for thermal management", *2D Materials*, 7(1), 012001, 2019

[F] Andreas Nylander, Marlene Bonmann, Andrei Vorobiev, **Josef Hansson**, Nan Wang, Yifeng Fu and Johan Liu, "RF Properties of Carbon Nanotube / Copper Composite Through Silicon Via Based CPW Structure for 3D Integrated Circuits", *Proceedings of the 14th IEEE Nanotechnology Materials and Devices Conference*, 2019

Contents

Dedicated to my soon to be wife, Jennifer

Acknowledgements

While this thesis represent the sum of my own work over the last five years, I did far from all of this by myself. There are a number of people, without whom this thesis would not exist, or at least not to this standard. First and foremost, I would like to thank Johan Liu for giving me this opportunity, continually guiding me through the work and trusting me to an extent I am not sure I would have myself.

In my daily work, it has been my two co-supervisors, Lilei Ye and Torbjörn Nilsson who have guided my work. Thank you for helping me and for caring about my research and my progress as a PhD student. Without Lilei's insight I am sure there would still be glaring errors in my work, and Torbjörn's proofreading has elevated the text several notches.

I would also like to thank all my current and former colleagues at the EMSL packaging group, with whom I have shared ups and downs during my time here. Thank you Yifeng Fu, Abelhafid Zehri, Ya Liu, Changdong Zhao, Majid Kabiri Samani, Nan Wang, Shuangxi Sun, Wei Mu, Di Jiang and Nikolaos Logothetis among others. Thank you for always helping out when asked, for support even when not, and all the fun times and interesting lunch-room discussions. A special thank you to Andreas Nylander who has been my PhD brother during all this time, if that is a thing.

I would also like to thank the rest of my colleagues in EMSL and MC2, not least the administration and infrastructure support. I have been consistently impressed with how things are run, both in the Myfab LIMS cleanroom and the administration of MC2. Special thanks to Henric Fjellstedt (in how many workplaces do the employees actually spontaneously praise the IT support?).

On a more personal note, I would like to thank everyone outside my work who nonetheless (or especially) contribute to my capability to achieve a work like this. Thanks to all my friends who have kept me grounded in the real world. I am fortunate that you are too numerous for me to mention here, although I would like to give a shoutout to Christmas, Shiny and Teabag. Mostly for your friendship, but also because I find it hilarious to mention those nicknames within an academic text.

Finally my family, who have managed to somehow support without pushing, and to show pride without expectations. It has been a great comfort to feel that I can count on you unconditionally. Foremost among them is of course my fiancee

Jennifer Panditha, who has shared every little up and down, seen me at my higher and my lowest and still showers me with enough love to light my darkest days. I cannot wait to share the rest of my life as well.

Chapter 1

Introduction

1.1 Background

The first and second law of thermodynamics state that energy is always conserved within a closed system, and that the entropy of a closed system always increases, respectively. In other words, that energy is never created or destroyed, only converted, and this conversion leads to a less ordered state. In general, the highest entropy state is the random movement of individual atoms, or in other words, heat. And as such, chemical and physical reactions tend to increase the temperature of the system.

Electrical currents are no exceptions, and, disregarding the case of superconductors, all electrical circuits create some amount of heat. In some cases, this is by design, but usually it is unwanted waste heat, which in certain applications can cause significant problems, in addition to the energy inefficiency. The field of microelectronics is one such field, where the decreasing feature size and increasing density has increased the thermal waste generation to the point where active cooling solutions are necessary to prevent overheating of the active components. In fact, cooling is responsible for a significant fraction of the total power consumption in modern data centers [1]. Even despite active cooling, thermal management presents a bottleneck towards further miniaturization. Therefore, there is a need for better materials to efficiently remove heat from heat generating components.

When designing the cooling solution for microelectronic systems, invariably, different materials and components will be included. Heat spreaders, heat pipes and heat sinks among others, can all have a place within the total system, and new materials and designs for all these components are continuously explored. However, regardless of the efficiency of individual components, in order to bring them together into a complete system, connections between different components and the heat

source itself is required. Since the surfaces of components are never perfectly flat, a simple mechanical connection between two surfaces usually results in a very limited fraction of the total area of the surfaces in actual contact, with air trapped between the contacting peaks. This severely restricts the heat flow between them, to the point where these interfaces are significant bottlenecks for the heat conduction. In order to fill these air gaps, thermal interface materials (TIMs) are used. A TIM is a material, placed between connecting surfaces, that can conform to irregularities and fill out the air gaps in order to facilitate heat transfer.

A perfect TIM would fill out only the original air gaps with a material of a thermal conductivity as high as the mating materials. Naturally, such a material does not actually exist for most applications, and so the results will be a compromise between thermal conductivity, conformability, ease of application, cost, reliability, etc. In the end, despite the application of TIM, thermal interfaces can still represent a large part of the thermal budget for a system, and the development of better TIM is crucial for the continued overall development in the field of microelectronics [2].

This need has led to a large variety of solutions in use in industry for different applications, and an even larger variety being actively researched. As a researcher or someone working in the field, having a broad knowledge of different types of existing and future TIM is vital, including their properties, features and applications. As a part of this thesis, a systematic review over TIM research has been done, focusing especially on nanostructured materials.

Based on the conclusions from the review of the field, we identified key areas where there is room for improvement over currently existing technologies. Two of these areas are especially relevant for the scope of this thesis: solder based TIM and carbon nanotube (CNT) array TIM.

1.1.1 Solder based TIM

In a solder based TIM, a low melting point metal alloy is used to join two surfaces in a similar manner to the attachment of electronic components on a printed circuit board (PCB). The molten metal can fill out surface irregularities, and when cooled and solidified, form metallurgical bonds to the joined surfaces. In addition, while the thermal conductivity of solder alloys are lower than most pure metals, it is still relatively high compared with most other TIM types.

However, solder can have reliability issues, due to its high stiffness, which makes it unable to absorb the stress created when the two joining surfaces are of materials with different coefficient of thermal expansion (CTE), which can lead to delamination or crack formation. In addition, solder can be difficult to process on large areas, such as molten solder pumping out of the interface, or a slight imbalance can cause the thickness of the TIM layer, or the bond line thickness (BLT), to become uneven over the surface. Parts of this thesis concerns the effort to create a composite structure which retains the thermal and connecting properties of solder TIMs, while addressing the mechanical and reliability issues that arise from using pure solder.

1.1.2 Carbon Nanotubes

Carbon nanotubes are one-dimensional allotropes of carbon, in which one or more single atom layers of carbon, called graphene, are rolled into tubes. First discovered by Iijima et al. [3], CNTs have since gathered significant research interest due to a number of exceptional electrical [4], mechanical [5] and thermal [6–8] properties, as well as their inherent one-dimensional structure.

Of note for TIM applications is the thermal conductivity of CNTs, which could theoretically reach more than 10 times that of copper [8]. This, together with a high degree of flexibility [9] and the possibility of synthesizing CNTs in the forms of densely packed forest or arrays, opened up research into a new type of TIM. This type of TIM uses CNTs that span the entire gap between joining materials to conduct the heat, allowing for a very high thermal conductivity along the CNTs and across the interface. CNT array TIMs show great promise in terms of thermal performance, and after more than a decade in the lab, CNT array technologies are approaching industrial applications. In principle, CNT array TIM should have thermal performance comparable with solder based TIM without the accompanying reliability issues. However, while much attention has been placed on achieving good thermal performance, the reliability of CNT array TIM has so far not been investigated in detail. For this reasons, this thesis includes a systematic study on the reliability of CNT array TIMs including what parameters that can affect it, failure modes and degradation mechanisms.

While the CNT array TIM is the driving force behind the studies of CNT arrays in this thesis, CNT arrays can have other uses as well, either due to inherent properties of the CNTs themselves, or the unique structural properties that comes from a highly oriented nanoscale tube forest. Similar to how TIM utilize thermal conductivity, it is possible to use the electrical conductivity for through-chip electrical interconnects [10], supercapacitor electrodes [11], field emmision [12] or even as blackbody absorber [13]. This means that improvements of CNT array synthesis and properties can have multiple applications, and the last part of the thesis concern CNT arrays in general rather than specifically for TIM applications. There are great challenges in developing fast, efficient and cheap synthesis of CNT arrays with sufficient quality. There are methods to produce very high quality CNTs, but in order to create vertically aligned arrays we are limited to chemical vapor deposition (CVD), which require high temperatures and tends to produce CNT with relatively low crystallinity and high amount of defects.

To improve on this situation there is an effort to improve both synthesis methods as well as post-synthesis treatment to improve the CNT quality. The final parts of this thesis concern our contribution to both of these areas.

1.2 This Thesis

This thesis is divided into five main parts. Chapter 2 introduces in detail the research area of thermal interface materials, based on the review in paper I. First, the working principle of TIMs is introduced together with important properties and figures of merit which are relevant for TIM selection. Second, a brief overview of existing TIMs used in industry is provided. Finally, novel research on TIMs is presented, divided into four general areas, together with a review of the status of the respective areas in terms of progress and research quality. The conclusions from this part motivates the work of the rest of the thesis.

The second part of this thesis, chapter 3, presents the experimental research into a specific type of TIM: the solder matrix fiber network composite (SMFC), which consists of a nonwoven horizontal randomly aligned fiber network inside a solder matrix. Two different kinds of fibers, carbon fiber (CF) from paper II and silver coated nylon (PA6,6) from paper III, and two different matrix alloys, Indium and Sn-Ag-Cu, are explored. The chapter details the fabrication of the composite materials, as well as the thermal and mechanical characterization of the TIM.

Chapter 4 deals with an investigation into the reliability of CNT array TIM. It includes an overview of CNTs, synthesis methods and reliability testing through accelerated aging. Two studies on different types of CNT array TIMs were done. From paper V a CNT array bonded with polymer was investigated. The result from this study then formed the basis for a more detailed study done on metal bonded CNT arrays in paper VIII.

Chapter 5 presents an improved method for synthesizing CNTs on both sides of thin electrically conducting foils, demonstrated using graphene and graphite films. The synthesis method from chapter 4 is expanded upon to highlight the problems we are trying to solve, before introducing the new method. This method is then used to fabricate CNT arrays for two different applications. From paper IV, CNT arrays on a graphene film are used as a TIM, and from paper VI CNT arrays on graphite paper are used as electrodes in a bipolar electrochemical capacitor.

The last main part, chapter 6, concerns the work on post synthesis heat treatment of carbon nanotube arrays in order to reduce defects of CNTs as well as to eliminate catalyst residue from the synthesis process. The influence of both crystallinity and catalyst residue on CNT arrays is discussed, together with the motivation for the treatment. After this, the characterization of the treated material is presented, with detailed investigation and explanation for an unexpected CNT bonding phenomenon which greatly impacts the end result.

Finally, in chapter 7 I give a brief outlook on future research based on the results from this work, and chapter 8 provides a brief summary of the papers this thesis is based on.

Chapter 2

Thermal Interface Materials

A surface is never completely flat, and will, at the microscopic scale, always have some degree of roughness. Pressing two such surfaces together will thus lead to a very limited contact, as seen in figure 2.1 a). These contacting choke points will constrict the heat flux (red lines) and lead to a large temperature drop over the interface.

To reduce the temperature drop, a thermal interface material (TIM) can be placed in between mating surfaces to fill the trapped voids and increase the effective contact area. The thermal conductivity of the TIM is normally lower than the mating substrates, and for this reason an ideal TIM would only fill out the voids between the mating surfaces as seen in figure 2.1 b). In reality, the application of a TIM will cause a gap between the surfaces, as seen in figure 2.1 c), called the bond line thickness (BLT).

The most important figure of merit for a TIM is the thermal interface resistance (R_{TIM}), which is a measure on how difficult it is for heat to dissipate over the interface. It is related to the temperature drop (ΔT) over the interface according to Fourier's law as

$$\Delta T = R_{TIM} Q \tag{2.1}$$

where Q is the heat flux. Minimizing R_{TIM} is a general goal of thermal interface materials development. The thermal interface resistance can be divided into resistive components, for a TIM typically

$$R_{TIM} = R_{c_1} + \frac{BLT}{\lambda_{TIM}} + R_{c_2} \tag{2.2}$$

where R_{TIM} is the total thermal interface resistance, R_{c_1} and R_{c_2} is the contact

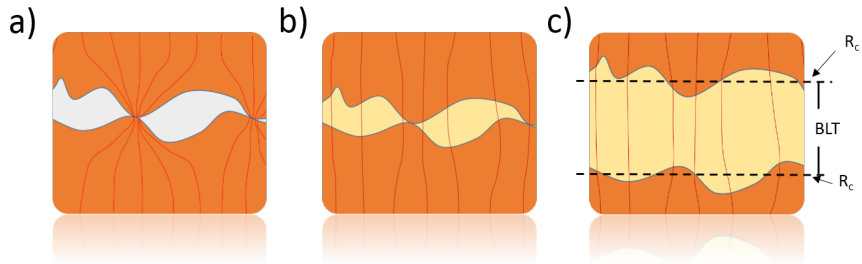

Fig. 2.1. a) The principle for the heat flow in a bare interface. b) In ideal TIM filling out the remaining voids. c) A realistic TIM with a bond line thickness. From paper I.

resistances at the interface between the TIM and the mating surfaces, λ_{TIM} the thermal conductivity of the TIM and BLT is the bond line thickness i.e. the thickness of the TIM. The different terms of this equation correspond to different TIM properties, and when designing a TIM we have to take each of these into consideration.

R_c - The contact resistance on each side of the TIM is a measure of the thermal contact between the TIM and the mating surface. This depends largely on how well the TIM can conform to the surface and have actual physical contact, which in turn depends on both TIM material properties as well as mating surface roughness and applied pressure. In addition, there is another effect, called the Kapitza resistance [14], which creates a resistance even at atomically smooth interfaces.

λ - The thermal conductivity is a measure of how well a material can conduct heat. Since the whole purpose of the TIM is to efficiently conduct heat, this is obviously a critical parameter within any TIM. A lot of research is focused on improving the thermal conductivity of TIM materials. However, due to trade-offs with other important parameters, the thermal conductivity of most TIMs remain much lower than that of the mating materials.

BLT - The bond line thickness of the TIM measures the thickness of the entire interface, as illustrated in figure 2.1 c). Since the thermal conductivity of a TIM is typically much lower than the mating materials, the BLT should be minimized in order to optimize the thermal performance, and ideal TIM

would like the one in figure 2.1 b). In practice, other considerations causes the BLT to range in the order of 10-1000 µm.

Aside from the thermal performance, there are a number of considerations to take into account when choosing or developing TIMs. Examples include:

- Whether the TIM is electrically conductive or not.
- Whether the TIM is in liquid or solid form, both when applied and in use. TIMs that are liquid during handling can lead to a somewhat messy process and uncertain BLT, but are generally able to infiltrate voids well if the viscosity is low enough. On the other hand, TIMs that are solid during application, like a pad, are easier to process but might not be able to conform to the substrates as well as liquid TIM.
- During operation, if the TIM is liquid it can be susceptible to pumping out of material from the interface.
- For TIMs that are solid in operation there can be significant stress induced due to difference in CTE between the mating surfaces. In this case, the TIM needs to be soft enough to flex and absorb this stress in order to prevent cracking or delamination.
- If the TIM has an adhesive function or if a constant pressure is required during operation. If a constant pressure is required, an additional challenge is to ensure that the pressure is maintained during the full lifetime of the device.

Depending on application, any and all of these parameters may be important, with different weights. Different types of TIM have different tradeoffs between these parameters, allowing for a large variety of TIMs to be used in applications. It also means that the research into novel TIMs can have a variety of focuses, not all of them necessarily on the thermal aspect.

Two different applications for TIMs can be seen in figure 2.2. It shows a typical ball grid array (BGA) package with a heat sink, which has two instances of TIM. The first instance is placed between the heat generating chip and the internal heat spreader (IHS), in a TIM1 application. TIMs not placed directly into contact with the heat generating chips are called TIM2, in this case between the IHS and the heat sink.

TIM1 application typically operate at higher temperatures and power densities, and thus have stricter requirements on thermal performance. They also connect a semiconductor on one side with a metal or ceramic on the other, which can have very different CTE (e.g. 3 ppm/K for silicon and 24 ppm/K for aluminum), which in turn means that TIM1 applications are at risk of reliability issues unless the TIM can absorb the stress due to thermal expansion mismatch.

In academia, the distinction between TIM1 and TIM2 is usually not considered, since the research is on a more fundamental level and rarely demonstrated in actual

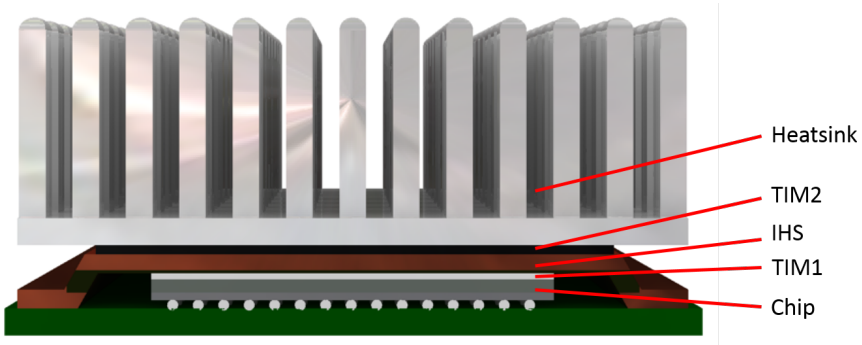

Fig. 2.2. A typical BGA package with TIMs between chip and internal heat spreader (IHS), and between IHS and heatsink. From paper I.

Type	λ (W/mK)	**BLT** (µm)	R_{TIM} (Kmm^2/W)	**Pump-out**	**Absorbs stress**	**Reusable**	**Replaceability**
Thermal grease	0.4 - 4	20-150	10 - 200	Yes	Well	No	Medium
Thermal Pad	0.8-3	200-1000	100-300	No	Well	Yes	Excellent
Phase Change Material	0.7-1.5	20-150	30-70	Yes	Well	No	Medium
Thermal Gel	2-5	75-250	40-80	No	Medium	No	Medium
Thermally Conductive Adhesive	1-2	50-200	15-100	No	Medium	No	Poor
Solder	20-80	25-200	<5	No	Poorly	No	Poor

Table 2.1. Common types of commercial thermal interface materials and typical properties [15–26].

applications, but is something that should be considered and sometimes needs to be taken into account.

2.1 Current Thermal Interface Materials

Current commercial TIMs can be divided into several categories, that each have different properties and applications. A summary of the properties of different common TIM types is given in table 2.1 with typical values for thermal conductivity, BLT and thermal interface resistance.

Thermal grease – Thermal grease, or thermal paste, is one of the most widely used TIMs in commercial applications. It is a particle laden polymer (PLP), consisting of thermally conductive fillers in a hydrocarbon oil, which results in a viscous paste that can be applied between surfaces that are clamped together. Thermal grease can conform well to substrates and can be squeezed into thin BLT, enabling thermal interface resistances as low as 10 Kmm^2/W for the highest

performing thermal greases [15]. The drawbacks mostly involve the fact that the TIM is liquid during operation, which means that it is susceptible to pump-out and the processing can be somewhat messy.

Thermal Pads – Similar to thermal grease, thermal pads are also a type of PLP. The difference is that the polymer is cured after mixing in fillers, forming a soft plastic sheet which is placed between the mating surfaces. As a pad, the handling is much easier and it can also easily be replaced. However, as a solid it is much more difficult to conform to substrates, and the BLT is relatively large, typically in the order of 200-1000 µm [16]. This means that the overall thermal performance is relatively poor. Nonetheless it sees use in applications where the thermal performance is not critical.

Phase Change Materials – Phase Change Materials (PCMs) are TIM that usually melt during operation i.e. have a matrix material with a melting temperature between room temperature and operating temperature. This can combine the best properties of liquid and metal TIMs, with solid handling characteristics, and liquid conformability [18].

Gels – As with grease and pads, gels is another PLP type TIM. The matrix generally consists of a weakly cross-linked silicone polymer [27] which is dispensed as a liquid and subsequently cured into a more solid structure [16] afterwards. This prevent pump-out which is otherwise a problem for thermal greases.

Thermal Conductive Adhesives – Similar to gels in application, thermal conductive adhesives (TCAs) also bonds the substrates together, eliminating the need for the application of pressure or some other fastening. They generally consists of a more heavily cross-linked polymer such as epoxy, creating a more rigid structure than gel TIMs. Solid version of TCAs also exists, which work as a double-sided tape that is applied in a similar manner to thermal pads.

Solders – Solders are the most high-performing TIMs in terms of thermal performance currently in commercial use. Solder alloys are reflowed in order to form metallurgical bonds between substrates, which conforms extremely well and nearly eliminates contact resistances [17]. In addition, since solders are pure metals the thermal conductivity of solder TIMs is much higher than PLPs. The drawbacks of solder TIMs are related to voids inside the joint [28] as well as the high stiffness of solder joints which can cause stress-induced failures during thermal cycling. In addition, the cost and complexity in processing is a concern [28].

2.2 Recent Thermal Interface Materials Development

For a large number of applications, it would be beneficial to use TIM with superior or alternative qualities compared to existing TIMs. This has led to large amount of research into new materials and structures that can be used for thermal interfacing. Paper I is a thorough review into the various research avenues of TIMs. In particular,

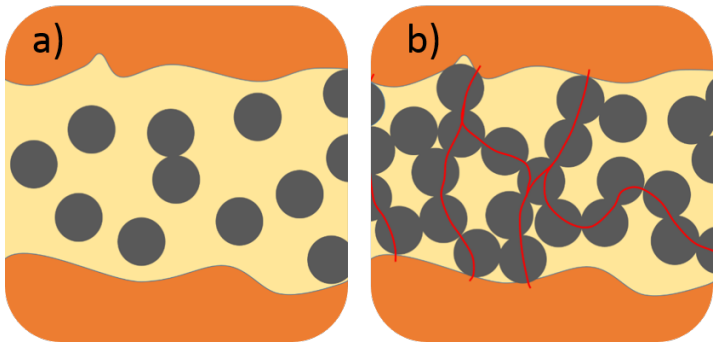

Fig. 2.3. Percolation in PLPs. a) Insufficient filler fraction for percolation and thus no continuous heat paths. b) Filler fractions above percolation threshold, and thus continuous heat paths between surfaces. From paper I.

three main categories of TIM which have attracted significant attention have been identified: Particle laden polymers (PLPs), continuous metal phase TIM and carbon nanotube (CNT) array TIM.

2.2.1 Particle Laden Polymers

Particle laden polymers (PLPs) are compounds which consist of filler micro- or nanoparticles inside a polymer matrix. PLP TIMs come in a variety of forms, and can be liquid, solid or cured after application. Most commonly used commercial TIMs fall under this category, such as thermal grease, thermal pads, PCMs, gels, or thermal conductive adhesives. Despite the large variety, from a research perspective they are quite similar, and focus is mainly on the fillers used, their material properties, shapes and filler fraction.

PLPs function by utilizing the polymer matrix to spread, adhere and conform to the mating surfaces. The polymers themselves generally have very low thermal conductivity (< 0.2 W/mK), and for this reason, filler particles with high thermal conductivity are introduced into the matrix in order to conduct the heat. Since the thermal conductivity of the matrix is so low, in order to create an efficient TIM, the heat needs to be able to flow between particles through inter-particle contact without going through the matrix. For this, the density of fillers needs to exceed the percolation threshold, as demonstrated in figure 2.3. At the percolation threshold, the composite thermal conductivity sharply increases. Further increase in filler fraction further increase the composite thermal conductivity, although at a continuous pace. Nonetheless, the final thermal conductivity of PLPs is usually much lower than the filler bulk thermal conductivity, and commercial PLP compounds usually range between 1-10 W/mK.

Material	Conductivity (W/mK)
Graphene	6000
SWCNT	3500
MWCNT	3000
Graphite	100-400 (in-plane)
BN	250-300
Ag	427
Cu	393
Au	315
Al	237
AlN	170
Al_2O_3	39

Table 2.2. Thermal conductivity of common types of fillers.

On the other hand, the mechanical properties, especially the viscosity, of the compound is dependent on the filler fraction. Too high filler fraction will cause the compound to become difficult to apply, and may not conform well to the surfaces and therefore cause significant contact resistances. The main goal of the research into PLPs is therefore to achieve as high thermal conductivity as possible at a sufficiently lower filler fraction.

As mentioned before, the most important figure of merit is the thermal interface resistance according to equation 2.2. However, in the case of PLPs, most reports only mention a value for the thermal conductivity, without any actual measurements of a TIM application. For this reason, the thermal conductivity and filler fraction are the comparative figures of merit for this section.

Filler materials

The filler particles in PLPs can consist of a number of different materials. A list of materials encountered within this study can be seen in table 2.2, together with their respective bulk thermal conductivity. Within these materials, three groups can be distinguished: ceramics, metals and carbon allotropes.

Ceramic materials are electrically insulating, which can be important for many applications. However, heat is transported partly by electrons, which means that insulating materials typically have lower total thermal conductivity. Boron Nitride has highest thermal conductivity ceramic, and thin sheets of hexagonal BN has even higher thermal conductivity as a 2D material. Using BN platelets, a composite thermal conductivity of 32.5 W/mK has been achieved [29], although at a very high

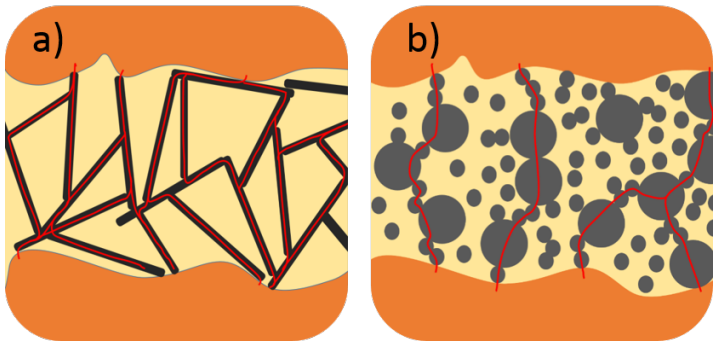

Fig. 2.4. Filler combinations to achieve percolation at lower filler fractions. a) High aspect ratio fillers. b) Bimodal particle size distribution. From paper I.

filler fraction (88%). Overall, higher filler fraction is required for similar thermal conductivity as other types of filler. Nonetheless, ceramic fillers are common in commercial PLPs for cost reasons. Academically, BN [30–34] and AlN [35, 36] are the most interesting ceramic filler materials.

Carbon allotropes come in many forms, such as diamond, graphite, CNTs or graphene. Out of these, CNTs and graphene stand out due to their potentially incredible thermal conductivity [6, 7, 37]. Another interesting property is the 1D and 2D nature of these materials respectively. By using fillers with a high aspect ratio, it is possible to achieve percolation at much lower filler fractions than by using spherical fillers, as seen in figure 2.4 a). For CNTs, percolation has been achieved at filler fractions as low as 0.1-0.2 wt% [38, 39].

However, there is a very high thermal contact resistance between CNT and matrix [40–43], as well as phonon dampening due to their interaction [44]. The thermal conductivity improvement of PLPs with CNTs is quite modest, and much lower than what would be expected from a rule of mixtures [45].

Unlike CNTs, graphene and graphite flakes has been shown to increase the thermal conductivity of epoxy by about 20-30 times at 20-30 wt% [46–50] filler fraction. The thermal conductivity improvements in graphene/graphite composites are much higher than for CNTs, even at the same filler fraction [51], as well as significantly cheaper and easier to manufacture.

Metals have very high intrinsic bulk thermal conductivity and good handling properties. The best commercially available thermal greases have a thermal conductivity of about 8 W/mK with a filler of Ag flakes. Most recent progress using metal fillers are focused on using metal nanowires (NWs) rather than spherical fillers. Similarly to CNTs, metal nanowires can, due to their 1-D shape, form percolating networks at very low filler fractions.

Ag is the most popular metallic filler in commercial compounds and is a natural candidate, and has been demonstrated as TIM filler by electrodeposition of a template [52, 53] or a chemical process [54, 55]. The electrodeposition method forms a highly aligned network, which allows for a significantly higher thermal conductivity than using a random dispersion, 30.3 W/mK [53] compared to 1.4 W/mK [55]. In addition to these methods, Pashayi et al. demonstrated a self-structured metallic nanowire network based on agglomeration and sintering of PVP-coated Ag-nanoparticles which exhibits a thermal conductivity of up to 38.5 W/mK at 48 vol% [56, 57].

Other metals have also been investigated. Wang et al. found that CuNWs gave a larger conductivity enhancement at a lower filler fraction than AgNWs, and achieved a thermal conductivity of 2.46 W/mK at a low filler fraction of 0.9 wt% [55]. Nanowires of Ni [58, 59] and Au [60] have also been investigated.

Filler combinations

A method of increasing the thermal conductivity at a lower filler fractions is to combine different fillers into the same TIM matrix. Different fillers create synergistic effects that increases the effective thermal conductivity beyond what would be expected from models. The most common mechanisms behind the synergistic effects are size variations and variations in aspect ratio of fillers. Size variation can help forming percolating networks (see figure 2.4 b) and improve packing ratio [34, 47, 61]. Variations in aspect ratio can combine the percolation-forming networks formed by high aspect ratio fillers with the thermal transport properties of bulk and 2D fillers [62].

Filler combinations reported typically includes filler materials with different dimensionality (1D, 2D or 3D). Lee et.al. demonstrated the concept of mixing 1D rods with spherical particles [63] in 2006. Recent progress includes studies of Boron Nitride (BN)/CNTs [64–66], BN/CNFs [67] and graphene oxide (GO)/CNT [68, 69] hybrid composites, which all combine 1D and 2D fillers, which are more effective for creating conducting networks than 1D/spherical filler combination [65].

Since spherical 3D and 2D flake fillers already exist as commercial compounds, the addition of a high aspect ratio filler into commercial thermal grease has proven a popular method of investigating the synergistic effects of spherical/high aspect ratio hybrid fillers [47, 70–72]. Among these the highest thermal conductivity value reported to date is 14 W/mK by the addition of an optimized mixture of graphene and multi-layer graphene into thermal grease at a low filler fraction of 2 vol% [47]. Also, the addition of MWCNTs to thermal grease has been directly shown to decrease the temperature of a running microprocessor [72].

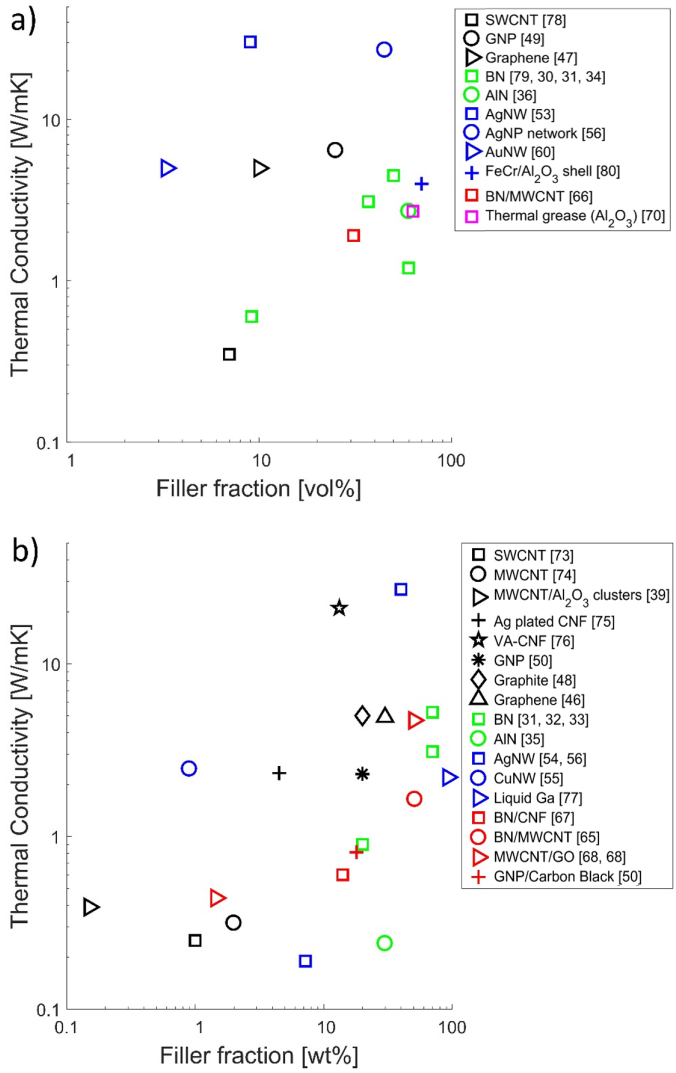

Fig. 2.5. Thermal conductivity as a function of filler fraction for various PLPs, colored based on different categories of fillers: carbon allotropes (black), ceramics (green), metal (blue), hybrid fillers (red) and a commercial compound (pink). The data is divided into two graphs depending on whether the filler fraction is measured in volume or weight percentage. From paper I.

Conclusion

A summary of recent reports on PLPs can be seen in figure 2.5, including some reports not otherwise discussed in this thesis [67, 73–80]. The thermal conductivity of the presented compound is plotted against total filler fraction. The figure is split into two graphs as filler fraction value reported is alternatively given in volume fraction or weight fraction. The volume fractions give a more accurate representation of the effect of higher filler fractions, but general trends can be distinguished in both cases.

It is clear that alignment of high-aspect ratio fillers such as carbon nanofibers and metal nanowires can provide a magnitude higher thermal conductivity at the same filler fraction compared to unaligned fillers, and is generally the only way to increase the thermal conductivity beyond 10 W/mK. Also noteworthy is that although CNTs have shown rather unimpressive performance as fillers, other carbon allotropes such as graphene and GNP have shown better performance than other kinds of fillers at similar fractions.

Aside from these few exceptions, the actual performance of PLPs has not increased significantly during the last decade, and recent reports have similar performance to commonly available industrial TIMs. Despite this, the research area of PLPs has seen a relatively large amount of publications. A possible explanation is that it is relatively easy experimentally to test new fillers or mix together a new combination, even though the end result is rarely groundbreaking. Further evidence of this is that there are few publications on PLPs in high impact journals compared to the other categories.

The current industry is dominated by PLPs in different varieties, and there is a large infrastructure already in place for developing new compounds. This means that any breakthrough in research has the potential to quickly reach the market. The matrix material has little effect on the thermal conductivity, allowing filler development to have an effect on a wide range of TIMs.

2.2.2 Continuous Metal Phase TIM

Solder based thermal interface materials are used in industry in applications where a low thermal interface resistance is critical. Solder is the only commercially available TIM which can provide low thermal interface resistances of <5 Kmm^2/W, due to the inherently high thermal conductivity of metals, and the reflow process which largely eliminates voids and forms metallurgical bonds. Solders can be applied either as solder paste or as a thin foil sheet with or without flux. It provides a continuous metal phase for heat transfer at a high thermal conductivity, nearly eliminating internal interface resistance. However, their rigid structure can lead to poor stress absorption further leading to cracking during thermal cycling due to CTE mismatch. Indeed, solder fatigue is often the most common failure mode in electronics. As such, research on metal TIM tends to focus on decreasing the Young's modulus or

otherwise improve the reliability of the TIM, rather than further thermal interface resistance improvements.

Another possible issue is the formation of intermetallic compounds (IMCs) at the interface between the solder and bonded surfaces. These IMCs consists of alloys of both solder and substrate, which are typically both more brittle and lower thermal conductivity than either solder or substrate.

Historically, the most widely used solder alloy is tin-lead (SnPb), however due to the toxicity of lead, their use is now mostly forbidden in the European Union [81]. This presents a challenge for both traditional soldering and solder based TIMs, as lead free solders typically have higher melting points, modulus and are more brittle than SnPb solder [82]. The development to find better replacements are ongoing, and for research into TIMs based on solders it is important to have an overview of this research field as well. Kotadia et al. [83] have recently provided an extensive and up to date review article for this purpose.

The most common solder to be used in thermal interface applications in industry today is indium. It is a comparatively soft metal, allowing it to conform to substrates and absorb stress, and has a relatively low melting temperature of 157°C. Both AMD [84] and Intel [85] have developed and used indium as TIM in TIM1-applications for high-end processors. On the other hand, Indium is a relatively rare metal with a high price and limited supply [86]. There is a drive away from indium dependency, and therefore alternative alloys are also under being investigated, such as Sn-Ag-Cu (SAC) [87] and Sn-Bi [88].

Solders are typically solid in operation, but there are alloys with very low melting temperature (LMAs), such as Ga, Ga-In and In-Bi-Sn with melting points at 30°C, 16°C and 60°C respectively. These alloys can be used as TIM, and melt during operation, which allows for simultaneous mechanical decoupling and wetting, resulting in a very low thermal interface resistance [89–91]. However, LMA TIMs are, like thermal paste, susceptible to material pumping out of the interface. Additionally, Ga containing alloys are corrosive to must substrates [92], and In-Bi-Sn has a rapid growth of brittle IMCs at the surfaces [90].

Metal TIMs are usually limited to alloys with a melting temperature low enough to prevent damage to components, which usually excludes any alloy with a melting temperature above that of the solder used for the electronics assembly. However, higher melting point materials can be used in the form of nanoparticles (NPs) which sinter together at a much lower temperature than the melting point. This has been demonstrated with AgNPs, which can achieve a thermal interface resistance of less than 1 Kmm^2/W [93].

Metal matrix composites

One of the most interesting avenues for potential breakthrough technologies is the research into novel nanostructured composite materials. A combination of different materials can, through careful structuring of the components at small scales, combine

the best thermal and mechanical properties of the different constituents. Since solder has an unmatched thermal performance, the use of solder alloys as a matrix material in a composite is attractive. By combining the solder matrix with fillers or other nanostructures the mechanical properties can be significantly enhanced while retaining the high thermal conductivity of the solder.

One such composite consists of bulk solder in a liquid phase sintered solder composite material [94]. High-melting phase material such as Sn or Cu was embedded in a matrix of a low-melting phase such as In. The resulting composite combines the attractive properties of In, such as high thermal conductivity, low melting point and low shear modulus, with the compressive creep strength and price of Sn or Cu [94, 95]. Surface modification of Cu particles to prevent IMC formation created a composite with high mechanical strength and a thermal interface resistance of 2.1 Kmm^2/W [96]. Modeling further suggests that the composite may be improved further by disc-shaped inclusions instead of spherical particles [97].

Raj et al. demonstrated a concept of coelectrodeposition of metal films with filler particles incorporated [98], using SiC and graphite fillers in a Sn matrix. A similar concept was used by Nagabandi et al., wherein functionalized boron nitride nanosheets were included into an Ag matrix [99]. They showed a composite with a thermal conductivity of over 80% of that of pure Ag, together with a significantly reduced modulus.

Alternatively fillers can be mixed with solder paste to produce the composite after reflow which has been reported with fillers of CNTs [100], graphite [101], Zn [102] and Cu [103] into various solders. Despite some successful results in increasing creep resistance [101, 103] and reducing CTE [100] and IMC formation [102], there has been no TIM applications reported until recently, when Sharma et al. [104] demonstrated a solder-graphite network composite. Graphite forms a self-assembling network through mechanical compression, after which a flux-less reflow forms a network in the solder matrix. The resulting composite provides thermal resistance as low as 1.4 Kmm^2/W at 0.92 MPa and a CTE of 10 ppm/K.

As an alternative to a self-assembling composite, Chen et al. [105] proposed a vertically aligned solder-graphite sheet composite in which alternating vertically aligned graphite sheets and solder forms a composite. By varying the amount of solder to graphite the CTE of the composite can be controlled directly. Finally, another top-down approach on metal matrix composite fabrication is the solder matrix fiber composite (SMFC) which is discussed in detail in chapter 3.

Outlook

Table 2.3 shows recent results on continuous metal phase TIMs. The thermal interface resistance is very consistent in the 2-5 Kmm^2/W range owing to the high thermal conductivity of metals and excellent compliancy after reflow. The challenge is still to increase the reliability through improving mechanical properties.

Solders already have widespread industrial applications and is a very mature

Description	R_{th} (Kmm^2/W)	BLT (µm)	Reference
In-Bi-Sn	3	<30	[90]
Gallium	2.6	3	[89]
Sn-Bi solder paste	5	50	[88]
Liquid Phase Sintered Sn-In Composite	21	25	[94]
Liquid Phase Sintered Cu-In Composite	2.1	100	[96]
Sintered AgNP (250°C)	2	10	[93]
Aligned Graphite Solder Composite	3.5	200	[71]
Solder Graphite Network Composite	3.8	50	[104]
SAC-Polymer Fiber Composite	2-4	35-65	[106]
SAC-Carbon Fiber Composite	2-7	65-160	[107]

Table 2.3. Summary of recent continuous metal phase TIM progress

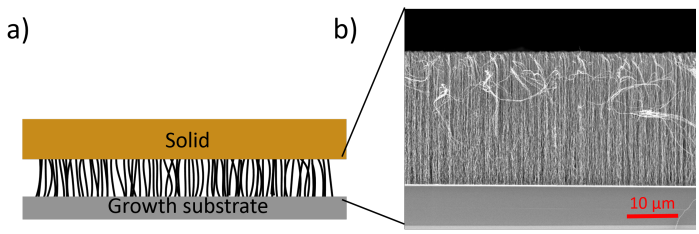

Fig. 2.6. a) Schematic of a CNT array TIM. b) Scanning electron microscopy (SEM) image of a CVD grown CNT array.

research field. As such, the path from new research to applications is, as with PLPs, relatively short. Much research is based on small incremental changes upon existing technology, where application and a large part of the manufacturing methods are already established. In addition, since solders are the sole currently existing alternative for high-performance TIMs, improvements would be relatively easy for industry to adopt compared with completely novel types of TIMs.

2.2.3 Carbon Nanotube Arrays

Instead of using CNTs as fillers in PLPs, having an array of CNTs that individually span the whole BLT, as seen in figure 2.6, would completely eliminate the internal resistances. Such a CNT array could therefore be a practical way of harnessing the

high thermal performance of CNTs in a TIM application [108]. Vertically aligned CNTs are grown by a chemical vapor deposition (CVD) process and pressed against an opposing surface. The mechanisms for CNT CVD is based on the thermal breakdown of a hydrocarbon gas in the presence of a metal catalyst particle [109]. The carbon then precipitates and crystallizes into a CNT that grows from the catalyst particle. With a high enough density of CNTs, geometrical constraints from neighbours will then align the CNTs vertically, forming an aligned array. The CVD process is described in more detail in chapter 4.

In a TIM application, the CNTs act like small springs, which bends and conforms to the surface. Additionally, each CNT would be independent in the x-y plane, in principle allowing the array to easily absorb any CTE mismatch between the two surfaces and completely avoid the large drawback of metal based TIMs.

The thermal conductivity of a carbon nanotube can reach as high as 3000 W/mK [6, 7], but the bulk value for CNT arrays is much lower, due to low CNT density, defects and imperfections in the CNTs themselves [110]. A typical value for a CNT array is on the order of 10 W/mK [110]. There is a large discrepancy between measured and theoretical thermal conductivity values. At moderate bond lines (<30 µm) the thermal conductivity will have relatively low effect on the thermal interface resistance compared to the contact resistances [111–113]. For instance, B. Cola et al. [114] measured the thermal interface resistance components for a Si-CNT-Ag interface at 0.241 MPa using a photoacoustic method, and while the contact resistance was found to be 1.7 Kmm^2/W at the Si-CNT and 14 Kmm^2/W at the CNT-Ag interface, the thermal resistance from the bulk CNT array was less than 0.1 Kmm^2/W.

The dominance of the contact resistance, especially at the attached surface, on the overall thermal interface resistance can mostly be explained by a limited number of the CNTs in actual contact to the opposing substrate [113, 115]. There is little conduction between adjacent CNTs in the array, and so only the fraction of CNTs in contact with both sides can significantly contribute to the heat transfer. Additionally, the intrinsic contact resistance (Kapitza resistance) between CNTs and metals is significant [116].

As shown by Cola et al., the bulk thermal conductivity of the CNT array has relatively little effect on the overall thermal interface resistance. However, the geometrical and mechanical properties of the CNT array are still important, and multiple studies have confirmed that the CVD growth parameters of the CNT array greatly affects the resulting TIM [117–120]. In particular the compliance of the CNT array is a dominant parameter, with lower modulus allowing more CNTs in effective contact with opposing substrate.

Bonding of CNT arrays

Since the largest contributor the thermal interface resistance of CNT array TIM is the contact between the tip of the CNT array and the opposing surface, much

research has been focused on reducing this contact resistance by bonding the surface to the tips. The goal is two-fold: increasing the number of CNTs in contact with the surface, and reducing the Kapitza resistance at individual CNT tips. Typically this is done by using an additional layer which partly penetrates into the CNT array to come into contact with additional CNTs.

An established method for bonding materials together is metal bonding, using metals as the intermediate layer. Tong et al.[112] demonstrated a bonding approach using a In solder layer at the free CNT ends, which partly penetrates the array and contacts a larger fraction of CNT. This results in a decrease in the total thermal interface resistance of an order of magnitude, down to 1.7 $\mathrm{Kmm}^2/\mathrm{W}$. Other metal bonding methods include metallization of Ti/Au onto both CNT array and bonding surface, which bonds at 220°C due to Au-Au self-diffusion [121], and palladium thiolate used to coat the sidewalls of CNTs with Pd nanoparticles [122], forming a Pd weld after baking at 250°C.

To avoid increased bonding temperatures, Barako et al. [123] proposed a bonding solution in which a Sn-coated foil comprised of many thin layers of alternating Au and Ni is used as a bonding layer. A pulsed electrical current initiates an exothermic reaction to alloy the layers into $Au_{0.5}Ni_{0.5}$, which locally heats up the foil enough to melt the Sn layer to the CNT array.

While metal bonding has shown significant improvements in thermal performance, it does nothing to address the large Kapitza resistance at the CNT-metal interface. For this reason, progress has been made towards non-metal bonding of CNT arrays using polymer coatings [124–126] or chemical functionalization [127–129]. Polymer bonding can serve to increase real contact area, as demonstrated using a spray on polymer coating together with a solvent, which pull CNTs into contact using capillary forces [125]. In addition, chemical functionalization, either directly or in conjunction with a polymer coating can create bonds between CNTs and substrate, greatly reducing the thermal contact resistance.

Ni et al. [124] introduced an azide polymer based thermal glue which also bonds covalently with CNTs through C-N bonds, achieving a low thermal interface resistance of 1.40 $\mathrm{Kmm}^2/\mathrm{W}$. They further suggests that bonding with an element lighter than carbon gives lower contact resistance due to higher vibrating frequencies. Kaur et al. [128] also managed a six-fold reduction of the thermal resistance at CNT-Al and CNT-Au interfaces using covalent bonding of short organic molecules, also bonding to CNTs with a covalent C-N bond. Taphouse et al. [129] showed a similar reduction of thermal resistance using a pyrenylpropyl-phosphonic acid surface modifier to bond CNT arrays to metal oxide substrates, although this bonds to CNTs using $\pi - \pi$ bonds rather than covalent bonds.

Transfer of CNT arrays

While CNT array bonding can reduce the thermal resistance of the interface, there is a fundamental problem to overcome before CNT arrays can be commercially

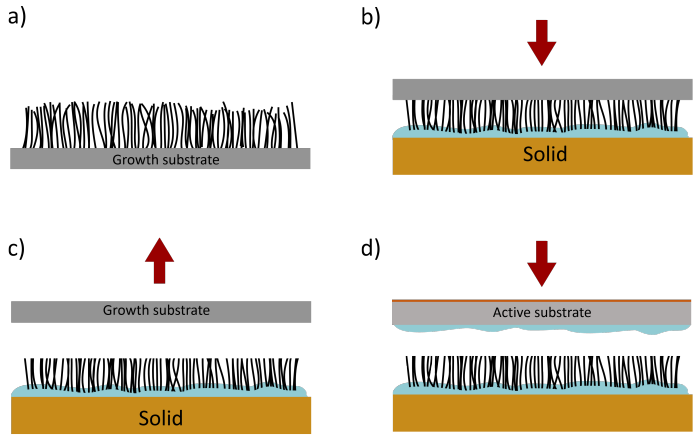

Fig. 2.7. Bonding and transfer process for a CNT array TIM. a) CNT array is grown on a sacrificial silicon chip. b) The array is bonded to another substrate. c) The sacrificial silicon chip is peeled off. d) A new active silicon chip can be attached instead.

viable. In a majority of studies, the CNT array is synthesized directly on the heat generating silicon chip. However, the CVD process require high temperature, typically at least 700°C, which is incompatible with modern CMOS electronics (max 500°C). There has been some effort into optimizing a low temperature CVD process [109, 118], but so far it has proven challenging to synthesize CNT arrays of sufficient quality at low enough temperatures. Another option is to grow the CNTs on the heat sink side, and this has been demonstrated on both Cu [130] and Al [131, 132].

However, the most promising alternative appears to be the transfer of the CNT array from a sacrificial growth substrate into the interface. A bonding method as discussed in the previous section can be used to attach the array onto one surface. Then, the original growth substrate can be peeled off, and the other mating surface can be attached. An illustration of this is seen in figure 2.7.

Transfer has been demonstrated for solder [133, 134], metallization [121] and thermocompression [135, 136] bonding. Despite bonding, the thermal contact resistance of the growth substrate/CNT array interface is an order of magnitude lower than at the bonding interface, and a corresponding increase in thermal interface resistance is seen after transfer compared to just bonding the free ends [121].

A more flexible alternative to transfer of bonded CNT arrays is to grow CNTs directly on both sides of a thin foil [137–139]. This allows the TIM to be applied anywhere in the same manner as a thermal pad. While the arrangement is in principle equal to two conventional CNT array TIMs, in reality the foil can conform

to the substrates, increasing the fraction of CNT contacts on both sides. Cola et al. achieved thermal interface resistance less than 10 Kmm^2/W at moderate pressures [137], on par with single-sided CNT array TIMs, suggesting that the added conformability and real contact outweighs the higher number of interfaces.

Another way to create a freestanding film that can be applied as a thermal pad is to infiltrate the CNT array with a polymer, forming a composite material which can easily be applied. Several investigations into CNT array polymer composites have been conducted, both as freestanding films [140–142] and attached to original substrate [43, 143]. However, in each case the thermal conductivity of the composite is lower than for a naked array. Possible explanations include polymer preventing some CNTs to contact with a substrate, decreased alignment due to processing and damping of phonon modes in the CNTs by the polymer matrix [141].

Outlook

Research done on CNT array TIMs is summarized in figure 2.8, which shows the reported thermal interface resistance values versus total CNT array height [144–148]. The correlation between thermal interface resistance and CNT array height is very weak, which is consistent with performance limited by contacts between CNT array and substrates. The importance of a good bonding is apparent, and further research should continue to investigate the possibilities of a facile, scalable bonding method.

The main limitation preventing widespread industrial use of CNT array TIMs is the production capacity of CNT arrays, which is currently lacking scale and process controllability. While production of randomly aligned CNTs are starting to reach industrial scale [109], growing a uniform vertically aligned CNT array poses additional limitations on scaling. For an introduction of commercial CNT array TIMs the CVD process has to be improved and scaled up significantly. Roll-to-roll CVD systems for graphene [149] and CNT [150] production have recently been demonstrated, which could potentially increase volume, although controlling the process remains an issue.

In addition to the manufacturing issues, unlike for PLPs and solder TIM, there is little research on the reliability of interfaces with CNT arrays. Theoretically, the mechanical decoupling of surfaces that CNT arrays allows for should result in excellent mechanical properties, but there is a lack of experimental studies to corroborate this. This lack of studies is the motivation behind the work on the reliability of CNT array TIM presented in chapter 4.

2.2.4 Other Novel Concepts

In addition to the previous categories of TIM research, there are a number of novel concepts which have been proposed. These can be divided into three additional smaller categories: mechanically deformed metal, thermally conductive polymer and carbon based TIM.

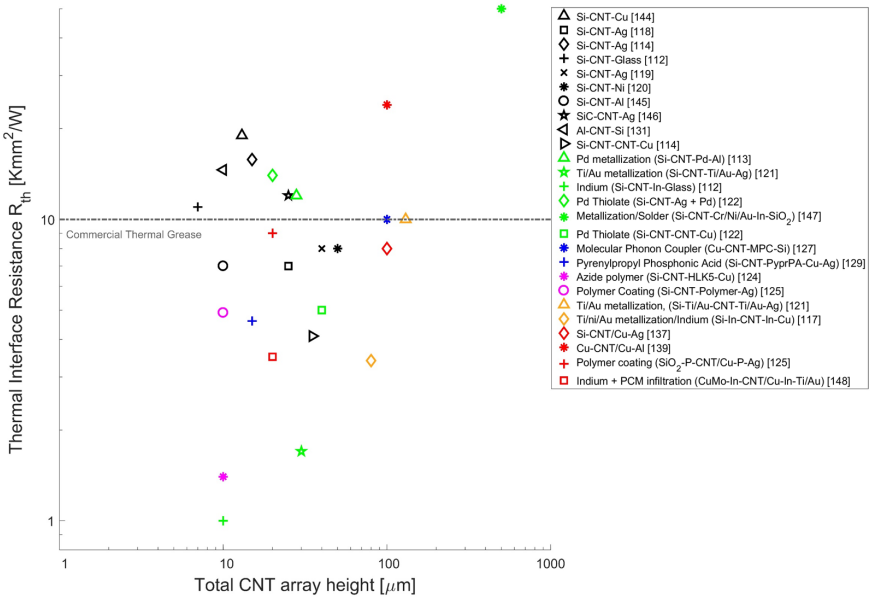

Fig. 2.8. Summary of CNT array TIM results, plotted as thermal interface resistance versus CNT array height. The results are divided into different categories: bare CNT arrays (black), Metal bonded CNT arrays (green), chemically bonded CNT arrays (blue), polymer bonded CNT arrays (magenta), transferred CNT arrays (orange) and double sided CNT array foils (red). Dashed line represents the thermal interface resistance of the best available thermal greases, at 10 Kmm^2/W. From paper I.

Unlike continuous metal phase TIM, a mechanically deformed metal does not use melting of the metal to create metallurgical bonds. Rather, in this category, the metal is textured in such a way that mechanical pressure allows it to bend and conform to the surfaces. This has been demonstrated for microtextured metal foils [151–153], tin [154] and copper [155] nanowire arrays and copper nanosprings [156]. The metal nanowire arrays could potentially combine the thermal stress absorption of CNT arrays with the low contact resistance associated with continuous metal phase TIM, if bonded with solder at the interface. This was demonstrated with copper nanosprings for a low thermal interface resistance of 1 Kmm^2/W.

The second category, thermally conductive polymers, utilize the recent discovery that polymers can be modified by increasing crystallinity and alignment of crystallites and chain orientation to increase the thermal conductivity by several orders of

magnitude [157, 158]. A polymer nanofiber array was found to be applicable similarly to CNT array TIM with a thermal interface resistance of 12.8 Kmm^2/W.

The third category is that of carbon based TIM aside from CNT array TIMs. The exceptional thermal properties of graphene-like structures can be harnessed in other ways than just CNT arrays and fillers in PLPs. The challenge is to create macroscale 3D structures out of what originates as 1D or 2D (CNT and graphene respectively). One way of creating such a 3D structure out of graphene is to deposit graphene on the surface of a highly porous template, and then selectively etch away the template. Left will be a freestanding graphene foam-like structure. Zhang et al. demonstrated the possibility of such a graphene foam as TIM, and found that the structure is exceptionally compliant and could achieve a thermal interface resistance as low as 4 Kmm^2/W at a contact pressure of only 0.1 MPa [159]. A similar foam like structure has also been created by a self-assembled method through a hydrothermal reduction of a graphene oxide (GO) dispersion [160].

Alternatively, instead of a random foam network, a more deliberate alignment can be done. Films of graphite or reduced GO can have a very high degree of alignment and a thermal conductivity in excess of 1600 W/mK [161]. However, this alignment is in the in-plane direction, orthogonal to the heat flow in a TIM application. If graphene sheets could be efficiently aligned in the z-direction instead, it could potentially provide a good TIM candidate. Direct stacking of multiple graphene films has been demonstrated to some success [162, 163], but a more efficient way of aligning the graphene sheets is needed for a practically usable TIM.

Finally, graphene is only the first out of many possible 2D materials, and the attractive properties of graphene could very well be found in other materials as well. One such interesting material is hexagonal boron nitride (h-BN), which has a similar structure to graphene and also high thermal conductivity. However, unlike graphene, it is electrically insulating, which may be important in certain applications. It has already been used as conducting fillers in polymers, both in the form of platelets [33], nanotubes [164], and as a BN foam [165], echoing the use of graphene while retaining its insulating properties.

2.2.5 Summary

Figure 2.9 shows the thermal interface resistance versus BLT from all reports treated within this review where such data could be obtained, including some reports not previously mentioned [166–169]. A few commercial compounds are also included as reference [148, 170]. It contains selected reports in which thermal interface resistance measurements have been done at a given BLT. While not exhaustive, it gives an overview of the field in its entirety, and some general trends can clearly be distinguished, as seen from the colored ellipses. Particle laden polymers, despite attracting much interest, has still not improved significantly over the last decade in terms of thermal performance. Indeed, where comparable the performance of commercial thermal grease actually performs better than newer compounds. Metal

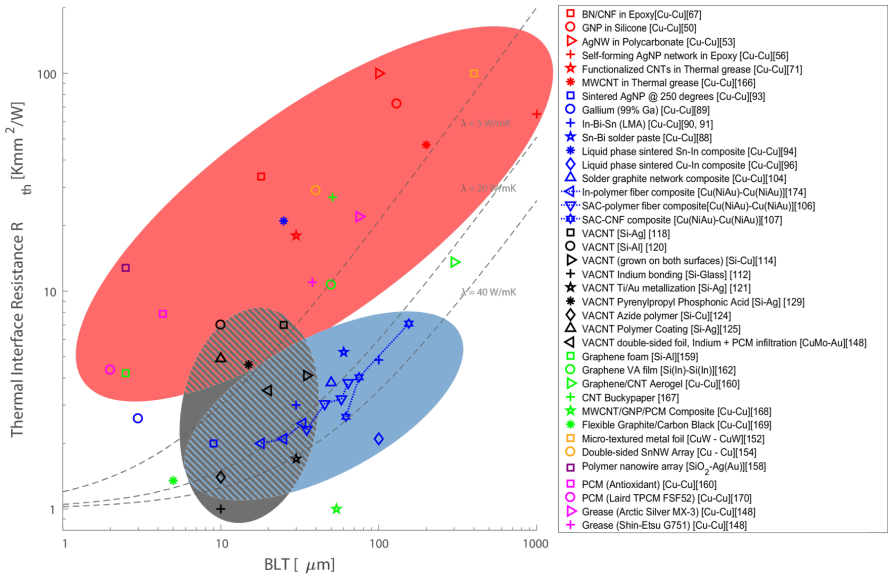

Fig. 2.9. Thermal Interface Resistance versus Bond Line Thickness for recent results, based on different categories: Particle Laden Polymers (red), Carbon Nanotube array TIMs (black), continuous metal phase TIMs (blue), other carbon based TIMs (green), mechanically compliant metal TIMs (orange), polymer nanowire array (purple) and commercial TIM references (pink). References for TIMs with a thermal contact resistance of 1 Kmm^2/W and a thermal conductivity of respectively 5, 20 and 40 W/mK are also plotted (dashed grey). The colored ellipses show the approximate region in which the different categories of TIM are found.

nanowire filler is a potential breakthrough technology, but as can be seen, despite a very high thermal conductivity, the thermal interface resistance is still very high due to high contact resistance and large BLTs.

Reports on continuous metal phase TIMs all follow a similar relationship between BLT and resistance, Which is consistent with the idea that research within this area is more focused on mechanical properties rather than thermal performance, and actual progress in that area will not be represented in this type of comparison. Rather, the challenge is to create a reliable, convenient and cheap TIM without sacrificing the thermal performance.

As previously discussed, CNT array TIMs perform slightly worse than solders with dry contact, and on par or even better when bonded to a substrate. There is no clear relationship between BLT and thermal interface resistance, which is

consistent with the resistance being dominated by contact resistances at the edge of the CNT arrays. It is clear that performance is not the factor limiting CNT array TIMs from becoming commercially available. On the other hand, the reliability of CNT array TIM is an open question, which we will address further in chapter 4. Nonetheless, CNT array TIM is the most promising new breakthrough technology to enter commercial markets within the relatively near future.

Chapter 3

Solder Matrix Fiber Composites

3.1 Introduction

The most common use of solder is to attach components on a PCB and to form electrical connections between them. However, the same properties and technologies that enable excellent electrical connections, also creates good thermal connections.

Due to their ability to form metallurgical bonds towards other metal surfaces together with their high thermal conductivity, solders have been widely used in TIM applications, and is the only commercially available alternative when thermal interface resistances of < 5 Kmm^2/W is required. However, as explained in section 2.2.2, solders can have significant drawbacks in terms of reliability due to a high elastic modulus and rigid structure. This issue is exacerbated as the size of the interface increases, as the strain due to CTE mismatch between the two surfaces is larger. In addition, solder can be difficult to handle during reflow, causing uneven and/or to thin BLT.

As a potential way to address these issues, the solder matrix fiber composite (SMFC) concept was introduced by Carlberg et al. in 2008 [171]. The concept consists of a randomly aligned network of fibers inside a metal matrix as seen in figure 3.1. The metal part of the composite acts as the solder in normal solder TIM. The fiber network is highly porous, which allows the metal to form continuous heat paths through the TIM. This allows for a high total thermal conductivity despite the presence of a fiber network, which is not necessarily a good thermal conductor. The end result is a composite material which has very similar thermal properties as regular solder TIM.

The fiber network serves several purposes within the metal martix:

- To tailor the mechanical properties of the TIM. Depending on fiber composition, the fiber can serve to make the material softer or stronger.
- To prevent crack propagation through the metal phase.
- To act as a spacer during reflow, in order to establish a well-defined and uniform BLT and prevent metal from escaping the interface during molten state.

Both metal matrix and fiber network can consist of a number of different materials. The metal matrix could be any suitable alloy, depending on the requirements for each application in terms of thermal properties, temperature and surface metallization. SMFCs have been demonstrated with In [172–175], Sn-Ag-Cu (SAC) alloys [106, 107] and In-Bi-Sn [171] as metal matrix component. The fiber network can consist of any material available as a non-woven fiber network, depending on desired end properties. So far, the concept has been demonstrated using fibers made out of Ag coated polyimide [106, 174, 175], carbon nanofibers [107] and BN [172].

All previous reports have relied on the electrospinning technique for the manufacturing of the fiber network. However, current electrospinning processes are too slow and expensive to be viable for a commercial application. In order to bring the technology closer to industry, it would be desirable to be able to simplify the fiber fabrication, or outright use existing commercial alternatives.

This chapter described the experimental research work done on SMFCs within the scope of this thesis. Instead of using electrospun nanofibers, commercially available non-woven fiber networks have been explored in order enable mass production and potentially commercially viable materials. Two different fibers have been investigated: carbon fiber (Paper II) and silver plated nylon fibers (Paper III).

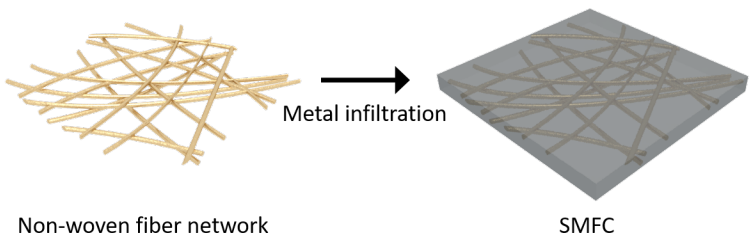

Fig. 3.1. SMFC concept, consisting of a non-woven fiber network which is infiltrated with molten metal to form a composite structure.

Pressure assisted infiltration of molten solder

Regardless of fiber and alloy composition, the principle for forming the composite structure is the same. It is based upon pressure assisted infiltration of solder in the molten state into the fiber network. The difficulty of infiltration depends on the wetting between the solder and fiber. Molten metal has a relatively large surface tension, and has poor wetting towards most polymers. Therefore, surface modifications such as metal coatings and high pressure during infiltration may be needed in order to ensure proper infiltration of the matrix [106, 176].

For the infiltration process, custom in-house constructed tools were used. The fiber network was placed inside a thin mold cavity, which was heated to 30°C above the melting point of the metal. Molten metal from a separate melt cavity was then injected under pressure into the mold, and the pressure was maintained for several seconds. The end result was a thin preform foil of the composite material, which can be cut into arbitrary shapes in order to fit desired application.

Two different versions of the infiltration tool were used. The first was a lab scale prototype which has been used in previous works in our group, which produces single round pieces with a diameter of 30 mm. The second was a newly developed automated machine, for volume production on a roll-to-roll basis with a production rate of tens of 100x100 mm pieces per hour.

Thermal characterization

To evaluate the performance of the fabricated SMFCs in a TIM application, the fabricated SMFCs were sandwiched between Electroless Nickel Immersion Gold (ENIG) coated Cu surfaces. A pressure of 200 kPa was applied to the stack, and fluxless reflow was carried out using a temperature profile optimized depending on solder material used. After reflow, the resulting three-layer sandwich structure was used to characterize the thermal properties of the TIM.

The main tool for thermal characterization used in this thesis was the transient laser flash method. The principle is based on heating one side of a specimen with a laser pulse and monitoring the time-dependent temperature change on the opposite side using an IR detector. Under perfect adiabatic conditions, the temperature response from the laser pulse depends on the thickness d and thermal diffusivity α of the specimen according to:

$$\alpha = \frac{1.38d^2}{\pi^2 t_{1/2}} \tag{3.1}$$

where $t_{1/2}$ is the half rise time of the temperature. With additional corrections, it is possible to extract the thermal diffusivity even under non-adiabatic conditions. The thermal diffusivity is further related to the thermal conductivity λ according to:

$$\lambda = \rho C_p \alpha \tag{3.2}$$

where ρ is the density and C_p is the specific heat capacity of the specimen.

From this we can calculate its effective thermal conductivity. In a multilayer setup, it is possible to extract the thermal resistance contribution of a single layer given that the the properties of the other layers is known. In a three-layer model, with a TIM between two substrates, the thermal interface resistance R_{TIM} relates to the measured $\lambda_{effective}$ by the following equation:

$$\frac{d_{total}}{\lambda_{effective}} = \frac{d_{s1}}{\lambda_{s1}} + \frac{d_{s2}}{\lambda_{s2}} + R_{TIM} \tag{3.3}$$

where d_{s1}, d_{s2} are the thickness and λ_{s1}, λ_{s2} the thermal conductivity of the two substrates. In practice, this is best done using more complex numerical analysis software, but the equation above serves to demonstrate the principle.

3.2 Carbon Fiber Composite

Carbon fiber (CF) is widely used as a component in high performing composite materials, primarily owing to its high strength. In addition, like other carbon allotropes, CFs have high thermal conductivity, which could be increase the thermal performance of a CF composite [177]. Murugesan et al. demonstrated a SMFC with SAC solder matrix and electrospun CFs from mesophase pitch [107]. However, as previously explained, it would be desirable to be able utilize fibers that are available at a commercially relevant scale.

In paper II we instead used a procured non-woven CF veil, which is available in large quantities on rolls. SEM images of the fiber network can be seen in figure 3.2 a) and b). The fiber networks consisted of CF with a diameter of 8 ± 2 µm and the total mat thickness is 82 ± 3 µm, with a total fiber volume fraction of around 4 %.

This fiber size is around one order of magnitude larger than that of the fibers produced by electrospinning, and the pore size between fibers is similarly larger. For the electrospun CF network, a metal coating to facilitate wetting between fiber and matrix was required in order to properly manage inflitration, despite the fact that the wetting between solder and graphite is relatively good [178]. However, with a more sparse matrix, this metal coating might not be required. Thus, the infiltration was attempted both with pristine fiber networks and with Ag coated fibers. The Ag coating was formed by a chemical method. A silver nitrate solution was saturated with ammonia to form diamine silver complex, which in turn was mixed with a mixture of glucose and tataric acid to form deposit silver on the fiber network. The silver plated fiber can be seen in figure 3.2 c) and d).

Despite the fact that the CF fiber is available as a roll, the manual prototype infiltration equipment was used for the fabrication of the CF-SMFC in this work, due to a process incompatibility. The problem is not insurmountable, and future works aims to adapt the process in order to create high volume TIM. SAC305 (96.5%Sn-3%Ag-0.5%Cu) alloy was used as matrix material, as it is one of the most common solders used in industry today.

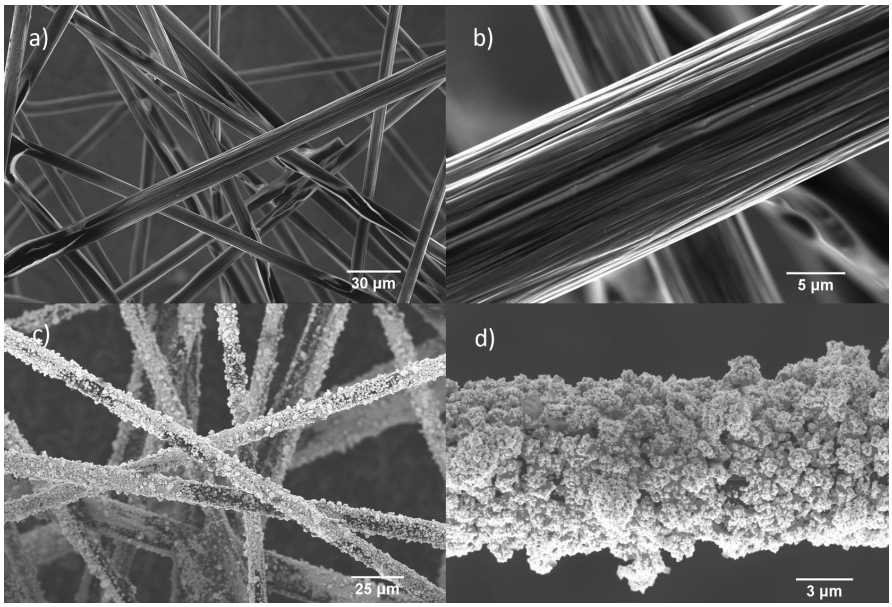

Fig. 3.2. SEM images of carbon fiber network, pristine (a,b) and with a Ag plating layer (c,d). From paper II

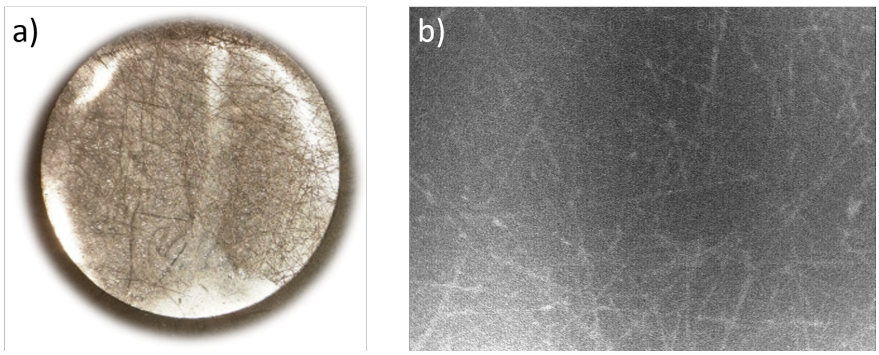

Fig. 3.3. a) Photo of the infiltrated CF-SMFC preform. b) X-ray image of the assembled TIM sandwich structure.

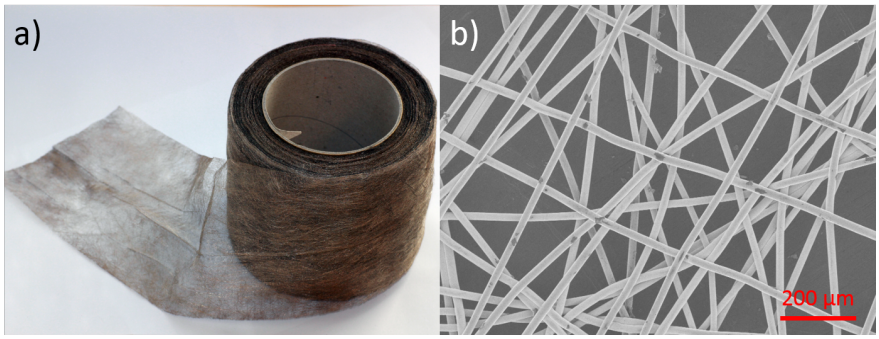

Fig. 3.4. A roll of the commercial Ag-plated PA6,6 fiber network.

The resulting preform TIM after infiltration can be seen in figure 3.3 a). After subsequent reflow the internal structure of the TIM without Ag plating was characterized using X-ray imaging, the result of which can be seen in figure 3.3 b). The x-ray image provides contrast based on difference in density, and is useful to detect voids and imperfect infiltration. As seen from the image, the density is uniform throughout the sample, with only the outline of the fibers themselves providing any contrast. This indicates that the wetting between the fibers and the matrix is good despite the lack of metallization on the fiber surface. This is further confirmed by later thermal characterization, and so only the pristine CF TIM was further investigated.

3.3 Nylon Fiber Network Composites

Among the different fiber compositions investigated for SMFCs in the past, the majority have used polymer fibers, mainly polyimide (PI) [173–175]. The reason for this is that polymers are soft materials which may help decrease the modulus of the TIM and reduce thermal stresses. Similarly to the case with CF, a commercially available fiber alternative would be desirable, and in paper III we investigate new version of SMFC based on commercially available polymer fibers.

Instead of PI fibers, these commercial fibers consists of polyamide (PA), or nylon, more specifically PA6,6. It is one of the most common type of nylon in the plastics and textile industries, making it cheap and abundant. The fiber procured (Statex, Bern) is a non-woven PA6,6 fabric with a Ag coating. The Ag coating is necessary since PA6,6, unlike CF, has very poor wetting towards solders. Since the fabric is already coated, no additional treatment of the fibers is needed before infiltration. The fiber is available on rolls, as can be seen in figure 3.4 a. The microstructure of the fiber network can be seen in figure 3.4 b. The fiber network consists of randomly

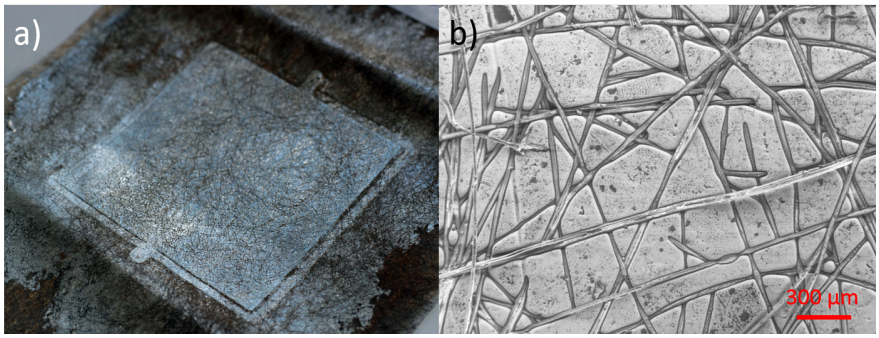

Fig. 3.5. a) Resulting TIM on the fiber roll. b) SEM image of fabricated TIM surface.

aligned fibers with a fiber diameter of 8 µm, which forms a mat with a thickness of 80 µm at a volumetric filling factor of 4%.

In this study, a newly developed automated infiltration equipment was used. Instead of placing the fiber inside a cavity into which the molten metal was injected, the cavity is formed from two tooling halves clamping onto the fiber, forming a cavity around part of the fiber, with the fiber mat itself sealing the cavity between the tooling halves. After sealing, molten metal was injected under high pressure, filling up the cavity and infiltrating the fibers.

The result is a 50x50 mm square TIM sample still attached to the fiber film, which can be seen in figure 3.5 a). Note that around the TIM sample, the fiber is compressed during infiltration, and is supposed to provide a seal. However, as can be seen in the image, some metal has penetrated the fiber around the sample, which may relax the pressure somewhat. Thus, it is difficult to tell the true pressure attained during this infiltration, though the infiltration appears to be successful from visual as well as SEM inspection (figure 3.5 b).

Multiple layers of fiber mat were stacked before infiltration in order to investigate the effect of fiber concentration in the SMFC. The fiber mat layers will compress into each other during reflow, increasing the concentration of fiber compared to the matrix with increasing number of fiber mat layers. Two different matrix materials were used, SAC305 and pure indium, as these are the two most common materials for solder TIM, as well as the most studied matrices in previous reports [106, 175]. In total, five different matrix/fiber configurations were investigated, according to table 3.1

The thickness of the TIM sample depends on the cavity halves together with the thickness of the fiber network, although it is significantly compressed. By exchanging cavity the thickness can be varied, while differing number of fiber layers compress into each other enough so that no discernible difference could be found on the final

Table 3.1. SMFC sample configurations

Sample configuration:	Metal	No. of fiber mat layers	Thickness after infiltration (µm)	BLT after reflow (µm)
A	SAC	1	220	68 ± 3
B	SAC	2	220	90 ± 13
C	SAC	3	220	117 ± 3
D	In	1	175	44 ± 3
E	In	2	175	86 ± 13

thickness. However, during the reflow process, excess material was pressed out of the interface, thinning the composite until the fiber phase supports the applied pressure, leading to a reduced BLT compared to the initial thickness.

To compare the SMFC to regular solder, reference samples with pure SAC and indium at the interface were prepared from solder preforms (Indalloy #4 and #256, Indium Co.) using an identical reflow profile. However, without the fiber component, the applied pressure will squeeze out almost all material from the interface, creating a very thin bond line. In order to make a comparison, copper spacers were created to ensure a similar BLT as for the SMFC TIM.

An X-ray microscope was used in order to investigate the internal structure of The assembled TIM structures. Figure 3.6 a-b), d-e) and g-h) show the assembled structure for sample condition A, B and C respectively. Light parts indicate regions of lower density, while the dark regions show continuous metallic thermal paths between the joined surfaces. The contrasting features consist of the fiber network together with intermittent small voids throughout the material. While voids inside a solder joint can affect the thermal and mechanical performance negatively [179, 180], it is mainly through large voids, which can lead to hot spots and delamination. Small, evenly spread voids do not necessarily contribute to decreased reliability at moderate void levels [181], and could even potentially be beneficial through stress relaxation and as crack propagation barriers. In this case the voids are evenly spread out at the millimeter scale, although the amount of voids starts to raise concerns at three fiber network layers. However, how much this affects the thermal properties can be measured directly by thermal interface resistance measurements.

Tensile analysis

One of the main motivations for the polymer composite is to modify the mechanical properties of the TIM compared to pure solder. To investigate this phenomenon, the samples were subjected to a pulling test in order to measure Young's modulus and tensile behavior of the different configurations. The SMFC was cut into strips of 10 x 50 mm, clamped at each edge and pulled with a strain rate of 0.1 mm/minute for

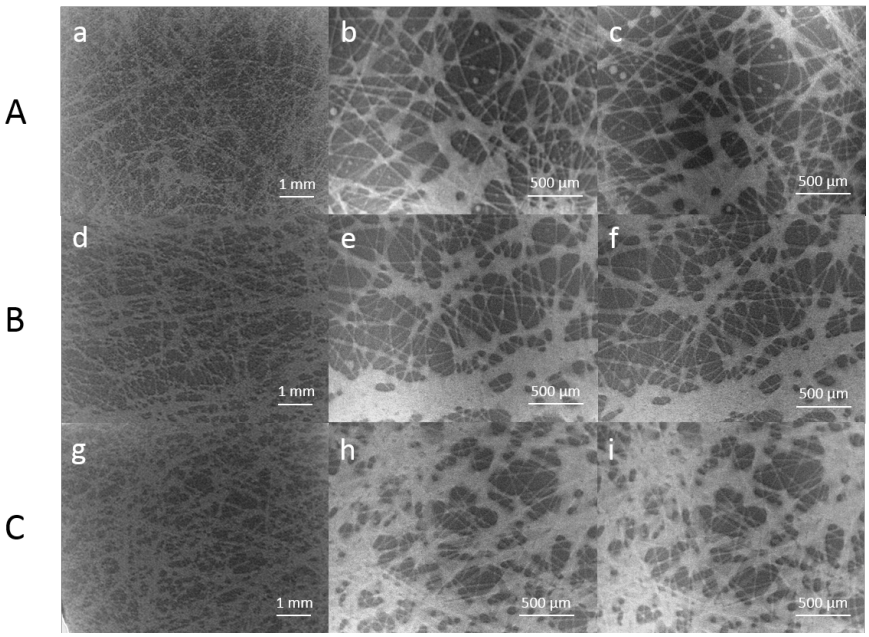

Fig. 3.6. X-ray images of the composite material in a TIM assembly, after reflow, for one (a,b), two (d,e) and three (g,h) fiber network layers (sample condition A, B and C respectively) Same samples after thermal cycling (c,f,i). From paper III

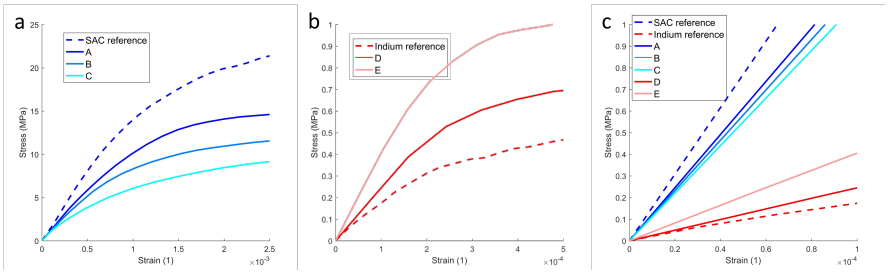

Fig. 3.7. Tensile behavior of a) SAC based SMFCs with pure SAC reference, b) Indium based SMFCs with pure indium reference. c) Initial linear regime tensile slope for all samples with pure solder references. From paper III

indium based samples and 0.3 mm/minute for SAC based samples, with metallic foils of pure indium and SAC as references.

Figures 3.7 a) and b) show the stress-strain curves for SAC based and Indium based composites respectively. Figure 3.7 c) shows all test conditions in the linear regime at low strain, from which the Young's modulus can be calculated. The values for the Young's modulus are presented later in this chapter in table 3.2.

The values of the reference SAC and indium foils significantly differ from the bulk literature values (Indium: 88 W/mK [182], SAC: 60 W/mK [21]) of the alloys. However, the tested material has been exposed to processing at high temperature and pressure, which may significantly alter the mechanical properties [183, 184]. In addition, size effects due to the low thickness can have a large effect on the properties of thin metallic foils [185]. The lower Young's modulus measured in this work is consistent with earlier reports of tensile measurements on thin metallic foils [186–188]. Thus, while the absolute values reported here should not be taken at face value, they can still be useful for comparative purposes.

For the SAC based composite, a clear trend of decreased stiffness with increased fiber content can be seen (figure 3.7 a). A contribution both from the low Young's modulus of the fibers as well as an increase in voids trapped inside the material can be expected to contribute to this decrease. This depression in stiffness is consistent with a similar report by Zandén et al. [106], in which a SMFC based on SAC and electrospun polyimide was investigated.

Indium based SMFCs on the other hand, show an inverse trend, with increased elastic modulus and increased strength with additional fiber network layers (figure 3.7 b). This behavior is more difficult to explain, as the individual components in the composite all have a lower modulus. But again, this is consistent with a previous work, where Luo et al. investigated the tensile behavior of a SMFC based on Indium and electrospun polyimide fiber [172]. Luo et al. found a mutual strengthening mechanism between the fiber and matrix, which increased the total strength of the

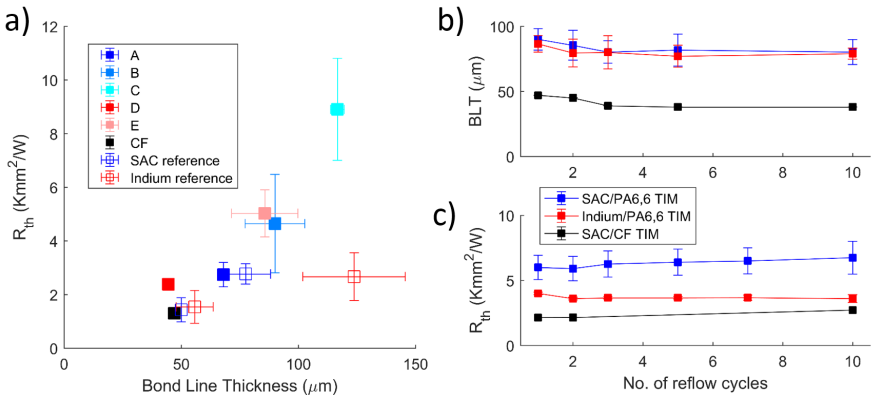

Fig. 3.8. a) Thermal interface resistance versus BLT for all test conditions (Filled squares) and pure solder references (unfilled squares). b) BLT as a function of number of reflow cycles for test condition B (blue), E (red) and CF (black). c) Thermal interface resistance as a function of number of reflow cycles for test condition B (blue), E (red) and CF (black).

composite. The tensile behaviour of the SMFC in this work indicates that the same mechanism plays a role in this case as well, despite a large difference in average fiber diameter (780 nm vs 8 µm in this work).

Figure 3.7 c) shows the linear regime of all sample configurations. By varying the matrix material and fiber density, the elastic modulus can be tailored in the regime between the two pure materials. Further optimisation would allow for the engineering of composite materials with very specific mechanical properties.

Note that the tensile testing is done directly on the SMFC prior to assembly and reflow in an application. Since a significant amount of metal is ejected from the interface during reflow, the actual fiber density of the TIM in application will be higher. Thus, the changes in mechanical properties can be expected to be even more pronounced, although to what degree is to be further investigated in future works.

3.4 Thermal Performance

As the most important figure of merit, the thermal interface resistance was measured for all configurations, both with CF and PA6,6 fibers. The results are shown in figure 3.8 a), plotted versus the BLT. As expected, increasing the amount of fiber network layers increases the BLT and the thermal interface resistance. However, the difference in thermal interface resistance with respect to variation of the number of layers is larger than for a material with uniform thermal conductivity. With

increasing amount of fiber network layers, the layers compress into each other and the total fiber network density increases. Increasing fiber density leads to a decreased thermal conductivity due to the drastically lower thermal conductivity of PA6,6 (0.25 W/mK) compared to SAC alloy (60 W/mK) and Indium (82 W/mK). The increased fiber density also reduces the infiltration effectiveness and traps additional voids in the interface, further reducing the effective composite thermal conductivity.

SAC based and Indium based samples have a similar thermal interface resistance compared to number of fiber mat layers. A lower thermal interface resistance of samples based on Indium could be expected considering the increased thermal conductivity of Indium compared to SAC, and the absence of such difference indicates that the bulk thermal conductivity of the solder material is not the limiting factor for the total thermal interface resistance, and that SAC is possibly slightly more compatible with the infiltration process. It should be noted however, that the higher effective thermal conductivity of configuration A as compared to configuration D can be explained by a higher fiber density due to the same amount of fibers inside a thinner interface. The total thermal interface resistance is instead primarily based on the number of fiber layers rather than the BLT.

Using a single fiber mat layer, the thermal interface resistance of the composite is still close to the reference samples with pure solder, which indicates that any extra voids due to the presence of the fiber network is limited for single-layer fiber networks. However, we can see the superior wetting characteristics of SAC/CF compared with the other configurations, as the thermal resistance here is almost identical with the SAC reference sample. This indicates that the presence of fibers in the CF TIM does not harm the thermal performance in any way.

While the thermal interface resistance of the SMFC is comparable to pure solders, a potential benefit of the composite compared to conventional solders is the possibility of a fluxless reflow process without using complicated spacers or frames to prevent metal pump-out of the interface. The fiber network in the composite acts as a spacer, ensuring a well-defined and uniform BLT throughout the sample. To confirm that a consistent BLT is achievable over several reflow cycles, samples from configuration B, D, and CF were subjected to additional reflow cycles while monitoring BLT and thermal interface resistance.

Figure 3.8 shows the BLT (3.8 b) and thermal interface resistance (3.8 c) across 10 reflow cycles. A slight decrease in BLT and increase in thermal interface resistance is seen at first, attributed to a slight additional compression of the fibers, but the performance subsequently remains stable. Note that the interface does compress during the initial reflow until the fiber network is compressed enough to withstand the applied pressure. However, subsequent additional melting of the interface does not cause additional material to escape.

A comparable reflow cycle with pure solder without the use of a spacer immediately collapses the interface (BLT <10 µm) and the melt leaks out of the interface. To be able to apply the composite in an application as a preform with built-in BLT control could potentially eliminate the need for spacer usage, and allow for

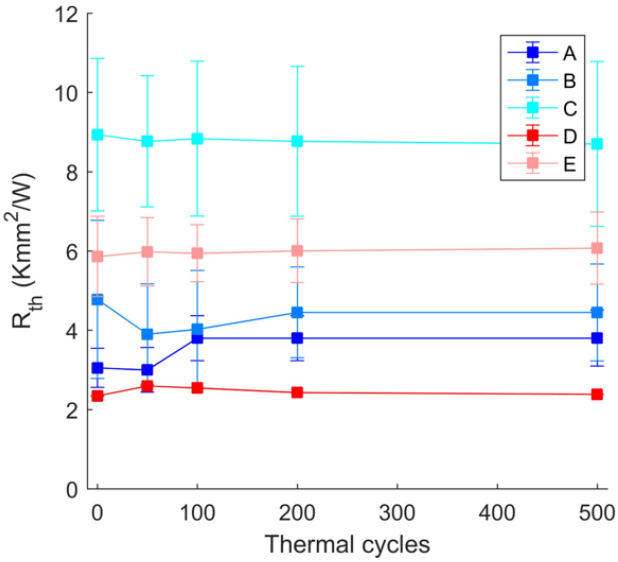

Fig. 3.9. Thermal interface resistance as a function of number of cycles during temperature cycling for PA6,6 based SMFCs. From paper III

significantly simplified process flow for TIM assembly.

Additionally, the reliability of the PA6,6 based SMFCs was tested using thermal cycling in accordance with JEDEC standard test condition 1. The samples were subjected to 500 cycles, with a temperature profile ranging from -40°C to 115°C, at 2 cycles/h and 5 min soak time at each extreme. Thermal interface resistance measurements were carried out periodically to monitor the change in thermal interface resistance. Figure 3.9 shows measured thermal interface resistance values during thermal cycling. Each test case is an average of at least 3 samples. All samples across showed a variation of less than 20% over the full amount of cycles, indicating that internal structure of the TIM does not change significantly due to thermal stress. This is seen clearly in figure 3.6, where images of the same spot before (b, e, h) and after (c, f, i) 500 thermal cycles show the same distribution of fibers and voids. The X-ray images show an absence of even minor structural changes which could be indicative of reliability issues further along.

Table 3.2. Thermal and mechanical results for SMFC configurations

Sample configuration	BLT (µm)	λ_{eff} (W/mK)	R_{TIM} (Kmm^2/W)	Young's modulus (GPa)
A	68 ± 3	25 ± 4	2.7 ± 0.5	11.6
B	90 ± 13	19 ± 5	4.6 ± 1.8	9.5
C	117 ± 3	13 ± 2	8.9 ± 1.9	7.8
D	44 ± 3	18 ± 1	2.4 ± 0.1	3.0
E	86 ± 13	17 ± 2	5.0 ± 0.9	3.8
CF	47 ± 1	35 ± 2	1.4 ± 0.4	
SAC references	50 ± 1	34 ± 1	1.4 ± 0.5	18.0
	78 ± 10	28 ± 4	2.8 ± 0.4	
Indium references	56 ± 8	36 ± 5	1.5 ± 0.6	1.9
	123 ± 22	46 ± 8	2.7 ± 0.9	

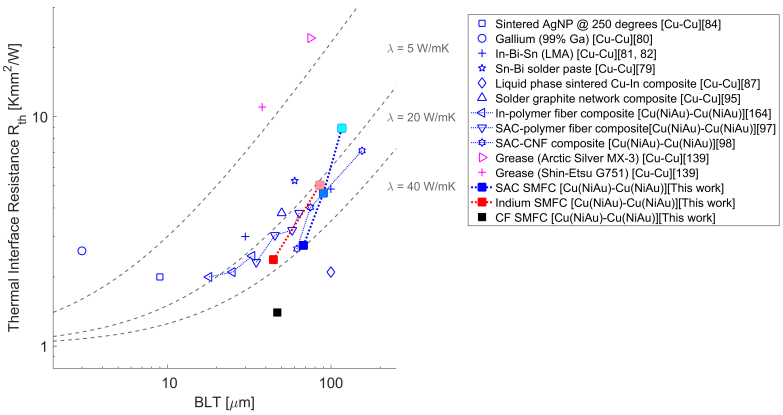

Fig. 3.10. Comparison of thermal interface resistance versus BLT for various metal based TIM (blue), commercial thermal grease (pink) and this work (blue, red and black filled squares). From paper III

3.5 Summary and Conclusion

The thermal and mechanical characterizations of the different versions of SMFCs are summarized in table 3.2. Figure 3.10 further shows the thermal performance versus BLT of the different SMFCs compared to a selection of previously reported metal

based TIM (blue) and commercial thermal greases (pink) from the earlier review in chapter 2. The dashed lines indicates hypothetical TIMs with thermal conductivity as indicated and a thermal contact resistance of 1 Kmm^2/W as comparison. SMFCs from earlier works typically fall in the range between the hypothetical 20 W/mK and 40 W/mK TIMs. Pure metals or alloys, such as Gallium [89, 90], In-Bi-Sn [90], Sn-Bi [88] and sintered silver nanoparticles [93] are typically slightly higher, although by achieving very thin bond lines it is still possible to achieve a low thermal interface resistance. Composite structures such as the solder-graphite network reported by Sharma et al. [104] follow the same trend, and the only outlier is a liquid phase sintered Cu-In composite [96] which takes advantage of the much higher thermal conductivity of Cu.

Most metal based TIMs still have a similar thermal performance as pure solder, and this will not change without the addition of other materials with significantly higher intrinsic thermal conductivity, such as carbon based materials [118] or non-solderable metals [96, 189]. However, despite little further improvement in thermal interface resistance, solder based TIMs can still be improved with regards to mechanical properties and handling characteristics. The TIMs in this work fall in the same range for one and two-layer samples, indicating that these SMFCs can act as replacement for solder. For the CF based TIM, the thermal interface resistance is even lower than previously reported metal TIM.

In conclusion, with the CF TIM, we have shown that it's possible to make SMFCs with very low thermal resistance using commercially available fibers. However, CFs have very high stiffness, and might not improve the mechanical properties of the TIM significantly, although the benefits in BLT control and handling are still applicable. For the PA6,6 based TIM, we have shown how the mechanical properties of the TIM can be modified based on different material selections and compositions, while retaining good thermal properties. This allows us to tailor the TIM towards specific applications where current materials are unsatisfactory.

Chapter 4

Reliability of Carbon Nanotube Array TIMs

The SMFC concept was aimed at improving the mechanical properties of continuous metal phase TIM, something we identified as one important development route for future TIM back in chapter 2. However, it was not the only concept where significant potential gains could be made. In this chapter, we will instead focus on another area which was identified as an area with a clear route forward: the carbon nanotube array TIM.

As seen in chapter 2.2.3, CNT array TIMs have the potential to surpass any commercially available TIM in terms of raw thermal performance. A significant amount of research has been done to optimize the thermal conductivity as well as bonding and transferring processes. However, none of that will ultimately be useful unless the TIM can withstand operating environments for the lifetime of the application device. Here there is a distinct lack of studies in the literature; it appears like the reliability of CNT array TIMs has never previously been investigated.

This chapter describes our efforts to rectify this situation. We conducted two major reliability studies of CNT array TIM, published as paper V and VIII respectively. Based on the results of these studies, we can draw some conclusions about the reliability of CNT array TIMs in general, and what considerations need to be taken into account in order to create a reliable interface.

4.1 Background

As discussed in chapter 2.2.3, a CNT array TIM consist of arrays of vertically aligned CNTs. In principle, each individual CNT spans the entire interface from

one side to the other, which in addition to allowing excellent thermal performance also allows mechanical decoupling between the mating surfaces. This is illustrated in figure (ref). Each CNT can bend independently of the others, causing the overall stress to be equal to the stress within a single CNT. However, despite the great promise, the reliability of CNT array TIMs had not previously been experimentally investigated.

4.1.1 Chemical Vapor Deposition

The first step in creating a CNT array TIM is to synthesize the CNT array itself, which is done by chemical vapor deposition (CVD). The principle for CNT CVD is the thermal composition of the carbon containing gas and absorption and diffusion of carbon into the metal nanoparticles. When the catalyst particle is saturated with carbon, it crystallizes as graphene layers on the surface of the nanoparticle, and finally when the surface is covered the carbon is pushed out from the particle into a tube by continuously crystallizing carbon.

This process can be achieved by a variety of catalyst materials, mostly depending on the carbon solubility within the material. The most common material is Fe, which we use in all the work within this thesis, but many others, such as Ni, Co and Mo [109, 190] and alloys thereof can also be used. Similarly, we use acetylene (C_2H_2 as carbon feedstock gas, but nearly any other carbon containing gas with a compatible thermal decomposition temperature will be able to produce CNTs.

A standard recipe, which we have used throughout this work, is shown in figure 4.1. This recipe produces arrays of MWCNTs with relatively high density up to a millimeter in length. In order to achieve aligned arrays, the catalyst particles have to be immobilized next to each other. In our case, this is done by an alumina (Al_2O_3) support layer. The process begins by preparation of catalyst structure on the desired substrate (usually Si). This is done by electron beam evaporation, which by localized heating of desired material vaporizes it and allows for redeposition on the substrate. Using this process, we deposit thin films of 10 nm Al_2O_3 and 1 nm Fe.

After catalyst preparation, the sample is placed in a CVD chamber (Axtron, Black Magic). First, the temperature ramps up to an annealing stage at 500°C under a flow of H_2 which acts as a reducing agent, removing oxides on the surface of the Fe layer. During this stage, the Fe layer partially melts and forms nanoscale droplets which wet to the alumina (step 2 in figure 4.1). The H_2 atmosphere removes and prevents oxides on the droplets, and the alumina layer immobilizes them, preventing diffusion into the underlying substrate as well as the agglomeration of the nanoscale droplets into larger ones. After 3 min annealing, the temperature is raised to 700°C and acetylene is introduced into the chamber. The acetylene decomposes in contact with the catalyst and the carbon diffuses in and crystallizes on the surface, until the surface is full and a CNT starts to grow (step 3 in figure 4.1). Since the catalysis site is immobilized, a crowding effect creates a vertical alignment of the CNTs. By

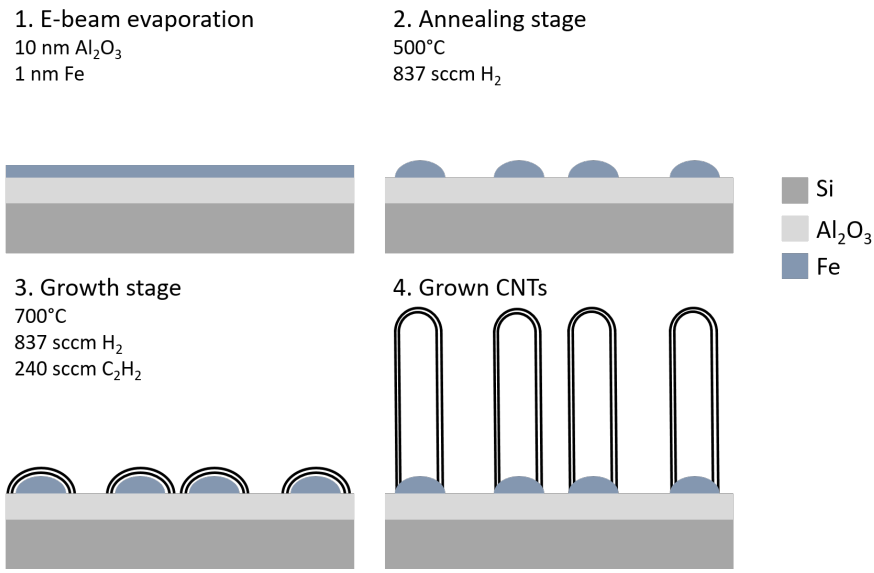

Fig. 4.1. Schematic of CVD of CNT arrays on silicon.

varying the growth time we can vary the CNT array height.

An example of CVD grown CNT arrays can be seen in figure 4.2. From afar the array has the appearance of a solid mass, but a closer inspection reveals the CNTs themselves. Note that the CNTs are not perfectly straight in themselves, but crowding effects makes the overall direction of the CNTs vertically aligned.

CNT array bonding and transfer

In order to create a CNT array TIM, in principle we only need to attach the grown CNT array to a mating surface. However, as discussed in chapter 2.2.3, in order to create a good interface some sort of bonding agent is required, and sometimes a transfer process from the growth substrate is needed as well. During the reliability studies, we tested both single bonded and transferred samples, with two different bonding techniques: one polymer based and one metal based.

4.1.2 Thermal Cycling

In order to investigate the reliability of a TIM, we need a controlled method for testing that mimics real usage within a much shorter time span. Most reliability issues arise from thermal expansion and contraction as devices heats up and cools down, which

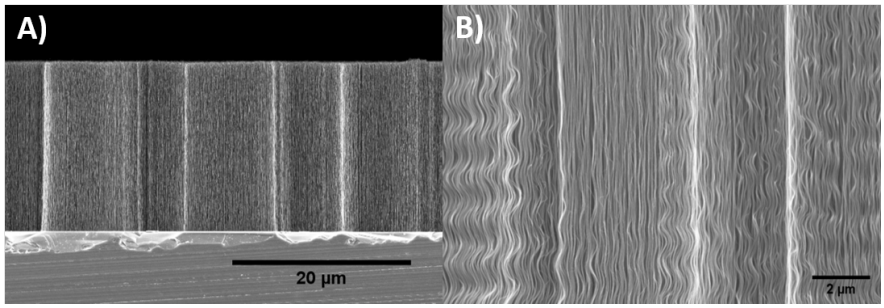

Fig. 4.2. SEM images of CVD grown CNT arrays. From paper V.

means that we can capture the most obvious reliability problems by temperature cycling of the interfaces. Using a thermal cycling oven with connected liquid nitrogen supply for rapid cooling, we cycled TIM samples using the JEDEC standard test condition B [191] thermal cycling profile. This correspond to temperature extremes of -55°C and 125°C, with a ramp time of 10 minute and holding time of 20 minutes. This is a common cycling procedure for accelerated aging, but much tougher than normal use cases in applications.

4.1.3 Characterization

The samples were characterized before, during and after thermal cycling. For the TIM performance, i.e. the thermal interface resistance, we used the laser flash method as described in chapter 3. However, in order to probe the interface in more detail, we also used some other methods to investigate the effect of thermal cycling on the CNT array TIM.

Pulsed Photothermal Reflectance

Pulsed Photothermal Reflectance (PPR) is a transient measurement technique which utilize the fact that certain metals change their reflectivity as the temperature change [192]. A low power probe beam laser is reflected on the sample surface, and the reflected intensity is measured. This allows for the monitoring of temperature changes on the surface of the sample at nanosecond timescales. Another laser fires picosecond long high-powered pulses (pump beam) onto the same spot, which locally heats up that spot. The reflectance, and thus the temperature, of the sample spot is monitored as the induced heat is spread into the material. If we model the heat diffusion as a one-dimensional heat equation it is possible to extract the thermal conductivity of up to three thin layers as well as the thermal boundary resistance between them.

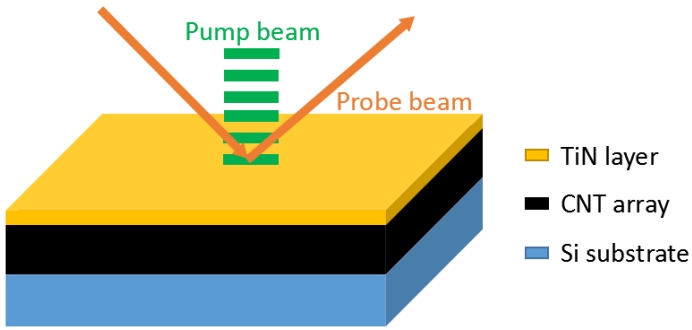

Fig. 4.3. Schematic of the Pulsed Photothermal Reflectance measurement technique. From paper V.

In our work, we used the PPR method to distinguish the different components of the thermal interface resistance as measured by laser flash. Remember from the basic equation for the thermal interface resistance of a TIM (equation 2.2) that there are three main components of the total thermal interface resistance, in this case the boundary resistance at both sides of the CNT arrays as well as the thermal resistance from conduction within the CNT array. By using the PPR method on a CNT array, we can extract the components from the CNT array itself as well as the boundary resistance at the CNT roots.

Figure 4.3 shows a schematic of our measurement setup. We used a picosecond Nd:YAG laser for the pump beam and a He-Ne laser for the probe beam. Since the principle for PPR depends on the known temperature dependent reflectivity of the surface, such a material is required as the topmost layer. For this, a 300 nm layer of TiN was sputtered onto the CNT array.

X-ray Photoelectron Spectroscopy

The basis for X-ray photoelectron spectroscopy (XPS) is the photoelectric effect, where an absorbed photon can cause an atom to release an electron. With XPS, high-energy X-rays are used to excite and free electrons. Some of these electrons will escape the material, and can be caught in a detector. By analyzing the kinetic energy of these electrons, the original binding energy can be extracted due to conservation of energy. This binding energy in turn provides a fingerprint of atomic composition of the material, giving rise to characteristic peaks in a spectrum. Each peak corresponds to the excitation of an electron in a specific atomic orbital.

The spectrum peaks are characteristics of elements, but that is not the only information available. Molecular bonds give rise to small energy shifts compared

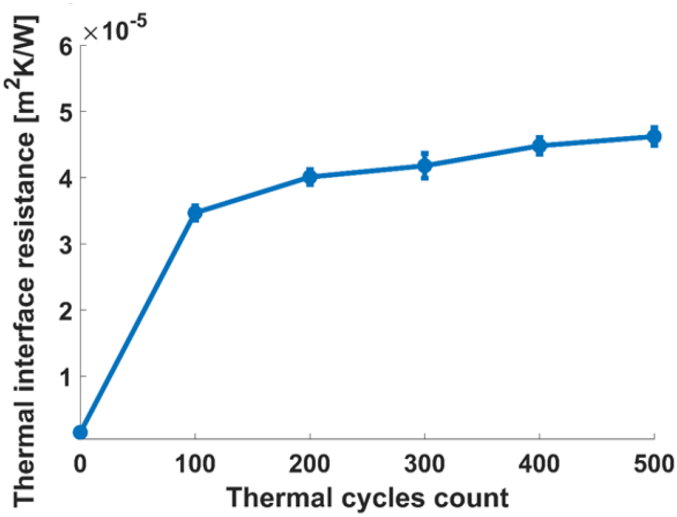

Fig. 4.4. Thermal interface resistance of polymer bonded CNT array TIM during thermal cycling. From paper V.

to the central peak. By deconvolution of the spectral shapes, contributions from different bonds can be extracted, giving a quantifiable measurement of both elemental composition as well as molecular structure.

4.2 Polymer bonded CNT array TIM

The first study, published in aper V, concerned a TIM for a specific application, a TIM1 application with a silicon chip attached to a copper surface. The CNT arrays were grown to a height of 15 µm on 280 µm thick 10x10 mm Si chips. The CNT arrays were then bonded to 2 mm thick Cu pieces using a bonding process with an azide based HKL polymer [193], creating a Si-CNT-HKL-Cu sandwich structure. This structure was measured using laser flash in order to determine the thermal interface resistance, and we found an average resistance of 1.7 ± 0.28 Kmm^2/W at 20 °C. In comparison to previous CNT array TIM, this is close to the state of the art.

4.2.1 Thermal Cycling Results

The polymer bonded CNT array TIM was measured by laser flash every 100 cycles. The results can be seen in figure 4.4, and we can immediately see a problem. Already

faliure surface.png

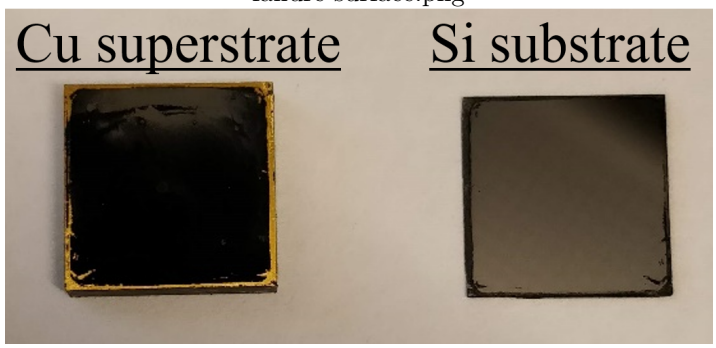

Fig. 4.5. The Cu mating surface and the Si growth substrate after delamination. The CNTs are all stuck on the Cu side. From paper V.

after only 100 cycles, the average thermal interface resistance has increased by over 2000%, and it continues to increase even more after that. In reality it is even worse, as several samples completely delaminated during the cycling process.

Already, this is a strong indication that CNT array TIM reliability is not something that can be ignored. However, it raises questions about what exactly has gone wrong, and whether anything can be done about it. In hindsight, since the degradation is so severe, the first measurement should have been done much earlier than after 100 cycles in order to see the degradation progress, and subsequent tests were run with much more measurements after few cycles.

4.2.2 Failure Analysis

To investigate the failure mode of the samples, the interface was opened, the results of which can be seen in figure 4.5. Very little mechanical force was required in order to break the interface, which was done by hand. The most immediate observation is that all the CNTs are stuck on the bonded side of the interface rather than the root side, as seen in figure 4.5. The Si substrate is almost completely clean, while the Cu surface is covered with CNTs. This means that at least in this case, the bonding is not the limiting factor for the reliability, and that we should expect the same behavior regardless of bonding method.

Since the failure surface is at the Si-CNT interface, we investigated this part further. We used XPS to probe the remains of the catalyst on the Si substrate. Figure 4.6 a) shows the spectrum for the Fe2p peak for both a forcibly delaminated pristine sample, and a spontaneously delaminated cycled sample. The Fe2p peak consists of clearly separated components which are marked with arrows in the figure [194]. The most obvious difference is that the ratio between metallic and oxidized Fe

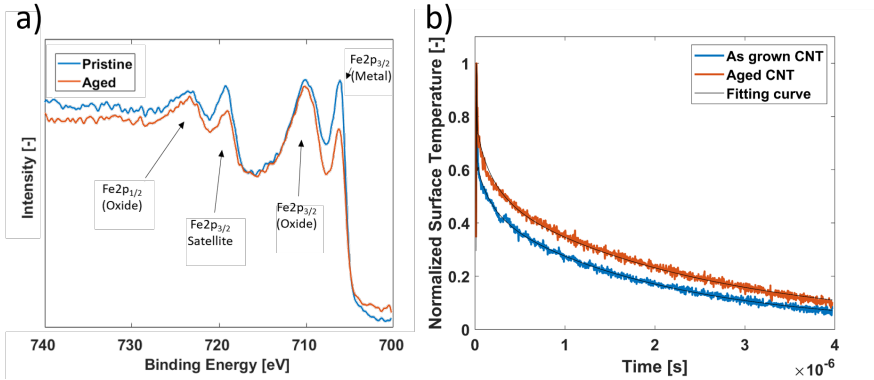

Fig. 4.6. a) XPS analysis of the Fe2p peak from the delaminated Si growth substrate for the pristine and cycled samples. b) PPR measurement signal from pristine and cycled samples. From paper V.

components has gone down substantially after thermal cycling. This is an indication that the thermal cycling oxidizes the iron catalyst particles that the CNTs are attached to. We also measured the Fe content on the roots of the CNTs and found that the total Fe content on the CNT roots is 70% lower on the cycled samples, which could mean that the bond between the Fe catalyst nanoparticles and the CNTs has weakened.

Further evidence of the Fe-CNT bond weakening is found through PPR measurements of CNT arrays without bonding to Cu. Figure 4.6 b) shows the normalized temperature response from the picosecond laser pulse for both as-grown arrays and arrays that have undergone 30 cycles. From the signal we can see that the temperature drops quicker for the as-grown CNT array, and from calculations we find that the thermal boundary resistance at the Si-CNT interface has increased from 0.96 mm^2K/W to 2.37 mm^2K/W.

An increase in thermal boundary resistance is further evidence of a weakening of the Si-CNT interface. However, the absolute thermal resistance increase of the CNT array TIM was an order of magnitude greater than the increase in Si-CNT boundary resistance, so it is not sufficient to explain the TIM failure.

Another contributing factor to the failure could be due to the CTE mismatch between the Si and Cu pieces. While CNT array TIMs should be good at absorbing the CTE mismatch stress by bending, unless the CNTs are long in comparison to the horisontal displacement due to thermal expansion, CNTs at the edges of the surface will be put under tensile stress as well. To keep a stress-free state, as the interface goes from room temperature to 125°C the CNTs at the outermost corners

would have to elongate according to:

$$l_{HT} = \sqrt{l_{RT}^2 + (\Delta\alpha\Delta T \cdot DNP)^2} \tag{4.1}$$

where l_{HT} and l_{RT} is the CNT length at 125°C and room temperature respectively, $\Delta\alpha$ is the CTE mismatch between the mating surfaces, ΔT the temperature difference and DNP is the distance to the neutral point, i.e. the distance from center to outer corner of the interface. Using this with the values of our system, we find that the CNTs would need to be elongated from 15 µm to 18 µm at the edges of the interface, or an elongation of 20%. In reality, the stress would be partially relieved by warpage of the substrates, and the CNTs are not perfectly straight in the array. However, the elongation at break for MWCNTs are typically as low as 0.2% to 0.4% [195], so this is an indication that CNT arrays may be unable to perfectly absorb CTE mismatch strain.

Of note is that this problem drops off quickly with longer CNTs, so if this is the limiting factor, longer CNT arrays should be much more reliable. For instance, at 100 µm the required strain is only 0.5%. However, as can be seen in chapter 2.2.3, most CNT array TIM studies have been done using CNT arrays with heights around 10 µm, and if this height is incompatible with reliable TIMs, then this should be taken into account in future studies.

4.3 Metal Bonded CNT Array TIM

In light of the previous results, a more thorough investigation was warranted. For this investigation, the polymer bonding was abandoned in favor of an indium based metal bonding approach. As will be evident, this creates TIM with higher thermal resistance, but has a fabrication process which allows us to rapidly create a large number of samples in order to investigate different parameters. As long as the CNT root side is the weak link rather than the bonding itself, the reliability behaviour should be similar.

The bonding is based on a previously developed transfer approach of CNT bundles [134]. This technique is based on indium solder bonding the CNT tips to the opposing substrate. A process schematic is shown in figure 4.7. In order to get good wetting for the indium, both the CNT array tips and the mating surface was covered by 20/100 nm Ti/Au by sputtering. After this, 1 µm of indium was deposited on the mating surface using e-beam evaporation. Using a flip chip bonder, the CNT arrays and Cu pieces were aligned and contacted, and the temperature was increased to 180°C for 2 minutes. During this process, the indium melted and bonded to both gold surfaces, creating a bonded structure.

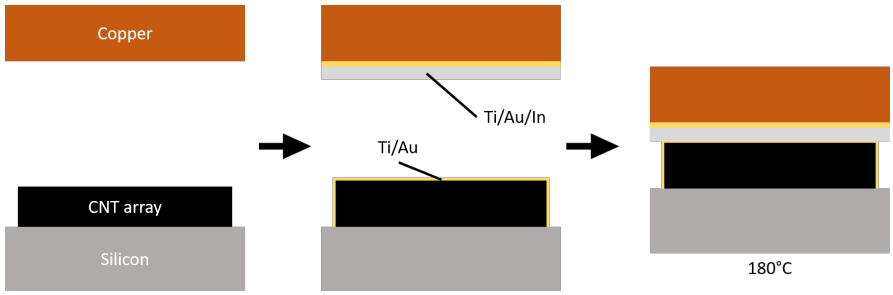

Fig. 4.7. Schematic of the indium bonding process for closing of CNT array TIM interfaces.

4.3.1 CNT Array Height Influence

One of the hypotheses was that the CNT array height might matter significantly for the reliability. In order to investigate the effect of CNT array height on the reliability of the TIMs, we cycled samples with CNT array heights of 10, 50, 80 and 200 µm. In the previous study, the performance was already severely degraded at the first measurement of cycled samples, after 100 cycles. This indicates that we are missing important information about the behaviour after only few cycles, so for this study we investigated a lower amount of cycles, with measurements after 0, 5, 10, 20 and 50 cycles. Again we used the same harsh temperature cycling profile between -55°C and 125°C.

Figure 4.8 a) shows the thermal interface resistance of CNT array TIM with varying array height during thermal cycling. The error bars show the standard deviation between samples and the dotted lines show a logarithmic fit to the data with an offset of one cycle. Figure 4.8 b) shows the initial thermal interface resistance as a function of CNT array height.

Figure 4.8 c) shows the logarithmic coefficient for the fitting curves in a), which in turn is fitted with a reciprocal function. The fact that the coefficients follow a reciprocal trend means that the thermal interface resistance increase during thermal cycling is rapidly decreases with increasing CNT array height, and that the height of the CNT array severely affects the reliability at low heights. Indeed, we can see that for the 10 µm CNT array TIM the thermal interface resistance increases by more than 30 Kmm^2/W after only 5 cycles. In fact, again reality is worse than the data, as some samples outright delaminated and could not be measured. Higher CNT arrays showed increasingly flat thermal interface resistance behavior, but also increased thermal interface resistance before cycling. We chose 80 µm as a compromise between resistance and thermal cycling stability for further testing.

The initial thermal interface resistance of the CNT array TIMs has a linear relationship with the CNT array height, corresponding to an effective CNT array

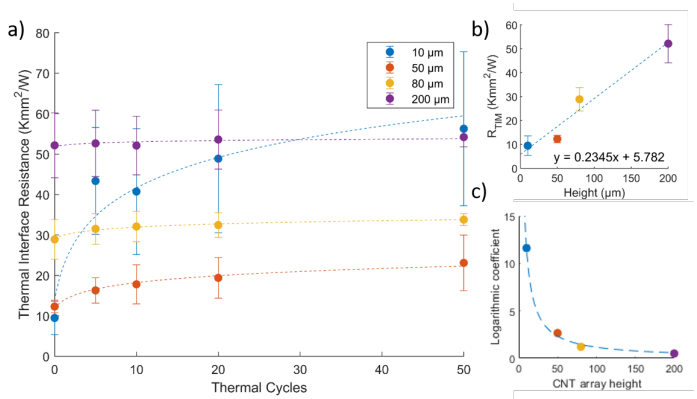

Fig. 4.8. a) Thermal interface resistance as a function of thermal cycles for different CNT array heights. b) Thermal interface resistance as a function of CNT array height before thermal cycling. c) Logarithmic coefficients of the fitted curves in a) as a function of CNT array height, with an exponential fitting.

thermal conductivity of 4.3 W/mK. This is much lower than would be expected, which is likely due to the metal bonding method not managing to engage all the CNTs, and any free CNT tips will barely contribute to the total heat transfer. This causes the total thermal interface resistance to be much higher than for the case of HKL bonded CNT arrays, and in order to create commercially viable TIM a better bonding method will be needed. However, since the degradation appears primarily on the root side of the CNTs, the resistance increase should be independent on bonding method.

4.3.2 Interface Type influence

The hypothesis that short CNT arrays are unable to absorb CTE mismatch strain appears to have merit, but we also had some evidence that oxidation of the catalyst weakens the Si-CNT interface. If this is the case, we should be able to see degradation of the interface even in the absence of any CTE mismatch. Additionally, if this is the case, doing a transfer of the CNT array and bonding it to the surfaces on both sides would solve this problem. In order to investigate this, we created a four sample configurations setup, which can be seen in figure 4.9. The samples we either bonded to copper in a Si-Cu interface as previously, or to another silicon substrate in a Si-Si interface which should not experience any CTE mismatch. For each of these interfaces, we created samples directly bonded to the mating surface as in the previous studies, but also transferred samples bonded on both sides.

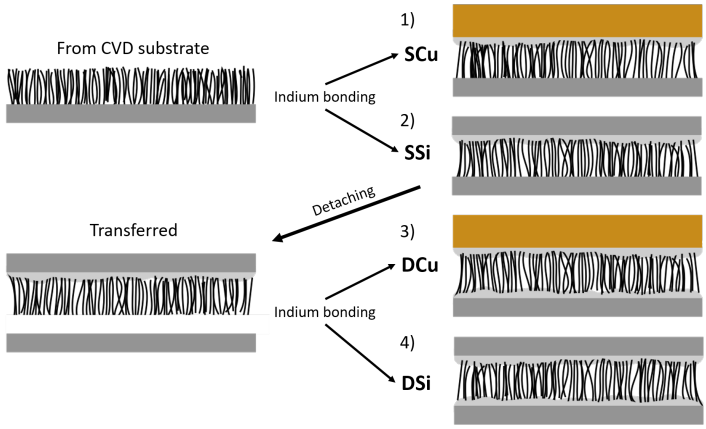

Fig. 4.9. Sample configurations for reliability testing of indium bonded CNT array TIM. The configurations are 1) single bonded Si-Cu (SCu), 2) single bonded Si-Si (SSi), double bonded Si-Cu (DCu) and 4) double bonded Si-Si (DSi).

The transfer process consisted of bonding the CNT array tips to opposing surface, shearing off the growth substrate and subsequently bonding the exposed CNT roots to another surface using the same bonding method. The four sample configurations were designated single bonded Si-Cu (SCu), single bonded Si-Si (SSi), double bonded Si-Cu (DCu) and double bonded Si-Si (DSi).

The thermal interface resistance of the different sample configurations before thermal cycling can be seen in figure 4.10 a). It is clear that the metal bonding method produces significantly higher thermal interface resistance, 29 Kmm^2/W for the SCu configuration compared to only 1.7 Kmm^2/W for the polymer bonded samples. This also means that the bonded interface side has higher thermal resistance than the root side, which in turn means that the overall thermal resistance of the double bonded samples is higher than the single bonded ones.

All sample configurations were subjected to 500 thermal cycles, with thermal interface resistance measurements at increasing intervals. Figure 4.10 b) shows the thermal interface resistance change over the 500 cycles for all sample configurations. Both Si-Si configurations, SSi and DSi, show essentially no change in thermal interface resistance over the full 500 cycles, while the SCu configuration exhibits a steady increase, from 29 to 43 Kmm^2/W.

This is consistent with a model where CTE mismatch induced stress is the main cause of CNT array TIM degradation. The increase is lower than for the polymer bonded TIMs, due to taller CNT arrays. Assuming that the increase in thermal resistance occurs primarily on the CNT root side, the absolute rather than

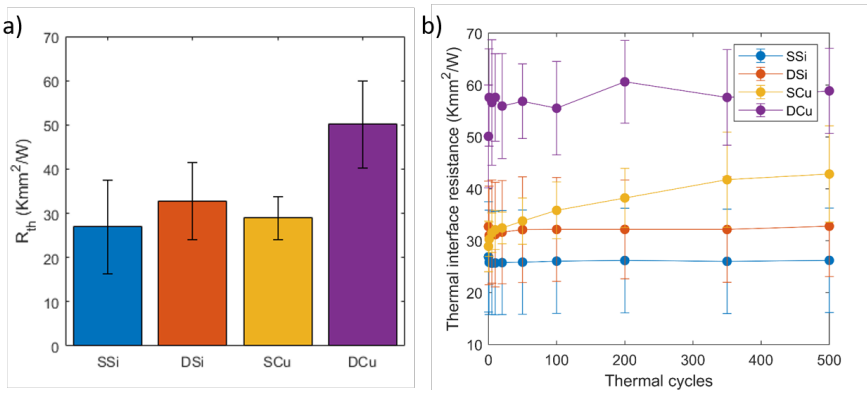

Fig. 4.10. a) Thermal interface resistance before thermal cycling for SSi, DSi, SCu and DCu sample configurations. b) Thermal interface resistance as a function of thermal cycles for the same samples. The error bars shows the standard deviation between samples.

proportional resistance increase is the relevant comparison. After 500 cycles, the 80 µm tall CNT array increased in resistance a third as much as the earlier 15 µm tall HKL bonded array, which is still considerable.

However, the DCu samples, aside from an increase in the first few cycles, show a relatively flat, thermal interface resistance. This is an indication that for this CNT array height, the CTE mismatch induced stress is enough to degrade the CNT root side, but not the bonded side. A reliable TIM may be possible at lower CNT array heights in double bonded configurations than in single bonded ones.

4.3.3 Catalyst Degradation

As in the case with polymer bonded CNT array TIM, we investigated the catalyst residues of pristine and aged samples using XPS. However, this time we did a more detailed analysis of the different peaks and their constituents. Figure 4.11 shows detailed XPS data for the peaks corresponding to the binding energy of the C1s and Fe2p electrons, and table 4.1 shows the quantitative composition of elements and bonds based on this data. Further details on the XPS analysis and peak deconvolution can be found in paper VIII.

The main finding is the same as we found previously, that the amount of iron bound in iron oxides, or rust, has increased. The hypothesis was that the oxidation would cause a weakening of the connection between the CNT roots and the silicon substrate. However, in this case we should be able to see a difference in thermal resistance change between the SSi and DSi samples, where we had eliminated the

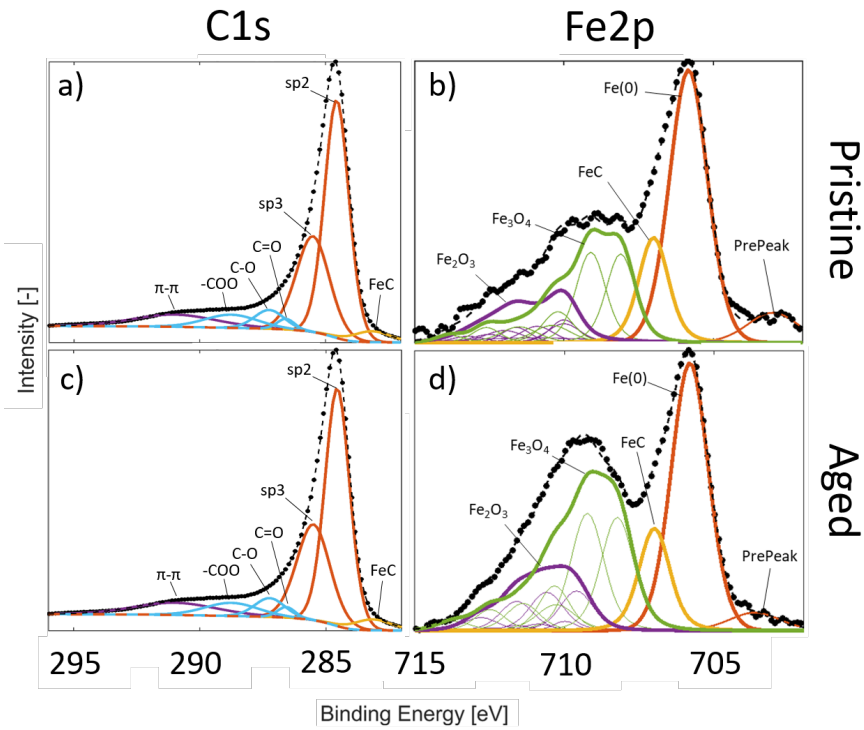

Fig. 4.11. XPS analysis of CNT array catalyst of pristine and aged samples. Data and deconvolution of peak contributions of the a),b) C1s, c), d) O1s and e), f) Fe2p peaks for pristine and aged samples respectively.

Bond type	**Presence (%)**	
	Pristine	Aged
C1s		
sp2	52.57	56.81
sp3	21.59	18.47
π-π	9.09	7.36
Carbide	2.71	3.21
C-O	5.16	4.69
C=O	5.48	6.09
-COO	3.41	3.32
Fe2p		
Fe(0)	38.18	32.35
Carbide	19.77	16.17
Fe_2O_3	26.24	30.68
Fe_3O_4	15.80	20.80

Table 4.1. XPS composition data of CNT array catalyst residues.

CTE mismatch. From table 4.1 we can see that the oxidation has happened, but the Si-Si interface configurations both showed no change during thermal cycling. We conclude oxidation of the catalyst does not appear to be a major factor in the total TIM reliability performance in either of our studies. Nonetheless, the same increase in thermal resistance as the one found in chapter 4.2 is within the margin of error for the metal bonded samples, and may still become an issue when using state of the art bonding methods combined with taller CNT arrays.

4.4 Conclusion

The most important parameter for the reliability of CNT array TIMs seems to be the array height. This should perhaps not come as a surprise, since TIMs in general exhibit the same behavior. Nonetheless, much of the research so far has been done using CNT array heights in the order of 10 µm, which will be unable to create reliable interfaces whenever there is CTE mismatch involved, and our studies conclusively show that taller CNT arrays will be required to solve this issue. Transfer and double bonding of the CNT arrays could potentially create stronger interfaces and allow for reliable interfaces despite shorter CNT arrays, although it is uncertain exactly to what extent.

The aim of these studies was to establish the limitations for CNT array TIM reliability, and to create a set of guidelines for how to construct a reliable TIM.

Based on the results from the studies in this chapter, we can create a set of guidelines consisting of the following three points:

- The height of the CNT array is an important parameter that needs to be taken into account when designing CNT array TIM aimed at interfaces with CTE mismatch.
- The root side of the CNT array is weaker than CNTs bonded to a surface. This means that the reliability performance for single bonded CNT array TIM will be independent of bonding method. Transfer and bonding of both CNT tips and roots can create a reliable TIM at lower CNT array heights.
- Aging of the catalyst causes a moderate increase in thermal boundary resistance at the CNT root side, which can become relevant if the bonding method is sufficiently good.

These points can act as guidelines for development of CNT array TIM, which will become increasingly relevant as CNT array TIM approaches commercial applications.

Chapter 5

Joule Self-heating Chemical Vapor Deposition of CNT arrays

In the previous chapter we were mostly concerned with the carbon nanotubes themselves, their properties and applications. In contrast, this chapter will be dedicated to the CVD itself, and how a modification of the normal process can enable new use cases and applications.

5.1 Chemical Vapor Deposition of CNT arrays

While the basic principle for the deposition of CNT arrays was described in chapter 4.1.1, there are possible variations in the process. The essential parts of any CVD process are catalyst, feeding gas and temperature. All three of these parameters can influence the resulting CNTs, but in this chapter we focus on the last parameter, the temperature..

As with any chemical reaction, temperature plays a large role in direction and rate of the reaction. In CVD processes, the reaction is limited by the decomposition of the feeding gas into atomic carbon. This process is usually temperature limited, and thus the resulting CNT array depends heavily on the process temperature [118]. Typical optimal temperature is around 700°C depending on catalyst structure and feeding gases. This is not ideal for integration of CNT arrays into electronics, as the highest processing temperature allowed within CMOS processes is around 500°C. Plasma enchanced CVD (PECVD) methods can enable CVD growth at lower temperature, but typically provides CNT arrays with vastly different morphology

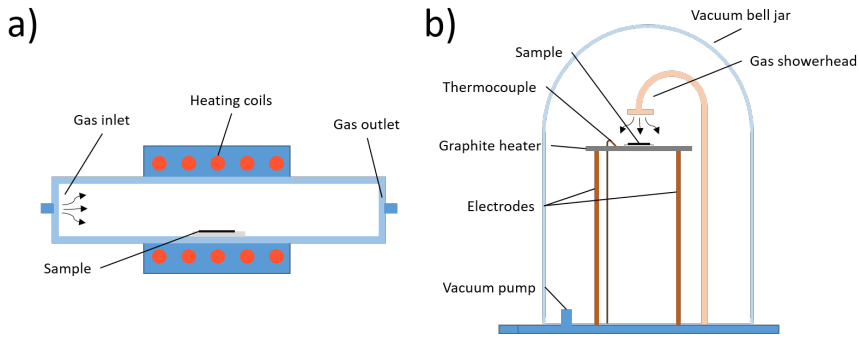

Fig. 5.1. a) Quartz tube hot-wall CVD system schematic. b) Cold-wall CVD system schematic.

compared to thermal CVD, creating CNT arrays with lower density and shorter but thicker CNTs. Creating a process that works at lower temperatures would be a big breakthrough, but has proven challenging, and today most solutions involve post-growth transfer processes like the one in chapter 4.

Aside from the question of which specific temperature the process should have, there can be large variation in how to practically induce the heating and ensure uniform temperature distribution over a large area. This is the main difference between different CVD setups, and also the question that the work in this chapter concerns.

5.1.1 Hot-wall Chemical Vapor Deposition

The hot-wall CVD system is the simplest and most common CVD system. A hot-wall system is essentially an oven with a variable gas feed. It is most commonly based on a quartz tube, heated from coils around the tube, with feeding gases flowing from one side. A schematic of such system can be seen in figure 5.1 a). Since the heating is done uniformly from all around, the temperature inside the chamber will be highly uniform. However, this process requires heating of the entire chamber, which consumes considerable power, and quartz tube furnaces are typically restricted to a heating rate of around 10°C/min, making high-temperature processes very time-consuming, considering normal CVD temperatures of around 700°C.

5.1.2 Cold-wall Chemical Vapor Deposition

In order to circumvent the drawbacks of hot-wall systems, cold-wall CVD aims at keeping the heat localized to only where necessary. Instead of heating the entire

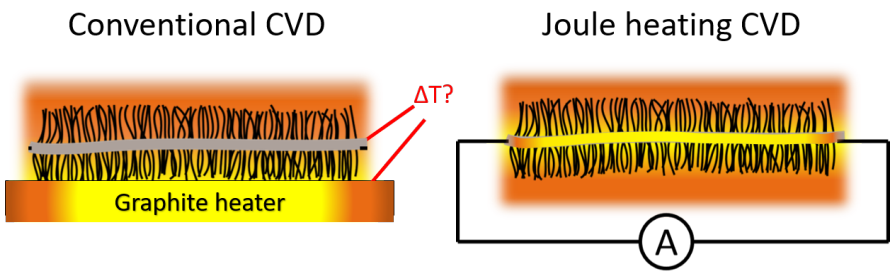

Fig. 5.2. The principle for Joule heating CVD in comparison with conventional cold-wall CVD methods.

chamber, the sample is placed on a small resistive heater. The setup is placed inside a vacuum chamber as shown in figure 5.1 b) and the process is conducted at lower pressures (< 0.1 mPa) in order to prevent diffusion of heat away from the heater. Cold-wall CVD systems enable a much faster and less energy intensive process, where the total processing time for a batch can be reduced from hours down to minutes. Cold-wall CVD systems enable rapid fabrication, but introduce a new set of problems, mainly related to the temperature. With localized heating the temperature may not be precisely the same at every point, and since the CVD process is very temperature dependent, this can cause significant variation in resulting CNT array depending on location on the heater. Even worse, the temperature at the reaction site (typically on the bottom of the CNT arrays) is not necessarily the same as on the heater.

5.1.3 Joule Self-heating Chemical Vapor Deposition

As seen in chapter 2.2.3, one CNT array TIM configuration consists of CNT arrays grown on both sides of a thin foil substrate [137, 148]. This type of structure is very difficult to reliably and uniformly produce in cold-wall CVD systems. This is due to distance from the heater to the CNT catalysis site varying as the CNT array on the bottom side grows, which in turn affects the termperature at the growth site, as illustrated in figure 5.2. In addition, the bottom side is hidden between substrate and heater, restricting the gas flow on that side. In total, these effects cause the grown CNT arrays to be short and uneven, with different properties in the top and bottom arrays.

We developed a new CVD method as a solution to the specific problem of achieving cold-wall CVD of double-sided CNT arrays: the Joule self-heating chemical vapor deposition method. This method utilizes the fact that most desirable foil substrates are metals or carbon based, and thus electrically conductive and can be

used as resistive heaters themselves. Instead of a separate graphite heater, we use the substrate itself as a heater by connecting it to electrodes and running a current through it.

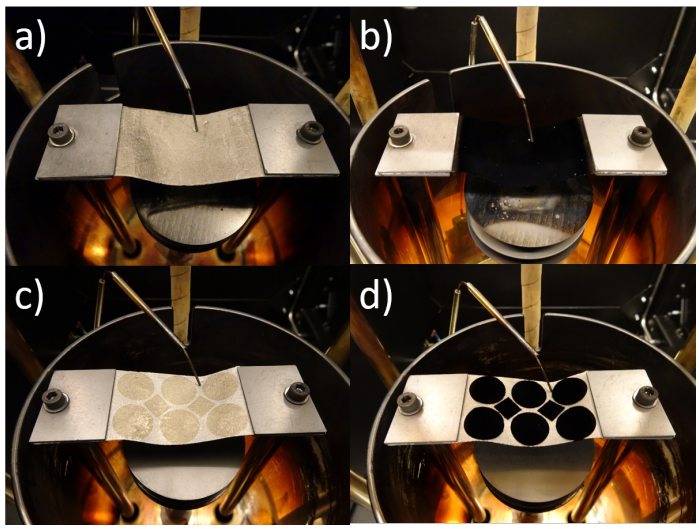

Fig. 5.3. The experimental setup for Joule heating CVD before (a) and after (b) growth using a graphene film as substrate. c) & d) Same setup with patterned catalyst, resulting in selective CNT array growth.

The sample processing is mostly similar to the CNT fabrication in chapter 4, and is independent of substrate material. The catalyst structure consists of 10 nm Al_2O_3 and 1 nm Fe which is deposited by electron beam evaporation on both sides of the film. We used a shadow mask of steel foil for rough patterning of the catalyst. The experimental setup can be seen in figure 5.3 for both unpatterned and patterned samples, using the same Aixtron system as before, but clamping the film instead of a heater between the electrodes. The temperature and gas flow recipe is then in principle same as in conventional growth. However, a thin foil is much easier to heat up compared to a graphite heater. This is good since it means that the process has a lower power consumption of around a quarter of conventional cold-wall CVD, which in itself requires orders of magnitude less power than hot-wall systems. This in turn is something which may become very important as the production of CNTs scales up towards commercial volumes. It does however mean that the automatic software regulation of the temperature, which is optimized for a graphite heater with a specific thickness, is unable to provide a stable heating, requiring manual adjustments on the fly instead. While not an inherent problem

with the Joule heating CVD method, it does mean that the process within this thesis is somewhat less stable than the normal CVD process. However, hypothetical equipment dedicated specifically for Joule heating CVD would not be more difficult to optimize than conventional CVD systems.

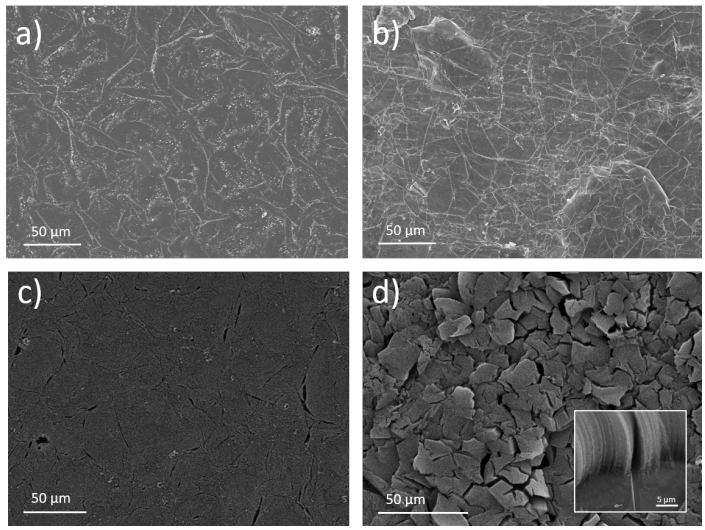

Fig. 5.4. SEM images of the substrate materials used in this thesis. a) Pyrolytic graphite sheet. b) Graphene film. c), d) Top view of resulting CNT array for PGS (c) and GF (d). The inset in d) shows the bottom of the array, where a wrinkle in the topmost graphene layer causes a separation between CNT bundles. Partially adapted from paper IV and VII.

In principle, any electrically conducting foil should be compatible with this method. However, within this thesis we have limited ourselves to two types of carbon based films, for the simple reason of trying to match the resistivity of the foil to the graphite heater normally there in order to minimize additional modifications to the system. The carbon based films were graphene films (GF) in paper IV and pyrolytic graphite sheets (PGS) in paper VI, both with a thickness of around 25 µm. These substrate materials can be seen in figure 5.4 a) and b) respectively. The graphene film was made by us by chemical methods based on the alignment and reduction of graphene oxide flakes [196], while the PGS is a commercially available product (Panasonic). Both consist of a highly ordered graphitic structure with very high in-plane thermal conductivity. As seen in the SEM image, they have a similar appearance with wrinkles in the top graphene layer visible, although the PGS has a somewhat lower degree of these wrinkles. This difference in wrinkling also creates a

difference in the resulting CNT array. Figure 5.4 c) d) show the top of the CNT array grown on PGS and GF respectively. On PGS, a uniform CNT array is formed with only a few cracks, while on GF the array is split up into bundles with clearly defined boundaries between them. These boundary arise from the wrinkles in the GF, as seen in the inset of figure 5.4 d).

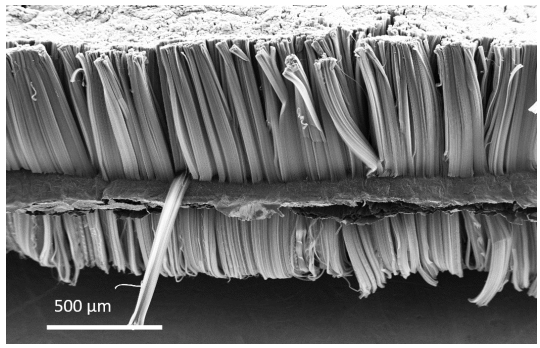

Fig. 5.5. Cross-sectional SEM view of a double-sided CNT array grown on GF with Joule heating CVD.

Aside from the bundling of CNTs from the wrinkles on the substrate, the CNT array is comparable to CNT arrays on silicon using conventional CVD: Figure 5.5 shows the as-grown double sided CNT array on GF (GF/CNT). The height of the CNT array is > 500 µm after 9 minutes, with a comparable degree of alignment to standard CNT growth.

5.2 Thermal Interface Material Application

As previously mentioned, the material fabricated using Joule heating CVD is useful for one configuration of CNT array TIM. One of the main benefit of this configuration is the possibility of applying it directly in an application like a thermal pad. Instead of bonding procedures, or reflow, simply place it between the interfacing surfaces and apply pressure.

To verify the usefulness of the GF/CNT in a TIM application, we first measured the CNT array thermal conductivity using the PPR method as described in chapter 4, finding an effective array thermal conductivity around 30 W/mK, similar to conventional arrays [110]. We then measured the thermal interface resistance in a TIM application using an ASTM D5470 standard compliant 1-D steady state measurement setup.

The ASTM D5470 measurement setup is illustrated in figure 5.6 a). It consists of two 4.5 cm long, 1.5 cm diameter aluminum rods with thermocouple temperature

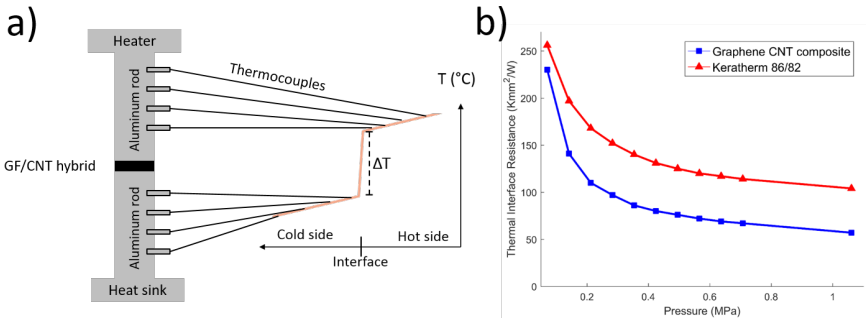

Fig. 5.6. a) The ASTM D5470 measurement setup and function. b) Thermal interface resistance of the graphene CNT hybrid compared to a commercial thermal pad as a function of applied pressure, measured by the ASTM D5470 setup. From paper IV.

sensors evenly spaced along their length. The rods are oriented on top of each other, with the TIM to measured sandwiched in between them. The top of the stack is connected to a heater, which is thermally isolated from the frame in order for all of the generated heat power to be dissipated through the column. The bottom of the lower rod is cooled by circulated water, creating a temperature gradient along the rods. This temperature gradient is similar to the one shown back in chapter 2 to explain the principle of a TIM. The thermocouples allows us to measure the linear slope of the gradient over the aluminum parts, from which we can calculate the temperature drop over the interface. From this temperature drop, together with the heat flux given by the heater power, we have everything we need to calculate the thermal interface resistance of the TIM according to equation (2.1),

The rod stack is then connected to a a mechanical tester which can apply pressure with very high accuracy. This allows us to measure the thermal interface resistance as a function of applied pressure. The results from the measurement is shown in figure 5.6 b), with a commercial thermal pad (Keratherm 86/82) as a reference. The thermal interface resistance is 60 Kmm^2/W at 1 MPa, compared to 105 Kmm^2/W for the reference material. While this is significantly higher than current state of the art CNT array TIM, compared to thermal pads it compares favorably (see table 2.1). Worth noting is that the CNT arrays in this TIM are 2x 500 µm, as compared to around 10 µm for the best-performing CNT array TIM and the 80 µm required in the reliability study in chapter 4. Plenty of further optimization is possible in terms of CNT array quality, thickness, substrate material and interfacial bonding, but this TIM acts as a proof of concept of Joule heating CVD for TIM fabrication.

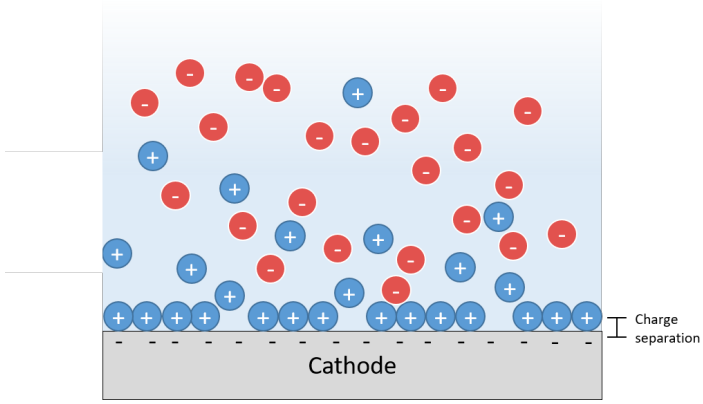

Fig. 5.7. Schematic of the working principle of a electrochemical double layer.

5.3 Supercapacitor Electrode Application

While the Joule heating CVD method was developed for thermal applications, it is not the only place where this type of structure can be useful. In paper VI, we utilize the Joule heating CVD method to create a double-sided porous electrode material, which we then demonstrate in a bipolar supercapacitor application.

5.3.1 Supercapacitors

Within energy storage, there is typically a trade-off between energy density and power density. The energy density decides how much energy you can store within your system, while the power density decides the rate of charge and discharge. In terms of energy density, fuel cells and batteries have high energy density, but low power density, useful for energy storage as long as long as the power requirements are limited. Batteries also degrade during charge/discharge cycling, making them unsuitable in application with rapid cycling or long lifetime requirements. Capacitors on the other hand, have rapid charge/discharge and can withstand nearly limitless charge cycling at the cost of total energy stored. Supercapacitors are a special type of capacitors which operates in the region between batteries and traditional capacitors, with enough energy density for useful energy storage but still rapid charging and long cycling lifetime.

The supercapacitors within this work are electrochemical double layer (EDL) capacitors, or just electrochemical capacitors (ECs). ECs consist of electrodes in contact with a liquid electrolyte, as seen schematically in figure 5.7. At the interface between electrode and electrolyte, an applied voltage repels equal charges and attracts opposite charges, forming a layer of opposite charges on the electrode

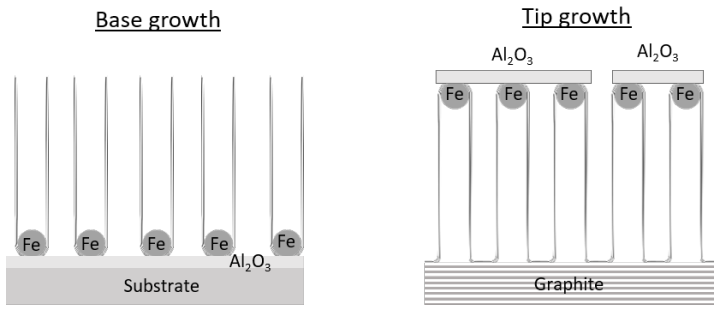

Fig. 5.8. Comparison of base growth and tip growth modes with an Fe/Al_2O_3 catalyst structure. From paper VI

surface. This is reminiscent of the simple parallel plate capacitor, with a capacitance C of:

$$C = \frac{\epsilon A}{d} \tag{5.1}$$

where ϵ is the permittivity of the material between the plates, A is the area of the plates and d is the separation between them. However, in the case of an EDL, the separation is less than 1 nm, instead of on the order of µm [197]. This allows for a much higher capacitance for an equivalent area. The other parameter from equation (5.1) which can be improved is the surface area. Electrochemical capacitors use porous electrode materials with as high specific surface area as possible, and this is where CNTs come in. VACNT arrays have been demonstrated to great effect as supercapacitor electrodes [11, 198–204] due the the 1-D structure of CNT giving a very high specific surface area.

Bipolar supercapacitors

In contrast to normal capacitors, ECs have a maximum operating voltage which depends on the electrolyte used. For many applications, this voltage is too low, often at around 1 V [205]. One way of increasing the operating voltage of capacitors is to connect them in series, i.e. stack more layers. Here, the double-sided CNT array obtained by Joule heating CVD can be used as a bipolar electrode, where the CNT array on one side acts as the positive electrode for one cell and the array on the other side acts as the negative electrode for the next. This way, an arbitrary number of layers can be stacked, increasing the maximum voltage by the electrolyte operating voltage for each layer.

5.3.2 Odako-growth of CNTs

Depending on catalyst structure, there are two different growth modes for CNT CVD: base growth and tip growth [109]. In base growth, the catalyst particles stay on the bottom of the CNT array, feeding the CNTs upwards, while in tip growth, the catalyst particle stays on top of the array instead, as shown in figure 5.8. In our normal CVD process, iron catalyst is immobilized by an underlying alumina layer, and the catalyst remains at the base of the array. This creates a barrier between substrate and CNT array for both the thermal and electrical connections. In thermal applications this is a modest problem [206] which was ignored in paper IV, but it is more problematic for an EC electrode as alumina is an insulator and can prevent good electrical connection.

A slight modification to the catalyst structure, where the iron layer is instead deposited first with the Al_2O_3 layer on top, changes the growth mode from base to tip. Instead of immobilizing the iron catalyst on the bottom, the alumina layer now floats on top of the CNT array, and brings the catalyst particles with it. The alumina breaks up into sheets like kites on the top of the array, allowing the feedstock gas to penetrate to the iron below, and is therefore called "odako" growth, from the Japanese word for giant kite [207]. This structure, with odako growth on PGS substrate, has previously been shown to work well for supercapacitor electrodes [11].

In paper VI, we adapted the Joule heating CVD method in order to make bipolar EC electrodes from double sided CNT arrays on PGS. Instead of 10 nm Al_2O_3/1 nm Fe, instead we deposited 2 nm Fe/3 nm Al_2O_3. A thicker iron layer is required as in this case we do not have a diffusion barrier between the iron and the substrate, and a thinner Al_2O_3 is to allow it to crack up into these kites. The CVD process was subsequently essentially the same as for the GF/CNT structure in paper IV, with some minor optimization for the new process.

The resulting material can be seen in figure 5.9 a-c). The odako structure means that the CNTs become separated into discrete bundles, which then grown at slightly different speed and alignment, which cause the overall structure to be less uniform, which is a drawback with this method. The alumina remains can clearly be seen on top of each bundle, especially highlighted in the single bundle shown in figure 5.9 c). Since the catalyst now remains on the top it is possible to remove after the CVD process by an oxygen plasma treatment for 30 s at 100 W. Corresponding images of the array after plasma treatment is shown in figure 5.9 d-i). The array height was around 30 µm, determined by a trade-off between longer CNTs but less uniformity for longer CVD growth times.

5.3.3 Bipolar capacitor performance

The fabricated electrode material was then put to use as electrode in a EC. As a proof of principle study, we made three versions of EC as shown in figure 5.10, one single EC, denoted as 1x, one two-layer stack with a bipolar EC, denoted as

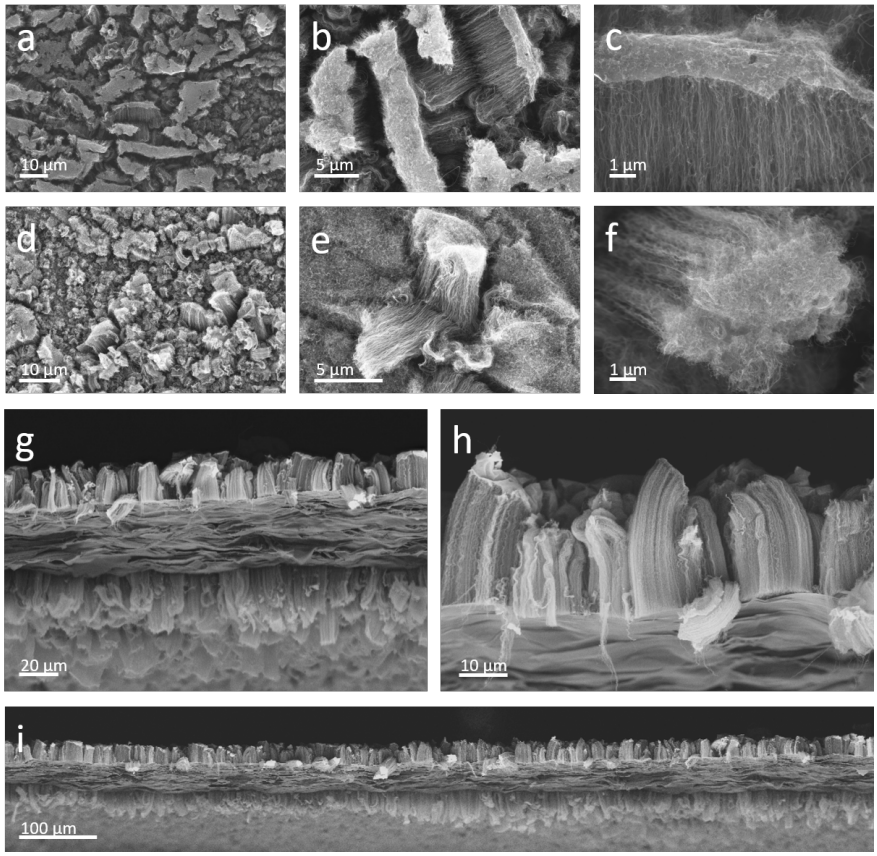

Fig. 5.9. SEM images of the double-sided CNT array on PGS electrode material, fabricated using odako growth Joule heating CVD. a-c) Top view of the as-grown CNT arrays to increasing magnification, with alumina flakes visible on top of the CNT bundles. d-f) Top view after plasma treatment, removing the alumina on top. g-i) Sideview of the electrode material. g) Section of the material showing both CNT arrays. h) Magnification of one of the sides. h) Overview of a large section of the material, showing the large scale uniformity. From paper VI

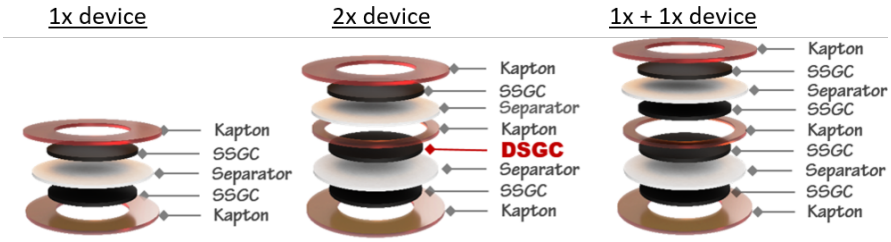

Fig. 5.10. EC device design. SSGC is Single-Sided Graphite/CNT and DSGC is Double-Sided Graphite/CNT. From paper VI

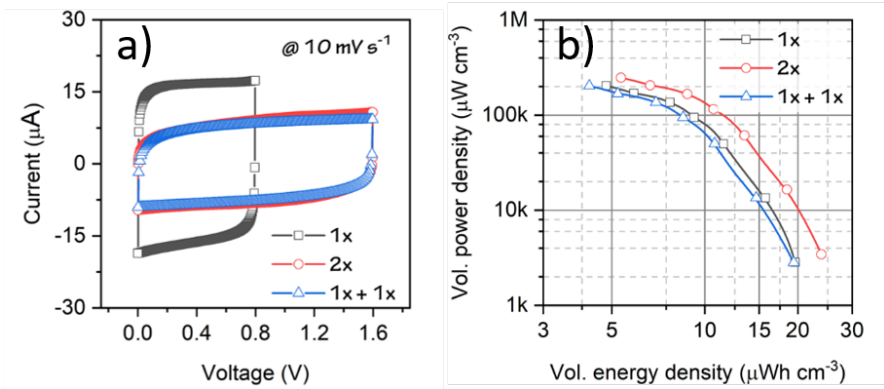

Fig. 5.11. Performance of the fabricated ECs. a) Cyclic voltammogram and b) Ragone plot. From paper VI

2x, and one version which is two single ECs connected in series, denoted as 1x + 1x. The end electrodes (SSGC in the figure) consisted on single-sided CNT arrays on graphite, fabricated using the same method as the double-sided version, but with catalyst on only one side. The basic structure consists of two CNT array electrodes with Polyvinyl Alcohol (PVA)/H_3PO_4 gel electrolyte and a separator inbetween. The separator prevents short circuiting of the electrodes while allowing the electrolyte to pass through. Kapton tape was used to seal the structure.

Figure 5.11 shows a few of the electrochemical measurements of the fabricated devices. Figure 5.11 a) shows a cyclic voltammogram (CV) of all devices. As expected, the 2x and 1x + 1x devices reach twice the voltage of the 1x device. In principle, the 2x and 1x + 1x devices should have identical properties, which also seems to be nearly the case, with almost complete overlap of the curves. Additional

electrochemical measurements, available in paper VI, further confirms that the identical performance. However, since the bipolar design is more compact, the 2x device achieves a 22% improvement in volumetric energy density compared to the 1x and 1x + 1x devices as seen in figure 5.11 b). This improvement could be expected to improve further with the stacking of additional layers.

Table 5.1. Volumetric performance comparison of CNT based ECs. From paper VI

Material (device)	Electrolyte	Voltage (V)	Vol. capacitance (F cm^{-3})	Vol. energy (µWh cm^{-3})	Vol. power (µW cm^{-3})	Ref.
DSGC (2×)	PVA/H_3PO_4	1.6	0.068	23.85	3454.35	This work
SSGC (1×)	PVA/H_3PO_4	0.8	0.22	19.61	2832.14	
Paper/CNTs	PVA/H_2SO_4	1.0	0.004	0.52	186.57	[208]
PET/CNTs	PVA/H_3PO_4	1.0	0.014	1.81	211.11	[209]
Al/CNTs	Na_2SO_4	0.8	0.089	7.9	1333.33	[210]
Graphene/CNTs	H_2SO_4	0.8	0.022	6.97	313.44	[211]

A comparison of volumetric performance between our devices and previously published reports, seen in table 5.1, shown how the combination of CNT arrays on graphite, using Joule heating CVD with odako growth, manages to create truly state of the art ECs.

5.4 Conclusion

The Joule heating CVD method was originally developed specifically to solve the challenge of cold-wall CVD synthesis of double sided CNT arrays. As is hopefully by now demonstrated, it does solve the problem, enabling CNT arrays with comparable quality to conventional growth on silicon substrates. In addition to this, it has other benefits such as lower power consumption and larger growth area. Indeed, even if CNTs are only desired on one side of the foil the Joule heating method is in many cases more suitable, for instance the single-sided electrodes in the EC demonstration, or the CNT arrays fabricated in the next chapter. While the setup used within this thesis is a modification of a conventional cold-wall CVD setup, a dedicated machine optimized for Joule heating CVD would easily enable even larger scale and allow for automatic control of the process further improving reproducibility.

Chapter 6

Heat Treatment of Carbon Nanotube Arrays

The method that the CNTs within this thesis is synthesized through, CVD, is not the only possible one. Indeed, the CNT produced by CVD are typically of significantly lower quality than those produced by other methods such as arc discharge or laser ablation [212–214]. However, CVD is currently the only method that can directly synthesize aligned arrays of CNTs, which is a key point for our purposes. In practice we are stuck with CNTs of far lower quality that theoretically possible. In this chapter, we explore whether we could potentially do something about this issue. Through heat treatment at extreme temperatures, CVD grown CNTs can change their structure into a more pure form. At the same time, this heat treatment could potentially solve the issue of catalyst residues on the bottom of the CNT arrays that we discussed in chapter 5.

6.0.1 Carbon Nanotube Crystallinity

When discussing CNT quality, there are two related concepts that are important: defects and crystallinity.

- **Defects** are imperfections in the crystal structure of the CNT. These can be on the atomic scale, such as vacancies (i.e. missing atoms), intermediary scale such as grain boundaries or larger structural defects such as kinks or buckling of the CNT structure. A CNT with a lot of defects is more disordered and less crystalline than a defect free CNT.
- **Crystallinity** is the inverse concept, a measure of how close the CNT is to the perfect crystal structure. Higher crystallinity means less defects and vice versa. Crystallinity is measured by the crystallite size, which is a measure

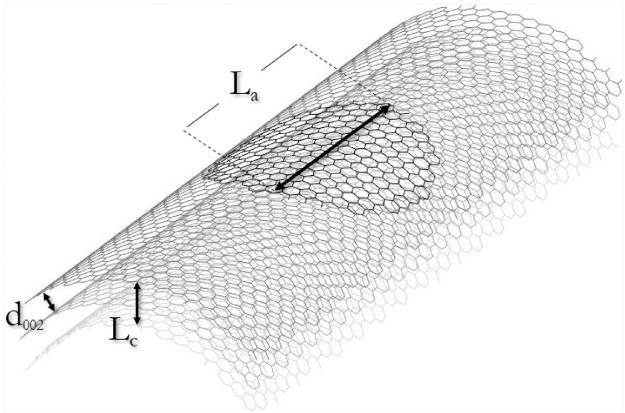

Fig. 6.1. Illustration of the in-plane and through-plane crystallites and interlayer spacing. From reference [215]

of how large regions with crystalline structure are. Since CNTs consist of graphene layers, it is mainly the in-plane crystallite size L_a that is important, as illustrated in figure 6.1.

Since these two measures are heavily correlated, they will be used somewhat interchangeably, with the crystallite size being a quntifiable measurement of the overall quality.

Chemical vapor deposition is a relatively low energy synthesis route for CNTs in comparison to the alternatives, and as a consequence the CVD CNTs are of relatively low quality. This has a consequence for the CNT properties, where both the electrical, thermal and mechanical properties suffer significantly [214–219]. By introducing enough energy for the CNTs to rearrange their crystal structure, the crystallinity can be improved after the CVD growth. This can be done by microwaves [220], but more commonly by heating it up to very high temperatures ($> 2500^{\circ}$C). This has been shown to anneal the CNTs and significantly improve the crystallinity and associated properties [221–226].

6.0.2 Carbon Nanotube Catalyst Residue

A seemingly unrelated problem is the one discussed in the previous chapter, where catalyst residues form a barrier between the CNT array and the underlying substrate. To circumvent this problem we used an inverted catalyst to form a seamless structure but, as mentioned, this has severe drawbacks in terms of CNT array height and uniformity. Ideally we would like to grow CNTs normally and remove the catalyst afterwards.

Here heat treatment again comes up as a possible solution. The boiling temperature of iron and alumina (2862°C and 2977°C respectively) are both lower than the sublimation temperature of carbon (3642°C), so there should be a temperature where the catalyst evaporates while the carbon structure remains. Heat treatment could then potentially improve CNT quality and eliminate catalyst residues at the same time.

6.0.3 Heat treatment of CNT arrays

The problem here, is that most substrate materials cannot withstand these temperatures. For this reason, so far studies on the effect of heat treatment of CNTs have used powder samples or very small freestanding arrays. However, as seen in the previous chapter, the Joule heating CVD method allows for rapid fabrication of CNT arrays on graphite substrates, which should be able to tolerate the heat. Also, temperatures high enough to alter the atomic structure of CNT will do the same for graphite, and possibly bond together CNTs and graphite with the same covalent bonding that odako growth can achieve. In paper VII we did exactly this experiment in order to study the effect of annealing on carbon nanotube arrays.

We fabricated the CNT arrays on PGS substrate using the Joule heating CVD method as described in chapter 5. Then, the fabricated samples were placed in a graphite crucible and put into a high temperature furnace. First, the temperature was increased to 1000°C at a heating rate of 5°C/min under a nitrogen flow of 100 sccm. Subsequently, the temperature was increased to 3000°C under an atmosphere of argon (3000 sccm) at a heating rate of 5°C/min, and the samples were kept at this temperature for 1 h.

6.1 Characterization of Annealed CNT Arrays

Our hypothesis was that the heat treatment would simultaneously increase the crystallinity and evaporate the catalyst. In order to verify whether this actually happened, we characterized the annealed CNT arrays in terms of crystallinity and defects using Raman Spectroscopy and Transmission Electron Microscope (TEM). We also did an elemental composition analysis using X-ray photoelectron spectroscopy (XPS) in order to verify that the catalyst has evaporated.

6.1.1 Carbon Nanotube Crystallinity

As discussed previously, a good quantitative measure of the quality of CNTs is the in-plane crystallite size L_a. In order to determine L_a for our samples, we used two different techniques: Raman spectroscopy and Transmission electron microscope (TEM) diffraction.

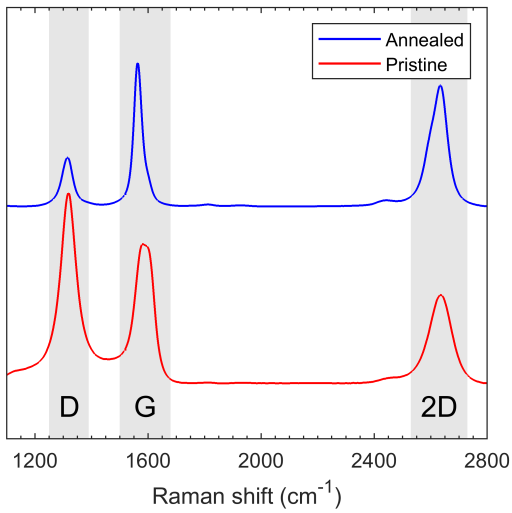

Fig. 6.2. Raman spectrum of annealed (blue) and pristine (red) CNTs. From paper VII.

Raman Spectroscopy

When light is shined onto a material, photons can interact with the material to temporarily excite electrons to a higher energy level. The electron relaxes back to the ground state by emitting a photon, typically of the same energy. Most of the time the emitted photon has the same energy as the absorbed, but a small fraction of excited electrons manage to interact with another excitation, typically a phonon i.e. a vibration within the material, before relaxing back to the ground state. During this interaction, energy is absorbed or emitted, and the emitted photon during relaxation will as a consequence have a shifted energy compared to the absorbed photon. This process is called Raman scattering. By measuring the spectrum of scattered light from a single wavelength excitation laser information about the vibrational modes of the material can be extracted, and can be used as a fingerprint for the material [227].

We used a Raman microscope (Horiba Xplora) with an excitation wavelength of 638 nm to investigate the annealed CNTs, with as-grown pristine CNTs as reference. The Resulting Raman spectra are shown in figure 6.2. There are three main features of interest in graphitic materials: the D band, G band and 2D band. The D band, at around 1320 cm^{-1}, is related to the disorder within the structure, while the G band, at around 1580 cm^{-1}, corresponds to an in-plane stretching mode in the crystal

lattice [228]. The 2D band, at around 2650 cm^{-1}, is the overtone of the D-band, but is somewhat counter-intuitively prominent even in a perfect lattice due to being a two-phonon scattering event. Further details on the Raman spectrum of graphitic materials can be found in reference [227]. The differences between the pristine and annealed CNTs are immediately obvious. The ratio between the D-peak and G-peak intensities (I_D/I_G) has decreased from 1.367 to 0.342, and the 2D-peak has also increased in comparison with the G-peak, although not quite to the same extent. Both of these changes are indications of a significant reduction of disorder within the material [222, 228, 229]. We can also see that the G-peak has narrowed and changed shape due to the reduction of another disorder related component within the G-band. This narrowing can be used to obtain a quantitative measure of L_a for the CNTs, by using the following empirical law [230]:

$$\Gamma_G = (68 \pm 4) - (5.2 \pm 0.5)L_a \tag{6.1}$$

where Γ_G is the half width at half maximum (HWHM) of the G-band peak. Using this equation we find that the average crystallite size has decreased from 9.8 ± 1.9 nm to 5.6 ± 1.4 nm.

Transmission Electron Microscopy

We can also look at the CNTs directly. A TEM is similarly to scanning electron microscopes (SEM) based on the principle that the wavelength of electrons is shorter than that of visible photons. The key difference between SEM and TEM is that, rather than scanning over the surface of the sample, the electrons pass through the sample onto a detector on the other side. This means you get 2D projection of the sample, and are limited to very thin samples, but you can use much higher accelerating voltage (typically < 10 keV for SEM vs. > 100 keV for TEM) and correspondingly better resolution. Using TEM we can image individual CNTs and directly see the sidewalls and their ordering.

Since what we see in TEM is a 2D projection, what we actually see is when rows of atoms line up in the same spot, which in the case of CNTs is the sidewalls. A perfect CNT structure will show as an even straight line of each wall on each side of the CNT, as shown in figure 6.3 a). Figure 6.3 b) and c) show actual TEM images of a pristine and an annealed CNT. The structural difference is apparent from the structure of the CNT walls. Before heat treatment, the walls of the CNTs are semi-aligned, wavy and disordered, while afterwards the walls appear close to the ideal CNT structure in figure 6.3 a). This is a good qualitative indication that the heat treatment has the desired effect.

A quantitative measurement of the crystallite size of individual CNT can be determined by TEM diffraction [215]. In this mode, instead of looking at the transmitted electrons, we instead look at how the electrons that has interacted with the CNT diffract. In this pattern there will be spots whose width correlate with the

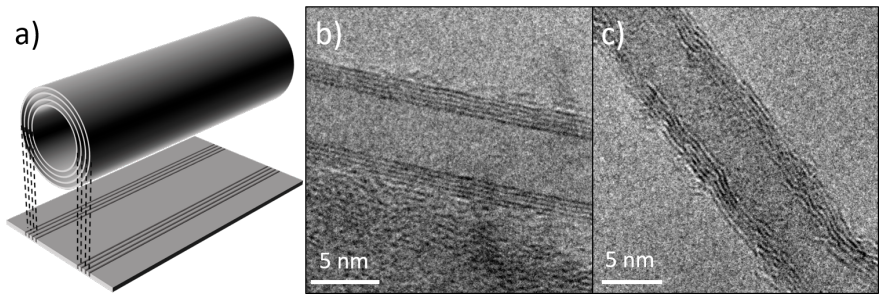

Fig. 6.3. a) Schematic for TEM imaging of an ideal CNT. Contrast in the TEM image (on the bottom) is found where the CNT walls are parallel to the incident electron beam. TEM images of pristine (b) and annealed (c) CNTs. From paper VII

in-plane crystallite L_a along the CNT axis. Further details on this method can be found in reference [215].

Figure 6.4 shows an example of such a spot in the diffraction pattern and the data and curve fitting of a scan along the marked line in the inset. By taking scans of multiple CNT we can obtain a measure of the average crystallite size for both pristine and annealed CNTs. For the pristine CNTs, this measurement yielded an average of $L_a = 5.4 \pm 2.1$ nm, and for the annealed an average of $L_a = 8.3 \pm 2.4$ nm. This is in agreement with the values obtained by Raman measurement with overlapping margin of error, which allows us to be confident in that we have accurate estimations of the crystallinity.

This increase in crystallinity will in turn affect the mechanical, electrical and thermal properties of the CNTs. Flygare et al. [215] determined the relationship between crystallite size and Young's modulus, which correlates well with desirable mechanical properties. Applying the relationship to our values, we get Young's modulus values of 78 ± 52 GPa and 175 ± 102 GPa for pristine and annealed CNTs respectively. While still lower than ideal CNTs, which can have a Young's modulus of around 1 TPa, it is still a significant improvement from as-grown tubes.

In addition to the atomic structure, the CNTs also undergo obvious changes on a larger scale. Figure 6.5 shows overview images of the CNTs at a lower magnification. Here we can see that the structure of the CNTs has changed from mainly wavy curves into straight jointed segments. This is also typical of higher quality CNTs.

6.1.2 Carbon Nanotube Bonding

In addition to the structural changes of individual CNTs, we also found that the interaction between adjacent CNTs changes after heat treatment. After annealing,

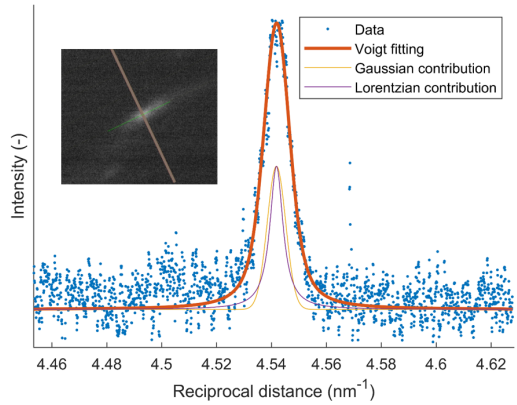

Fig. 6.4. Example of TEM diffraction data and curve fitting. From a signle CNT. The inset shows a diffraction spot and the graph shows the intensity variation along the marked line in the inset. From paper VII

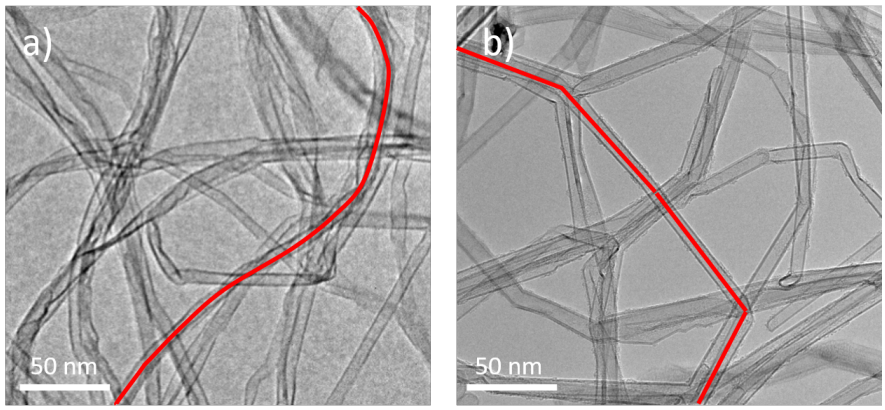

Fig. 6.5. Overview TEM images of a) pristine and b) annealed CNTs. A single CNT is marked in red in each case, highlighting the different between the continuous curving in a) and the straight jointed segments in b). From paper VII

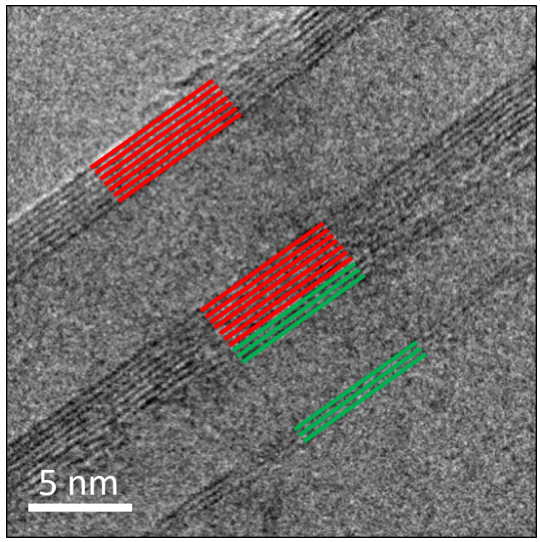

Fig. 6.6. TEM image of two bonded CNTs, with the CNT walls of the two tubes marked in red and green respectively. From paper VII

CNTs tend to align and bond together for long stretches. This can faintly be seen in figure 6.5 b), where a large fraction of the CNTs appear side by side for significant lengths, to a higher degree than in figure 6.5 a).

Figure 6.6 shows a magnification on two of these bonded CNTs. The red and green lines mark the walls of the two CNTs. As we can see, the distance between the outermost red and green walls appear to be the same as between two walls within the same tube, approximately 3.5 Å [231]. The similar bond distance indicates a similar mechanism as well.

van der Waals bonding

Within graphite, graphene layers are bonded together by van der Waals (vdW) forces [232]. In CNTs, the curvature of the CNTs prevents perfect graphite interlayer structure, and is rather more like turbostratic graphite where the layers are still bonded by vdW forces, but not neccessarily aligned in a crystal structure [233]. A similar vdW bonding between the outer walls of adjacent CNTs seems likely.

To verify that this is what happens, we calculated the vdW binding energy of the CNTs based on the works by Tao et al. [234], who used the consistent exchange version of the van der Waals density functional (vdW-DF-cx) method for nonlocal correlation density functional theory (DFT) [235–237] to calculate the vdW binding

energy of various carbon nanostructures, CNTs among them.

Our calculations, available in paper VII, show that CNTs tend to bond to each other, and when bonded at some degree will tend to further align themselves and grow the bonded regions. This fits well with what we have seen except for one important consideration: why does this not happen until heat treatment? In principle, according to the calculations, this should happen regardless of temperature.

An explanation for the apparent contradiction could be functional groups on the CNT walls, preventing close enough contact for vdW bonding. As previously mentioned, CVD grown CNts have a large amount of defects, which tends to react with atmospheric oxygen to form groups on the walls. During annealing, both these functional groups and the defect sites themselves will largely be eliminated, enabling close contact and bonding.

CNT array densification

The inter-CNT bonding is not just an interesting observation, it also has significant implications for the overall CNT array structure. When looking at the array with a lower magnification in figure 6.7 a) and b), we can see that the structure of the CNT array has changed dramatically from normal as-grown CNT arrays (such as the one back in figure 5.4 c)). Instead of a uniform array, it has broken up into discrete regions, with the CNT tips densified into much smaller areas.

The reason why this happens is illustrated in figure 6.7 c). When individual CNTs randomly come into contact they bond to each other in the absence of defects or functional groups. These bonded regions, marked in red, then grow, pulling adjacent CNTs closer together. The array splits along lines with relatively few initial contacting CNTs into discrete bundles which then further densify.

This densification effect allows us to directly see when and to what extent the CNTs bond to each other. With TEM we can see that the inter-CNT bonding happens, but to what extent is much harder and time-consuming to find out. However, by looking at the densification degree instead we can indirectly get a measure of the extent of CNT bonding.

We used this to look at the effects of annealing at various temperatures. Figure 6.8 shows CNT arrays after annealing at 1000°C, 1200°C and 3000°C. Here we can see that the array annealed at 1000°C looks essentially pristine. Some minor cracks are visible, but no overall densification can be ascertained. After 1200°C however, the CNT array has clearly started to break up, although not to the same extent as after annealing at 3000°C. This shows that the onset of densification starts between 1000°C and 1200°C.

The densification onset temperature fits well with the hypothesis that functional groups normally prevents vdW bonding of CNTs. While many functional groups decompose at lower temperatures than 1000°C, the most stable groups such as carbonyl or quinone groups decompose somewhere between 1000°C and 1200°C [238, 239], which fits well with the onset of densification.

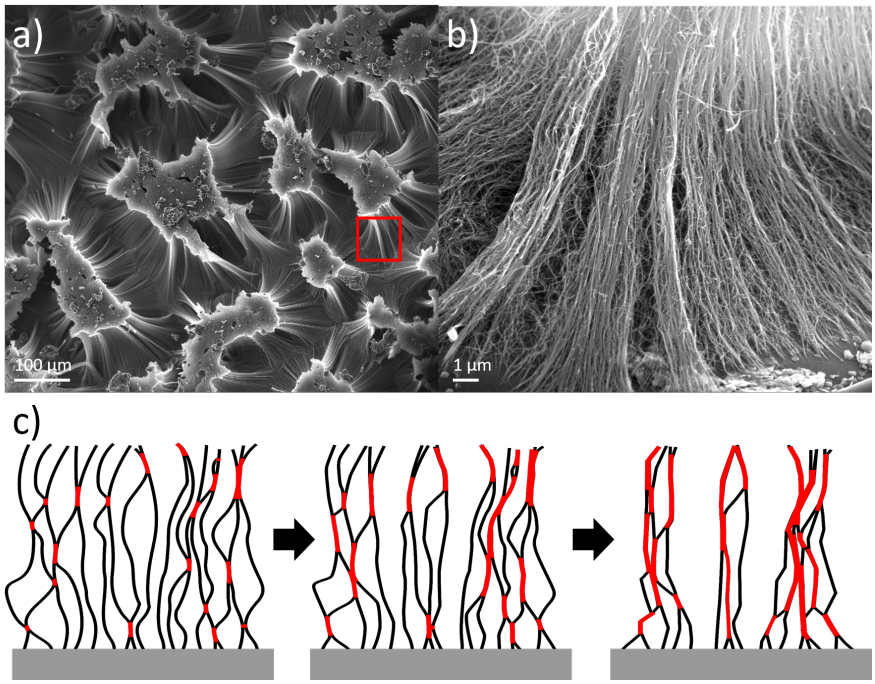

Fig. 6.7. a,b) SEM image of annealed CNT arrays. a) Overview of the structure from the top. b) Tilted view of the region marked in red in a). c) Illustration of the densification process due to individual CNTs bonding and aligning. Bonded regions are marked in red. From paper VII

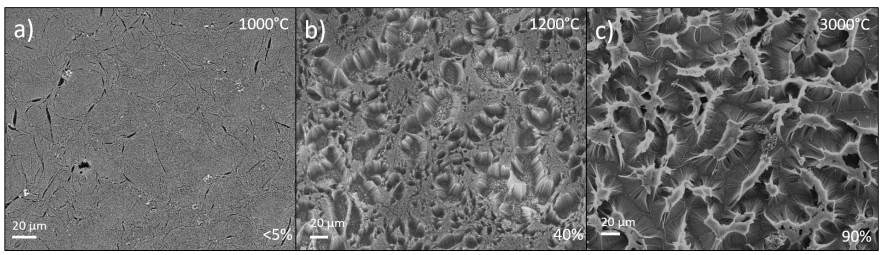

Fig. 6.8. SEM image of CNT arrays annealed at a) 1000°C, b) 1200°C and c) 3000°C. From paper VII

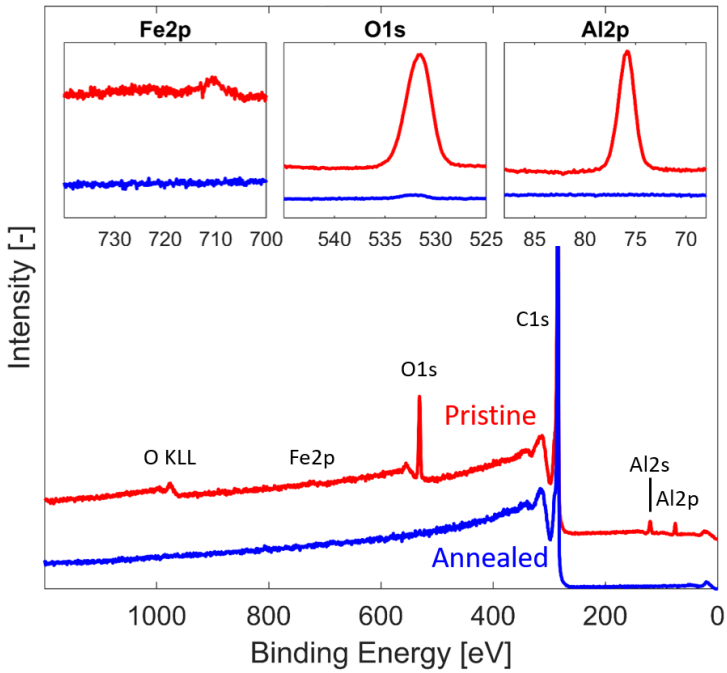

Fig. 6.9. XPS spectrum of annealed (3000°C, blue) and pristine (red) CNT arrays on graphite. The insets shows detailed scans of the Fe2p, O1s and Al2p peaks. From paper VII

6.1.3 Catalyst Evaporation

Finally, one of the expected results of annealing of CNTs on graphite was that the catalyst residues which remain on the bottom of the CNT array should evaporate and disappear, and the CNTs should anchor themselves directly to the graphite. To verify this, we did an elemental composition analysis using X-ray photoelectron spectroscopy (XPS).

Figure 6.9 shows the complete XPS spectrum of pristine (red) and annealed (blue) CNT arrays. A number of peaks can be identified, corresponding to electrons from different elements. In particular, we can see that the annealed sample shows a nearly perfect carbon spectrum, while the pristine sample shows several additional peaks. The insets show more detailed scans of the peaks corresponding to the Fe2p, O1s and Al2p electron orbitals. Again, we can se clear peaks in the pristine sample and nothing in the annealed, expect in the O1s peak, where we can see a small

trace.

(wt%)	C	O	Fe	Al
Pristine	91.19	5.23	0.12	3.46
Annealed	99.66	0.27	0.00	0.07

Table 6.1. Elemental composition of CNT graphite structure determined by XPS.

By taking the area under the peaks, subtracting the background and comparing their relative area, a measure of the elemental composition can be estimated. Table 6.1 shows the relative abundance of different elements for the pristine and annealed samples. The quantitative data confirms what we can see in the figure, that the heat treatment has eliminated essentially all traces of non-carbon elements.

The great reduction in oxygen content also indicates that not just the oxygen within the Al_2O_3 in the catalyst is gone, but also the oxygen from functional groups on the CNT sides. Normally significant traces of oxygen is always found on CVD grown CNTs, and these results show that not only are impurities removed, but the defect sites where atmospheric oxygen can bind have also largely been removed.

6.2 Discussion & Conclusion

Taken together, our hypothesis that heat treatment of CNT arrays should improve CNT crystallinity and eliminate catalyst can be considered confirmed. The data is clear, with a 124% improvement in crystallite size and a near total elimination of non-carbon elements.

However, the main finding in this study might very well be the vdW bonding between CNTs and the resulting array level densification. This was not something that we had foreseen, nor is it something that other researchers have reported on previously. However, despite not being directly investigated before, hints of the same effect can be found in previous literature. For instance, Yang et al. [240] found a reduction in intertube distance after spark plasma sintering at 1500°C of freestanding aligned MWCNT samples. While they do not go into more detail on the cause of this intertube distance reduction, it is likely that it is the same densification effect that we have seen.

This densification effect also has important implications for the practical use of the material in applications. Remember that the motivation for this work is primarily to create improved thermal interface materials. However, in this case, the densification effect severely limits the usefulness of the material compared to a uniform array. The same goes for supercapacitor electrodes like in the previous chapter, where bonded CNT exhibit lower effective surface area. To make this heat

treatment useful for real applications further research will be needed, to see if we can circumvent or possibly even harness the densification effect. Some of the most promising avenues towards this goal are presented in chapter 7.

In summary, heat treatment of CNTs is a viable method for improving their quality, and can also serve to eliminate catalyst residues. At the same time, the heat causes the CNTs to bond together and align, creating an overall densification of the entire array. For annealing to be an effective method for CNT quality improvement on an array level, this densification effect needs to be taken into account.

Chapter 7

Future Outlook

At the end of all this, one question remains: now what? How will the research I have presented affect the world? A work like this is only useful if it actually changes something. This could mean opening up new avenues for further research, recommendations for other studies, or perhaps simply a better understanding for certain phenomena. Or it could be more direct impacts such as technologies which could be applied in society today.

Below are my suggestions or predictions for how the findings within this thesis can be applied to further research or otherwise make an impact. It is nowhere an exhaustive list, but these are the areas which I believe have the most potential. In the end, it may very well be something else that I have completely overlooked which will turn out to be the most important finding.

Commercialization of SMFCs

The work on SMFCs in this thesis is based on a concept which has been developed over a decade by three generations of PhD students. I believe that the work presented here is the last push up to the line between scientific research work and development engineering. While there are further scientific questions remaining regarding the detailed infiltration and solidification process, further developments will be more targeted towards scaling up production and commercialization of a new product. We have set up a production scale prototype, but significant work remains in order to create a stable high-volume production process. After that, it is up to the market to decide whether the concept will find use in real applications.

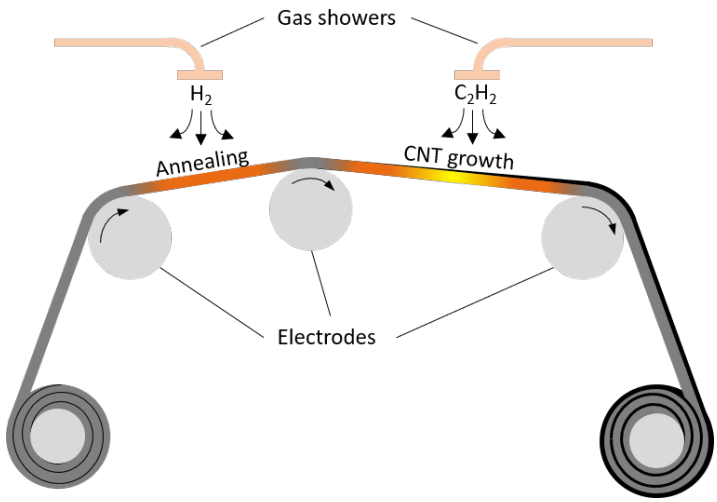

Fig. 7.1. Proposed schematic for a roll-to-roll Joule self heating CVD setup.

Reliable CNT array TIM

Carbon nanotube array TIMs are also relatively close to real applications, if not quite as far. Due to the promise they hold, industrial companies are starting to look into adapting CNT array TIMs for their own applications. In fact, our reliability study started within a project to do precisely that. When a technology is being adapted towards industry, the reliability becomes an acute concern, and thus the studies within this thesis should be very useful. This is the first time the reliability of CNT array TIMs has been thoroughly studied, and the results show that care must be taken in order to create reliable interfaces. We hope that the conclusion from our studies can be used as guidelines for others, both within academia developing without losing sight of the end usage, and within industry trying to implement the concept within their systems. Had a study like ours existed when we began our project, we most certainly would have done several things very differently.

Continuous roll-to-roll Joule heating CVD

One of the proposed advantages with the Joule heating CVD compared to convential cold-wall CVD is that it is more scalable. But what does this really mean? Part of it is that it utilizes the entire heater area, and changing heater size is as easy as changing substrate size. However, a much more dramatic difference is that the Joule heating CVD method should in principle be possible to scale up into a continuous roll-to-roll fabrication scheme as shown in figure 7.1. This proposed setup would

be for single-sided growth, but through further modification a double-sided variant should also be possible. This scaling potential is something that is to the best of my knowledge unique for the Joule heating CVD method, and could potentially be a driver for the adoption of VACNTs in industry.

Joule heating CVD on metallic foils

Within this thesis, we demonstrated the Joule heating CVD method on graphene and graphite films. However, the method does not have to be limited to carbon based materials. Indeed, any electrically conducting material should work. Both iron and copper are easily available in foils with a thickness on the order of tens of micrometers, and should be possible to run in the same process with minor modifications. The limiting factor so far has been the available current, since metallic foils have a much lower resistivity, a significantly higher current is required for the same amount of heating. However, with some minor modifications in the current CVD setup, this concept should be demonstrable.

Joule heat annealing of graphite CNT hybrid materials

Within this thesis we employed a furnace in order to heat the CNT arrays to 3000°C. However, this has the same type of drawbacks as I discussed about the hot-walled CVD systems in chapter 5.1.1 in that it is a slow and energy intense process. In principle, we should be able to use the same solution as well. Instead of a furnace, Joule heating of the graphite substrate inside of a vacuum chamber would allow us to study the heat treatment process in much more detail. This would allow us to answer questions regarding the relation between the CNT structural changes, the array densification and the catalyst evaporation, and if it is possible to achieve some of the effects and not others.

Annealed and densified CNT bundles for through silicon vias

The densification effect from annealing of CNT arrays is unwanted in most applications, but not necessarily in all. CNT based through silicon vias (TSV) are based on discrete CNT bundles which are either grown or transferred into holes in a silicon wafer in order to form connections from one side of a chip to the other [10]. In order to increase the conductivity of the TSV is to increase the CNT density, and fit a larger number of CNTs into the same hole. Several densification methods have been developed toward this end [241–244], which appear to result in a similar degree of densification as the heat treatment. By heat treating discrete bundles of CNT instead of a uniform array, each bundle will densify as a unit towards the center of each bundle rather than crack and split up. The result should be an array of well-defined densified CNT bundles which could subsequently be transferred into holes for TSV fabrication. By using heat treatment rather than an alternate densification method, we can take advantage of the higher CNT quality of heat

treated CNTs as well, potentially improving both the electrical and mechanical quality of the TSV.

Annealing of large freestanding CNT arrays

The same reasoning, to exploit rather than avoid the heat treatment densification effect, can be applied to more concepts. The CNT array splits up into different bundles largely because of one end being anchored to the substrate. Without this anchoring, in a free-standing array, larger areas of a CNT array may densify as a unit, creating a smaller but much denser CNT array, combining the increasing density with higher intrinsic thermal conductivity due to increased crystallinity. The result should be an array with a order of magnitude increased thermal conductivity which could be applied as a TIM.

A prerequisite for the feasibility of this idea is a large area freestanding CNT array. Wang et al. [245] have shown that a weak oxidative agent is enough to detach CVD grown CNT arrays from the growth substrate, allowing for wafer scale freestanding arrays. Combining this detaching method with heat treatment of the resulting freestanding CNT array could yield interesting and potentially highly useful results.

Chapter 8

Summary of Papers

Paper I

Novel nanostructured thermal interface materials: a review
Josef Hansson, Torbjörn MJ Nilsson, Lilei Ye and Johan Liu, *International Materials Reviews*, Vol. 63, no. 1, pp. 22-45, 2017

This paper provides a thorough review of thermal interface materials as a research field. Data from reports within the last ten years is analyzed and presented in a comparable format. Trends and challenges for different subfields are identified.

My contribution: I gathered all necessary data and references, analyzed and visualized the content and wrote the paper.

Paper II

Fabrication and Characterization of a Carbon Fiber Solder Composite Thermal Interface Material
Josef Hansson, Lilei Ye and Johan Liu, *Proceedings of IMAPS Nordic Conference on Microelectronics Packaging (NordPac)*, 2017

This paper presents a new composite thermal interface material consisting of carbon fiber reinforced solder matrix. Molten solder is injected into a carbon fiber under high pressure, forming a composite applicable as a preform TIM. The CF-TIM has low thermal resistance and good compatibility between fiber and matrix. In addition, the fiber phase keeps a constant bond line thickness independent of applied pressure during reflow.

My contribution: I developed the concept together with L.Y and J.L. I developed the fabrication method based on previous research and did all characterization of the material. I wrote the paper.

Paper III

Effect of fiber concentration on mechanical and thermal properties of a solder matrix fiber composite thermal interface material
Josef Hansson, Torbjörn MJ Nilsson, Lilei Ye and Johan Liu, *IEEE Transactions on Components, Packaging and Manufacturing Technology*, vol. 9, no. 6, pp. 1045-1053, 2019

This paper presents solder matrix fiber composite thermal interface materials based on commercially available components fabricated using developed automated equipment. Two different solder matrix materials, indium and a Sn-Ag-Cu alloy were explored together with varying fiber concentration within the TIM. The thermal interface resistance is comparable to pure metal alloy at lower fiber concentrations. In tensile measurements, the tensile modulus decreased with increased fiber concentration with Sn-Ag-Cu as matrix material, with opposite behavior with indium, allowing for a new trade-off regime between mechanical and thermal properties. Both TIM underwent 500 thermal cycles without degradation of thermal resistance.

My contribution: I oversaw the construction and testing of the automated equipment. I did all fabrication and characterization of the materials. I wrote the paper.

Paper IV

Synthesis of a Graphene Carbon Nanotube Hybrid Film by Joule Self-heating CVD for Thermal Applications
Josef Hansson, Majid Kabiri Samani, Andreas Nylander, Lilei Ye, Nan Wang, Torbjörn MJ Nilsson and Johan Liu, *Proceedings of IEEE 68th Electronic Components and Technology Conference*, 2018

This paper presents a novel joule heating based CVD method for synthesis of carbon nanotube arrays on both sides of a graphene based film. This method allows a cold-wall based CVD system to create double-sided CNT arrays on conducting films by using joule self heating as heat source. The CNT array has similar quality and alignment and thermal conductivity as CNT arrays grown using traditional CNT CVD. The hybrid graphene CNT film is used as a thermal pad, performing significantly better than commercially available alternatives.

My contribution: I developed the concept of Joule self heating CVD. N.W. fabricated the graphene film, and I implemented the CVD method and fabricated the hybrid material. I did the characterization with assistance from A.N. and M.K.S. I wrote the paper.

Paper V

Reliability Investigation of a Carbon Nanotube Array Thermal Interface Material
Andreas Nylander, **Josef Hansson**, Majid Kabiri Samani, Christian Chandra Darmawan, Ana Borta Boyon, Laurent Divay, Lilei Ye, Yifeng Fu, Afshin Ziaei and Johan Liu, *Energies*, vol. 12, no. 11, paper no. 2080, 2019

This paper investigates the reliability of a polymer bonded carbon nanotube array TIM during thermal cycling. The thermal interface resistance increases dramatically after relatively few thermal cycles. Shearing of the interface reveals that the CNTs delaminate from the CVD growth substrate, and stick with the polymer bonded CNT tips to the bonding surface. PPR and XPS measurements show that the connection between CNT array and substrate degrades during thermal cycling. Since one of the main proposed benefits of CNT array TIM is based on the reliability, this study highlights the importance of further research on how to realize this benefit.

My contribution: I helped develop the work from a previous conference paper into a complete journal paper. A.N. did the extra experimental work with my assistance. I wrote the paper together with A.N.

Paper VI

Bipolar Electrochemical Capacitors using Double-sided Carbon Nanotubes on Graphite Electrodes
Josef Hansson*, Qi Li*, Anderson Smith, Isaac Zakaria, Torbjörn MJ Nilsson, Andreas Nylander, Lilei Ye, Per Lundgren, Johan Liu and Peter Enoksson, *Journal of Power Sources*, Vol. 451, 2277652019, 2020. **Equal first co-author.*

This paper describes the realization of a bipolar electrochemical capacitor using a graphite CNT array hybrid structure as electrode material. The CVD method introduced in paper IV was adopted for use with a graphite paper as substrate and a modified catalyst structure to create double-sided CNT arrays covalently bonded to the graphite paper. The capacitor fabricated using this structure showed similar performance to two separately fabricated one-layer capacitors in a series connection, enabling a 22% volumetric energy density improvement. This study acts as a proof-of-concept for this type of bipolar capacitor design, which could enable more compact high voltage supercapacitors with a scalable manufacturing route.

My contribution: Q.L. developed the concept with my assistance. I developed the CVD method for the CNT synthesis and fabricated the electrodes. I did the material characterization with the assistance of A.N. Q.L. assembled the capacitor and performed all electrical measurements. Q.L. and I wrote the paper.

Paper VII

Effects of high temperature treatment of carbon nanotube arrays on graphite: increased crystallinity, anchoring and inter-tube bonding
Josef Hansson, Andreas Nylander, Mattias Flygare, Krister Svensson, Lilei Ye, Torbjörn MJ Nilsson, Yifeng Fu and Johan Liu, Under review by *Nanotechnology*

This paper investigates the effects of thermal annealing at graphitization temperatures of CNT arrays on graphite. CNT arrays were grown on graphite using the CVD method from paper IV, and subsequently annealed at 3000°C. Raman and TEM measurements show a dramatic increase in crystallinity and reduction in defects of individual CNTs. Resulting in CNT appearance changing from curved irregular tubes to straight tube segments connected with sharp corners. In addition, CNTs fuse together with adjacent tubes with a graphite interlayer-like van der Waals bonding. We show how this nanoscale fusing causes macro-scale densification of the CNT arrays. In addition, XPS measurements show that the catalyst remains from the CVD process are eliminated. This work provides hints towards further research for CNT based structures with better thermal, mechanical and electrical properties.

My contribution: I developed the concept and fabricated the samples. M.F and K.S performed the TEM diffraction measurements, and I performed the rest of the material characterization with assistance from A.N. and L.Y. I did the derivation and calculations on vdW binding energy. I wrote the paper.

Paper VIII

Degradation of Carbon Nanotube Array Thermal Interface Materials Through Thermal Aging: Effects of Bonding, Array Height and Catalyst Oxidation
Andreas Nylander*, **Josef Hansson***, Torbjörn Nilsson, Lilei Ye, Yifeng Fu and Johan Liu, in manuscript

This paper is an in-depth study of the parameters which influence the reliability of carbon nanotube array TIM, based on the concerns raised in paper V. We investigate the effect of different CNT lengths, the degradation of the growth substrate anchoring and show that bonding is required on both sides of the CNT array in order to achieve a CNT interface that can withstand CTE mismatch.

My contribution: A.N. and I jointly came up with the concept, designed the experiments and performed the fabrication, testing and characterization. We wrote the paper together.

References

[1] K. Ebrahimi, G. F. Jones, and A. S. Fleischer, "A review of data center cooling technology , operating conditions and the corresponding low-grade waste heat recovery opportunities", *Renewable and Sustainable Energy Reviews*, vol. 31, pp. 622–638, 2014.

[2] ITRS, "International Technology Roadmap for Semiconductors - Emerging Research Materials Summary", 2013.

[3] S. Iijima, "Helical microtubules of graphitic carbon", *Nature*, vol. 354, no. 6348, pp. 56–58, 1991.

[4] E. A. Laird, F. Kuemmeth, G. A. Steele, K. Grove-Rasmussen, J. Nygård, K. Flensberg, and L. P. Kouwenhoven, "Quantum transport in carbon nanotubes", *Reviews of Modern Physics*, vol. 87, no. 3, pp. 703–764, 2015.

[5] M. F. Yu, O. Lourie, M. J. Dyer, K. Moloni, T. F. Kelly, and R. S. Ruoff, "Strength and breaking mechanism of multiwalled carbon nanotubes under tensile load", *Science*, vol. 287, no. 5453, pp. 637–640, 2000.

[6] P. Kim, L. Shi, A. Majumdar, and P. L. McEuen, "Thermal Transport Measurements of Individual Multiwalled Nanotubes", *Physical Review Letters*, vol. 87, no. 21, p. 215 502, 2001.

[7] E. Pop, D. Mann, Q. Wang, K. Goodson, and H. Dai, "Thermal Conductance of an Individual Single-Wall Carbon Nanotube above Room Temperature", *Nano Letters*, vol. 6, no. 1, pp. 96–100, 2006.

[8] S. Berber, Y.-K. Kwon, and D. Tománek, "Unusually High Thermal Conductivity of Carbon Nanotubes", *Physical Review Letters*, vol. 84, no. 20, pp. 4613–4616, 2000.

[9] B. Demczyk, Y. Wang, J. Cumings, M. Hetman, W. Han, A. Zettl, and R. Ritchie, "Direct mechanical measurement of the tensile strength and elastic modulus of multiwalled carbon nanotubes", *Materials Science and Engineering: A*, vol. 334, no. 1-2, pp. 173–178, 2002.

[10] T. Wang, K. Jeppson, L. Ye, and J. Liu, "Carbon-Nanotube Through-Silicon Via Interconnects for Three-Dimensional Integration", *Small*, vol. 7, no. 16, pp. 2313–2317, 2011.

[11] Q. Li, S. Sun, A. D. Smith, P. Lundgren, Y. Fu, P. Su, T. Xu, L. Ye, L. Sun, J. Liu, and P. Enoksson, "Compact and low loss electrochemical capacitors using a graphite / carbon nanotube hybrid material for miniaturized systems", *Journal of Power Sources*, vol. 412, pp. 374–383, 2019.

[12] Y. Sun, D. H. Shin, K. N. Yun, Y. M. Hwang, Y. Song, G. Leti, S.-G. Jeon, J.-I. Kim, Y. Saito, and C. J. Lee, "Field emission behavior of carbon nanotube field emitters after high temperature thermal annealing", *AIP Advances*, vol. 4, no. 7, p. 077 110, 2014.

[13] K. Mizuno, J. Ishii, H. Kishida, Y. Hayamizu, S. Yasuda, D. N. Futaba, M. Yumura, and K. Hata, "A black body absorber from vertically aligned single-walled carbon nanotubes.", *Proceedings of the National Academy of Sciences of the United States of America*, vol. 106, no. 15, pp. 6044–7, 2009.

[14] G. L. Pollack, "Kapitza Resistance", *Reviews of Modern Physics*, vol. 41-81, no. 1, p. 48, 1969.

[15] S. Narumanchi, M. Mihalic, K. Kelly, and G. Eesley, "Thermal interface materials for power electronics applications", *2008 11th Intersociety Conference on Thermal and Thermomechanical Phenomena in Electronic Systems*, pp. 395–404, 2008.

[16] R. Viswanath, M. Group, and I. Corp, "Thermal Performance Challenges from Silicon to Systems", *Intel Technology Journal Q3,*, pp. 1–16, 2000.

[17] D. Blazej, *Thermal Interface Materials*, 2003.

[18] X. C. Tong, *Advanced Materials for Thermal Management of Electronic Packaging*. Springer, 2011, vol. 30, p. 347.

[19] L. Maguire, M. Behnia, and G. Morrison, "Systematic evaluation of thermal interface materials—a case study in high power amplifier design", *Microelectronics and Reliability*, vol. 45, no. 3-4, pp. 711–725, 2005.

[20] M. Ekpu, R. Bhatti, N. Ekere, S. Mallik, and K. Otiaba, "Effects of Thermal Interface Materials (Solders) on Thermal Performance of a Microelectronic Package", *Dtip*, no. April, 2012.

[21] J. Wilson, *Thermal Conductivity of Solders*, 2006.

[22] J. A. Emerson, M. J. Rightley, J. A. Galloway, D. F. Rae, D. L. Huber, and E. J. Cotts, "Minimizing the Bondline Thermal Resistance in Thermal Interface", *Physics*, pp. 106–111, 2005.

[23] R. S. Prasher and J. C. Matayabas, "Thermal contact resistance of cured gel polymeric thermal interface material", *IEEE Transactions on Components and Packaging Technologies*, vol. 27, no. 4, pp. 702–709, 2004.

[24] *Gap Pad Products*, 2016.

[25] M. de Sorgo, *Understanding Phase Change Materials*, 2002.

[26] *Thermally Conductive Adhesives*, 2016.

[27] G. Bischak and C. Vogdes, "Thermal management design criteria and solutions", in *Wescon/98. Conference Proceedings (Cat. No.98CH36265)*, 1998, pp. 188–193.

[28] R. Prasher, "Thermal Interface Materials: Historical Perspective, Status, and Future Directions", *Proceedings of the IEEE*, vol. 94, no. 8, pp. 1571–1586, 2006.

[29] H. Ishida and S. Rimdusit, "Very high thermal conductivity obtained by boron nitride-filled polybenzoxazine", *Thermochimica Acta*, vol. 320, no. 1-2, pp. 177–186, 1998.

[30] W.-Y. Zhou, S.-H. Qi, H.-Z. Zhao, and N.-L. Liu, "Thermally Conductive Silicone Rubber Reinforced With Boron Nitride Particle", *Polymers and Polymer Composites*, vol. 28, no. 2, pp. 23–28, 2007.

[31] K. Ahn, K. Kim, and J. Kim, "Fabrication of surface-treated BN/ETDS composites for enhanced thermal and mechanical properties", *Ceramics International*, vol. 41, no. 8, pp. 9488–9495, 2015.

[32] Z. Wang, Y. Fu, W. Meng, and C. Zhi, "Solvent-free fabrication of thermally conductive insulating epoxy composites with boron nitride nanoplatelets as fillers.", *Nanoscale research letters*, vol. 9, no. 1, p. 643, 2014.

[33] Z. Lin, Y. Liu, S. Raghavan, K. S. Moon, S. K. Sitaraman, and C. P. Wong, "Magnetic alignment of hexagonal boron nitride platelets in polymer matrix: Toward high performance anisotropic polymer composites for electronic encapsulation", *ACS Applied Materials and Interfaces*, vol. 5, no. 15, pp. 7633–7640, 2013.

[34] Y. K. Shin, W. S. Lee, M. J. Yoo, and E. S. Kim, "Effect of BN filler on thermal properties of HDPE matrix composites", *Ceramics International*, vol. 39, no. SUPPL.1, S569–S573, 2013.

[35] Z. Yuan, J. Yu, Z. He, X. Wu, B. Rao, S. Lu, and N. Jiang, "Improved thermal properties of epoxy composites filled with thermotropic liquid crystalline epoxy grafted aluminum nitride", *Fibers and Polymers*, vol. 15, no. 12, pp. 2581–2590, 2014.

[36] H. Yu, L. Li, T. Kido, G. Xi, G. Xu, and F. Guo, "Thermal and insulating properties of epoxy/aluminum nitride composites used for thermal interface material", *Journal of Applied Polymer Science*, pp. 1763–1772, 2011.

[37] K. S. Novoselov, A. K. Geim, S. V. Morozov, D. Jiang, Y. Zhang, S. V. Dubonos, I. V. Grigorieva, and A. A. Firsov, "Electric field effect in atomically thin carbon films.", *Science*, vol. 306, no. 5696, pp. 666–669, 2004.

[38] M. J. Biercuk, M. C. Llaguno, M. Radosavljevic, J. K. Hyun, A. T. Johnson, and J. E. Fischer, "Carbon nanotube composites for thermal management", *Appl. Phys. Lett.*, vol. 80, no. 15, pp. 2767–2769, 2002.

[39] B. M. Bozlar, D. He, J. Bai, Y. Chalopin, N. Mingo, and S. Volz, "Carbon Nanotube Microarchitectures for Enhanced Thermal Conduction at Ultralow Mass Fraction in Polymer Composites", *Advanced Materials*, pp. 1654–1658, 2010.

[40] M. B. Bryning, D. E. Milkie, M. F. Islam, J. M. Kikkawa, and A. G. Yodh, "Thermal conductivity and interfacial resistance in single-wall carbon nanotube epoxy composites", *Applied Physics Letters*, vol. 87, no. 16, pp. 1–3, 2005.

[41] S. T. Huxtable, D. G. Cahill, S. Shenogin, L. Xue, R. Ozisik, P. Barone, M. Usrey, M. S. Strano, G. Siddons, M. Shim, and P. Keblinski, "Interfacial heat flow in carbon nanotube suspensions.", *Nature materials*, vol. 2, no. 11, pp. 731–4, 2003.

[42] S. Shenogin, L. Xue, R. Ozisik, P. Keblinski, and D. G. Cahill, "Role of thermal boundary resistance on the heat flow in carbon-nanotube composites", *Journal of Applied Physics*, vol. 95, no. 12, pp. 8136–8144, 2004.

[43] W. Lin, K. S. Moon, and C. P. Wong, "A combined process of in situ functionalization and microwave treatment to achieve ultrasmall thermal expansion of aligned carbon nanotube-polymer nanocomposites: Toward applications as thermal interface materials", *Advanced Materials*, vol. 21, no. 23, pp. 2421–2424, 2009.

[44] F. H. Gojny, M. H. G. Wichmann, B. Fiedler, I. A. Kinloch, W. Bauhofer, A. H. Windle, and K. Schulte, "Evaluation and identification of electrical and thermal conduction mechanisms in carbon nanotube/epoxy composites", *Polymer*, vol. 47, no. 6, pp. 2036–2045, 2006.

[45] Z. Han and A. Fina, "Thermal conductivity of carbon nanotubes and their polymer nanocomposites: A review", *Progress in Polymer Science (Oxford)*, vol. 36, no. 7, pp. 914–944, 2011.

[46] B. Tang, G. Hu, H. Gao, and L. Hai, "Application of graphene as filler to improve thermal transport property of epoxy resin for thermal interface materials", *International Journal of Heat and Mass Transfer*, vol. 85, pp. 420–429, 2015.

[47] K. M. F. Shahil and A. A. Balandin, "Graphene-multilayer graphene nanocomposites as highly efficient thermal interface materials", *Nano Letters*, vol. 12, no. 2, pp. 861–867, 2012.

[48] B. Debelak and K. Lafdi, "Use of exfoliated graphite filler to enhance polymer physical properties", *Carbon*, vol. 45, no. 9, pp. 1727–1734, 2007.

[49] A. Yu, P. Ramesh, M. E. Itkis, E. Bekyarova, and R. C. Haddon, "Graphite Nanoplatelet - Epoxy Composite Thermal Interface Materials", *Phys. Chem C*, vol. 111, no. 21, pp. 7565–7569, 2007.

[50] M. A. Raza, A. V. K. Westwood, A. P. Brown, and C. Stirling, "Performance of graphite nanoplatelet/silicone composites as thermal interface adhesives", *Journal of Materials Science: Materials in Electronics*, vol. 23, no. 10, pp. 1855–1863, 2012.

[51] W.-L. Song, W. Wang, L. M. Veca, C. Y. Kong, M.-S. Cao, P. Wang, M. J. Meziani, H. Qian, G. E. LeCroy, L. Cao, and Y.-P. Sun, "Polymer/carbon nanocomposites for enhanced thermal transport properties – carbon nanotubes versus graphene sheets as nanoscale fillers", *Journal of Materials Chemistry*, vol. 22, p. 17 133, 2012.

[52] K. M. Razeeb and E. Dalton, "Nanowire polymer nanocomposites as Thermal Interface Material", in *Advances in Nanocomposites - Synthesis, Characterization and Industrial Applications*, 2011, ch. Nanowire p, pp. 685–706.

[53] J. Xu, A. Munari, E. Dalton, A. Mathewson, and K. M. Razeeb, "Silver nanowire array-polymer composite as thermal interface material", *Journal of Applied Physics*, vol. 106, no. 12, p. 124 310, 2009.

[54] A. Munari, J. Xu, E. Dalton, A. Mathewson, and K. M. Razeeb, "Metal nanowire-polymer nanocomposite as thermal interface material", *2009 59th Electronic Components and Technology Conference*, pp. 448–452, 2009.

[55] S. Wang, Y. Cheng, R. Wang, J. Sun, and L. Gao, "Highly thermal conductive copper nanowire composites with ultralow loading: Toward applications as thermal interface materials", *ACS Applied Materials and Interfaces*, vol. 6, no. 9, pp. 6481–6486, 2014.

[56] K. Pashayi, H. R. Fard, F. Lai, S. Iruvanti, J. Plawsky, and T. Borca-Tasciuc, "High thermal conductivity epoxy-silver composites based on self-constructed nanostructured metallic networks", *Journal of Applied Physics*, vol. 111, no. 10, p. 104 310, 2012.

[57] K. Pashayi, H. R. Fard, F. Lai, S. Iruvanti, J. Plawsky, and T. Borca-Tasciuc, "Self-constructed tree-shape high thermal conductivity nanosilver networks in epoxy", *Nanoscale*, vol. 6, no. 8, p. 4292, 2014.

[58] H.-G. Lee and K.-W. Paik, "Vertically aligned nickel nanowire/epoxy composite for electrical and thermal conducting material", *2012 IEEE 62nd Electronic Components and Technology Conference*, pp. 2087–2090, 2012.

[59] K. M. Razeeb and S. Roy, "Thermal diffusivity of nonfractal and fractal nickel nanowires", *Journal of Applied Physics*, vol. 103, no. 8, p. 084 302, 2008.

[60] N. Balachander, I. Seshadri, R. J. Mehta, L. S. Schadler, T. Borca-Tasciuc, P. Keblinski, and G. Ramanath, "Nanowire-filled polymer composites with ultrahigh thermal conductivity", *Applied Physics Letters*, vol. 102, no. 9, p. 093 117, 2013.

[61] V. Goyal and A. A. Balandin, "Thermal properties of the hybrid graphene-metal nano-micro-composites: Applications in thermal interface materials", *Applied Physics Letters*, vol. 100, no. 7, p. 073 113, 2012.

[62] L. Chen, Y.-Y. Sun, J. Lin, X.-Z. Du, G.-S. Wei, S.-J. He, and S. Nazarenko, "Modeling and analysis of synergistic effect in thermal conductivity enhancement of polymer composites with hybrid filler", *International Journal of Heat and Mass Transfer*, vol. 81, no. 0, pp. 457–464, 2015.

[63] G. W. Lee, M. Park, J. Kim, J. I. Lee, and H. G. Yoon, "Enhanced thermal conductivity of polymer composites filled with hybrid filler", *Composites Part A: Applied Science and Manufacturing*, vol. 37, no. 5, pp. 727–734, 2006.

[64] S. Y. Pak, H. M. Kim, S. Y. Kim, and J. R. Youn, "Synergistic improvement of thermal conductivity of thermoplastic composites with mixed boron nitride and multi-walled carbon nanotube fillers", *Carbon*, vol. 50, no. 13, pp. 4830–4838, 2012.

[65] P.-G. Ren, X.-H. Si, Z.-F. Sun, F. Ren, L. Pei, and S.-Y. Hou, "Synergistic effect of BN and MWCNT hybrid fillers on thermal conductivity and thermal stability of ultra-high-molecular-weight polyethylene composites with a segregated structure", *Journal of Polymer Research*, vol. 23, no. 2, p. 21, 2016.

[66] C.-C. Teng, C.-C. M. Ma, K.-C. Chiou, T.-M. Lee, and Y.-F. Shih, "Synergetic effect of hybrid boron nitride and multi-walled carbon nanotubes on the thermal conductivity of epoxy composites", *Materials Chemistry and Physics*, vol. 126, no. 3, pp. 722–728, 2011.

[67] M. Raza, A. Westwood, C. Stirling, and R. Ahmad, "Effect of boron nitride addition on properties of vapour grown carbon nanofiber/rubbery epoxy composites for thermal interface applications", *Composites Science and Technology*, vol. 120, pp. 9–16, 2015.

[68] Y. Hwang, M. Kim, and J. Kim, "Improvement of the mechanical properties and thermal conductivity of poly(ether-ether-ketone) with the addition of graphene oxide-carbon nanotube hybrid fillers", *Composites Part A: Applied Science and Manufacturing*, vol. 55, pp. 195–202, 2013.

[69] H. Im and J. Kim, "Thermal conductivity of a graphene oxide–carbon nanotube hybrid/epoxy composite", *Carbon*, vol. 50, no. 15, pp. 5429–5440, 2012.

[70] W. Yu, H. Xie, L. Yin, J. Zhao, L. Xia, and L. Chen, "Exceptionally high thermal conductivity of thermal grease: Synergistic effects of graphene and alumina", *International Journal of Thermal Sciences*, vol. 91, pp. 76–82, 2015.

[71] H. Chen, H. Wei, M. Chen, F. Meng, H. Li, and Q. Li, "Enhancing the effectiveness of silicone thermal grease by the addition of functionalized carbon nanotubes", *Applied Surface Science*, vol. 283, pp. 525–531, 2013.

[72] B. H. Thang, P. N. Hong, P. H. Khoi, and P. N. Minh, "Application of multiwall carbon nanotubes for thermal dissipation in a microprocessor", *Journal of Physics: Conference Series*, vol. 187, p. 012 051, 2009.

[73] M. B. Jakubinek, M. A. White, M. Mu, and K. I. Winey, "Temperature dependence of thermal conductivity enhancement in single-walled carbon nanotube/polystyrene composites", *Applied Physics Letters*, vol. 96, pp. 94–97, 2010.

[74] J. Hong, J. Lee, C. K. Hong, and S. E. Shim, "Effect of dispersion state of carbon nanotube on the thermal conductivity of poly(dimethyl siloxane) composites", *Current Applied Physics*, vol. 10, no. 1, pp. 359–363, 2010.

[75] J. Li, S. Qi, M. Zhang, and Z. Wang, "Thermal conductivity and electromagnetic shielding effectiveness of composites based on Ag-plating carbon fiber and epoxy", *Journal of Applied Polymer Science*, vol. 132, no. 33, 2015.

[76] K. Uetani, S. Ata, S. Tomonoh, T. Yamada, M. Yumura, and K. Hata, "Elastomeric Thermal Interface Materials with High Through-Plane Thermal Conductivity from Carbon Fiber Fillers Vertically Aligned by Electrostatic Flocking", *Advanced Materials*, vol. 26, no. 33, pp. 5857–5862, 2014.

[77] S. H. Jeong, S. Chen, J. Huo, E. K. Gamstedt, J. Liu, S.-L. Zhang, Z.-B. Zhang, K. Hjort, and Z. Wu, "Mechanically Stretchable and Electrically Insulating Thermal Elastomer Composite by Liquid Alloy Droplet Embedment", *Scientific Reports*, vol. 5, no. November, p. 18 257, 2015.

[78] P. Bonnet, D. Sireude, B. Garnier, and O. Chauvet, "Thermal properties and percolation in carbon nanotube-polymer composites", *Applied Physics Letters*, vol. 91, no. 20, p. 201 910, 2007.

[79] C. Yuan, B. Duan, L. Li, B. Xie, M. Huang, and X. Luo, "Thermal Conductivity of Polymer-Based Composites with Magnetic Aligned Hexagonal Boron Nitride Platelets.", *ACS applied materials & interfaces*, vol. 7, no. 23, pp. 13 000–6, 2015.

[80] S. W. Kim, H.-s. Choi, and K.-s. Lee, "Thermal conductivity of thermally conductive composites consisting of core–shell particles with nanostructured shell layers", *Materials Research Bulletin*, vol. 60, pp. 843–848, 2014.

[81] THE EUROPEAN PARLIAMENT AND THE COUNCIL OF THE EUROPEAN UNION, "DIRECTIVE 2002/95/EC OF THE EUROPEAN PARLIAMENT AND OF THE COUNCIL", *Official Journal of the European Union*, no. 37, pp. 19–23, 2003.

[82] K. Stinson-Bagby, D. Huff, D. Katsis, D. Van Wyk, and G. Q. Lu, "Thermal performance and microstructure of lead versus lead-free solder die attach interface in power device packages", *Electronics and the Environment, 2004. Conference Record. 2004 IEEE International Symposium on*, pp. 27–32, 2004.

[83] H. R. Kotadia, P. D. Howes, and S. H. Mannan, "A review: On the development of low melting temperature Pb-free solders", *Microelectronics Reliability*, vol. 54, no. 6-7, pp. 1253–1273, 2014.

[84] S. S. Too, M. Touzelbaev, M. Khan, R. Master, J. Diep, and K.-H. Keok, "Indium thermal interface material development for microprocessors", *2009 25th Annual IEEE Semiconductor Thermal Measurement and Management Symposium*, pp. 186–192, 2009.

[85] C. Deppisch, T. Fitzgerald, A. Raman, F. Hua, C. Zhang, P. Liu, and M. Miller, "The material optimization and reliability characterization of an indium-solder thermal interface material for CPU packaging", *Jom*, vol. 58, no. 6, pp. 67–74, 2006.

[86] T. E. Graedel, E. M. Harper, N. T. Nassar, P. Nuss, and B. K. Reck, "Criticality of metals and metalloids", *Proceedings of the National Academy of Sciences of the United States of America*, vol. 112, no. 14, pp. 4257–4262, 2015.

[87] M. Ekpu, R. Bhatti, M. I. Okereke, S. Mallik, and K. Otiaba, "Fatigue life of lead-free solder thermal interface materials at varying bond line thickness in microelectronics", *Microelectronics Reliability*, vol. 54, no. 1, pp. 239–244, 2014.

[88] R. Zhang, J. Cai, Q. Wang, J. Li, Y. Hu, H. Du, and L. Li, "Thermal Resistance Analysis of Sn-Bi Solder Paste Used as Thermal Interface Material for Power Electronics Applications", *Journal of Electronic Packaging*, vol. 136, no. 1, p. 011 012, 2014.

[89] Y. Gao and J. Liu, "Gallium-based thermal interface material with high compliance and wettability", *Applied Physics A: Materials Science & Processing*, vol. 107, no. 3, pp. 701–708, 2012.

[90] C. K. Roy, S. Bhavnani, M. C. Hamilton, R. W. Johnson, J. L. Nguyen, R. W. Knight, and D. K. Harris, "Investigation into the application of low melting temperature alloys as wet thermal interface materials", *International Journal of Heat and Mass Transfer*, vol. 85, pp. 996–1002, 2015.

[91] E. Yang, H. Guo, J. Guo, J. Shang, and M. Wang, "Thermal Performance of Low-Melting-Temperature Alloy Thermal Interface Materials", *Acta Metallurgica Sinica (English Letters)*, vol. 27, no. 2, pp. 290–294, 2014.

[92] Y.-G. Deng and J. Liu, "Corrosion development between liquid gallium and four typical metal substrates used in chip cooling device", *Applied Physics A*, vol. 95, no. 3, pp. 907–915, 2009.

[93] H. Yu, L. Li, and Y. Zhang, "Silver nanoparticle-based thermal interface materials with ultra-low thermal resistance for power electronics applications", *Scripta Materialia*, vol. 66, no. 11, pp. 931–934, 2012.

[94] I. Dutta, R. Raj, P. Kumar, T. Chen, C. M. Nagaraj, J. Liu, M. Renavikar, and V. Wakharkar, "Liquid phase sintered solders with indium as minority phase for next generation thermal interface material applications", *Journal of Electronic Materials*, vol. 38, no. 12, pp. 2735–2745, 2009.

[95] J. Liu, P. Kumar, I. Dutta, R. Raj, R. Sidhu, M. Renavikar, and R. Mahajan, "Liquid phase sintered Cu – In composite solders for thermal interface material and interconnect applications", *Journal of Materials Science*, no. 46, pp. 7012–7025, 2011.

[96] J. Liu, U. Sahaym, I. Dutta, R. Raj, M. Renavikar, R. S. Sidhu, and R. Mahajan, "Interfacially engineered liquid-phase-sintered Cu–In composite solders for thermal interface material applications", *Journal of Materials Science*, vol. 49, no. 22, pp. 7844–7854, 2014.

[97] P. Kumar and S. Awasthi, "Mechanical and thermal modeling of In-Cu composites for thermal interface materials applications", *Journal of Composite Materials*, vol. 48, no. 11, pp. 1391–1398, 2013.

[98] P. M. Raj, P. R. Gangidi, N. Nataraj, N. Kumbhat, G. C. Jha, R. Tummala, and N. Brese, "Coelectrodeposited Solder Composite Films for Advanced Thermal Interface Materials", *IEEE Transactions on Components, Packaging and Manufacturing Technology*, vol. 3, no. 6, pp. 989–996, 2013.

[99] N. Nagabandi, C. Yegin, X. Feng, C. King, J. K. Oh, E. A. Scholar, S. Narumanchi, and M. Akbulut, "Chemically linked metal-matrix nanocomposites of boron nitride nanosheets and silver as thermal interface materials", *Nanotechnology*, vol. 29, no. 10, 2018.

[100] S. M. L. Nai, J. Wei, and M. Gupta, "Improving the performance of lead-free solder reinforced with multi-walled carbon nanotubes", *Materials Science and Engineering A*, vol. 423, no. 1-2, pp. 166–169, 2006.

[101] L. Yang, C. Du, J. Dai, N. Zhang, and Y. Jing, "Effect of nanosized graphite on properties of Sn-Bi solder", *Journal of Materials Science: Materials in Electronics*, vol. 24, no. 11, pp. 4180–4185, 2013.

[102] H. R. Kotadia, A. Panneerselvam, M. W. Sugden, H. Steen, M. Green, S. H. Mannan, and S. Member, "Electronics Assembly and High Temperature Paste With Zn Additives", *IEEE Transactions on Components, Packaging and Manufacturing Technology*, vol. 3, no. 10, pp. 1786–1793, 2013.

[103] H. Huang, X. Wei, F. Liao, and L. Zhou, "Preparation and properties of particle reinforced Sn-Zn-based composite solder", *Journal Wuhan University of Technology, Materials Science Edition*, vol. 24, no. 2, pp. 206–209, 2009.

[104] M. Sharma and D. D. L. Chung, "Solder–Graphite Network Composite Sheets as High-Performance Thermal Interface Materials", *Journal of Electronic Materials*, vol. 44, no. 3, pp. 929–947, 2015.

[105] H.-H. Chen, Y. Zhao, and C.-L. Chen, "Experimental Study of Coefficient of Thermal Expansion of Aligned Graphite Thermal Interface Materials", *Frontiers in Heat and Mass Transfer*, vol. 4, no. 1, pp. 1–7, 2013.

[106] C. Zandén, X. Luo, L. Ye, and J. Liu, "A new solder matrix nano polymer composite for thermal management applications", *Composites Science and Technology*, vol. 94, pp. 54–61, 2014.

[107] M. Murugesan, C. Zandén, X. Luo, L. Ye, V. Jokubavicius, M. Syväjärvi, and J. Liu, "A carbon fiber solder matrix composite for thermal management of microelectronic devices", *Journal of Materials Chemistry C*, vol. 2, no. 35, p. 7184, 2014.

[108] B. A. Cola, T. S. Fisher, and X. Xu, "Carbon Nanotube Array Thermal Interfaces", in *Carbon Nanotubes: New Research*, 2009.

[109] M. Kumar and Y. Ando, "Chemical Vapor Deposition of Carbon Nanotubes: A Review on Growth Mechanism and Mass Production", *Journal of Nanoscience and Nanotechnology*, vol. 10, no. 6, pp. 3739–3758, 2010.

[110] A. M. Marconnet, M. A. Panzer, and K. E. Goodson, "Thermal conduction phenomena in carbon nanotubes and related nanostructured materials", *Reviews of Modern Physics*, vol. 85, no. 3, pp. 1295–1326, 2013.

[111] B. A. Cola, J. Xu, and T. S. Fisher, "Contact mechanics and thermal conductance of carbon nanotube array interfaces", *International Journal of Heat and Mass Transfer*, vol. 52, no. 15-16, pp. 3490–3503, 2009.

[112] T. Tong, Y. Zhao, L. Delzeit, A. Kashani, M. Meyyappan, and A. Majumdar, "Dense Vertically Aligned Multiwalled Carbon Nanotube Arrays as Thermal Interface Materials", *IEEE Transactions on Components and Packaging Technologies*, vol. 30, no. 1, pp. 92–100, 2007.

[113] M. A. Panzer, G. Zhang, D. Mann, X. Hu, E. Pop, H. Dai, and K. E. Goodson, "Thermal Properties of Metal-Coated Vertically Aligned Single-Wall Nanotube Arrays", *Journal of Heat Transfer*, vol. 130, no. 5, p. 052 401, 2008.

[114] B. A. Cola, J. Xu, C. Cheng, X. Xu, T. S. Fisher, and H. Hu, "Photoacoustic characterization of carbon nanotube array thermal interfaces", *Journal of Applied Physics*, vol. 101, no. 5, pp. 1–9, 2007.

[115] M. A. Panzer, H. M. Duong, J. Okawa, J. Shiomi, B. L. Wardle, S. Maruyama, and K. E. Goodson, "Temperature-dependent phonon conduction and nanotube engagement in metalized single wall carbon nanotube films", *Nano Letters*, vol. 10, no. 7, pp. 2395–2400, 2010.

[116] Q. Li, C. Liu, and S. Fan, "Thermal boundary resistances of carbon nanotubes in contact with metals and polymers", *Nano Letters*, vol. 9, pp. 3805–3809, 2009.

[117] Y. Yao, J. N. Tey, Z. Li, J. Wei, K. Bennett, A. McNamara, Y. Joshi, R. L. S. Tan, S. N. M. Ling, and C. P. Wong, "High-quality vertically aligned carbon nanotubes for applications as thermal interface materials", *IEEE Transactions on Components, Packaging and Manufacturing Technology*, vol. 4, no. 2, pp. 232–239, 2014.

[118] B. A. Cola, P. B. Amama, X. Xu, and T. S. Fisher, "Effects of Growth Temperature on Carbon Nanotube Array Thermal Interfaces", *Journal of Heat Transfer*, vol. 130, p. 114 503, 2008.

[119] P. B. Amama, B. A. Cola, T. D. Sands, X. F. Xu, and T. S. Fisher, "Dendrimer-assisted controlled growth of carbon nanotubes for enhanced thermal interface conductance", *Nanotechnology*, vol. 18, no. 38, p. 385 303, 2007.

[120] X. Liu, Y. Zhang, A. M. Cassell, and B. A. Cruden, "Implications of catalyst control for carbon nanotube based thermal interface materials", *Journal of Applied Physics*, vol. 104, no. 8, p. 084 310, 2008.

[121] R. Cross, B. A. Cola, T. Fisher, X. Xu, K. Gall, and S. Graham, "A metallization and bonding approach for high performance carbon nanotube thermal interface materials.", *Nanotechnology*, vol. 21, no. 44, p. 445 705, 2010.

[122] S. L. Hodson, T. Bhuvana, B. A. Cola, X. Xu, G. U. Kulkarni, and T. S. Fisher, "Palladium Thiolate Bonding of Carbon Nanotube Thermal Interfaces", *Journal of Electronic Packaging*, vol. 133, no. 2, p. 20 907, 2011.

[123] M. T. Barako, Y. Gao, Y. Won, A. M. Marconnet, M. Asheghi, and K. E. Goodson, "Reactive Metal Bonding of Carbon Nanotube Arrays for Thermal Interface Applications", *IEEE Transactions on Components, Packaging and Manufacturing Technology*, vol. 4, no. 12, pp. 1906–1913, 2014.

[124] Y. Ni, H. Le Khanh, Y. Chalopin, J. Bai, P. Lebarny, L. Divay, and S. Volz, "Highly efficient thermal glue for carbon nanotubes based on azide polymers", *Applied Physics Letters*, vol. 100, no. 19, p. 193 118, 2012.

[125] J. H. Taphouse, T. L. Bougher, V. Singh, P. P. S. S. Abadi, S. Graham, and B. A. Cola, "Carbon nanotube thermal interfaces enhanced with sprayed on nanoscale polymer coatings", *Nanotechnology*, vol. 24, no. 10, p. 105 401, 2013.

[126] J. Daon, S. Sun, D. Jiang, G. Cibien, E. Leveugle, C. Galindo, A. Ziaei, L. Ye, Y. Fu, J. Bai, and J. Liu, "Electrically conductive thermal interface materials based on vertically aligned carbon nanotubes mats", in *Therminic 20th International workshop*, 2014, pp. 1–4.

[127] W. Lin, R. Zhang, K.-S. Moon, and C. Wong, "Molecular phonon couplers at carbon nanotube/substrate interface to enhance interfacial thermal transport", *Carbon*, vol. 48, no. 1, pp. 107–113, 2010.

[128] S. Kaur, N. Raravikar, B. A. Helms, R. Prasher, and D. F. Ogletree, "Enhanced thermal transport at covalently functionalized carbon nanotube array interfaces", *Nature Communications*, vol. 5, pp. 1–8, 2014.

[129] J. H. Taphouse, O. L. Smith, S. R. Marder, and B. A. Cola, "A pyrenylpropyl phosphonic acid surface modifier for mitigating the thermal resistance of carbon nanotube contacts", *Advanced Functional Materials*, vol. 24, no. 4, pp. 465–471, 2014.

[130] W. Lin, R. Zhang, K. S. Moon, and C. P. Wong, "Synthesis of high-quality vertically aligned carbon nanotubes on bulk copper substrate for thermal management", *IEEE Transactions on Advanced Packaging*, vol. 33, no. 2, pp. 370–376, 2010.

[131] Z. L. Gao, K. Zhang, and M. M. F. Yuen, "Fabrication of carbon nanotube thermal interface material on aluminum alloy substrates with low pressure CVD.", *Nanotechnology*, vol. 22, no. 26, p. 265 611, 2011.

[132] Z. Kai, M. M. F. Yuen, D. G. W. Xiao, Y. Y. Fu, and P. Chan, "Directly synthesizing CNT-TIM on aluminum alloy heat sink for HB-LED thermal management", *Proceedings - Electronic Components and Technology Conference*, pp. 1659–1663, 2008.

[133] A. Kumar, V. L. Pushparaj, S. Kar, O. Nalamasu, P. M. Ajayan, and R. Baskaran, "Contact transfer of aligned carbon nanotube arrays onto conducting substrates", *Applied Physics Letters*, vol. 89, no. 16, pp. 14–17, 2006.

[134] Y. Fu, Y. Qin, T. Wang, S. Chen, and J. Liu, "Ultrafast transfer of metal-enhanced carbon nanotubes at low temperature for large-scale electronics assembly", *Advanced Materials*, vol. 22, no. 44, pp. 5039–5042, 2010.

[135] A. Hamdan, J. Cho, R. Johnson, J. Jiao, D. Bahr, R. Richards, and C. Richards, "Evaluation of a thermal interface material fabricated using thermocompression bonding of carbon nanotube turf.", *Nanotechnology*, vol. 21, no. 1, p. 015 702, 2010.

[136] M. X. Chen, X. H. Song, Z. Y. Gan, and S. Liu, "Low temperature thermocompression bonding between aligned carbon nanotubes and metallized substrate.", *Nanotechnology*, vol. 22, no. 34, p. 345 704, 2011.

[137] B. A. Cola, X. Xu, and T. S. Fisher, "Increased real contact in thermal interfaces: A carbon nanotube/foil material", *Applied Physics Letters*, vol. 90, no. 9, pp. 9–11, 2007.

[138] H. Wang, J. Y. Feng, X. J. Hu, and K. M. Ng, "Reducing thermal contact resistance using a bilayer aligned CNT thermal interface material", *Chemical Engineering Science*, vol. 65, no. 3, pp. 1101–1108, 2010.

[139] N. Na, K. Hasegawa, X. Zhou, M. Nihei, and S. Noda, "Denser and taller carbon nanotube arrays on Cu foils useable as thermal interface materials", *Japanese Journal of Applied Physics*, vol. 54, no. 9, 2015.

[140] H. Huang, C. Liu, Y. Wu, and S. Fan, "Aligned carbon nanotube composite films for thermal management", *Advanced Materials*, vol. 17, pp. 1652–1656, 2005.

[141] A. M. Marconnet, N. Yamamoto, M. A. Panzer, B. L. Wardle, and K. E. Goodson, "Thermal conduction in aligned carbon nanotube-polymer nanocomposites with high packing density", *ACS Nano*, vol. 5, no. 6, pp. 4818–4825, 2011.

[142] M. Wang, H. Chen, W. Lin, Z. Li, Q. Li, M. Chen, F. Meng, Y. Xing, Y. Yao, C.-p. Wong, and Q. Li, "Crack-free and scalable transfer of carbon nanotube arrays into flexible and highly thermal conductive composite film.", *ACS applied materials & interfaces*, vol. 6, no. 1, pp. 539–44, 2014.

[143] Y. T. Lee, S. Shanmugan, and D. Mutharasu, "Thermal resistance of CNTs-based thermal interface material for high power solid state device packages", *Applied Physics A: Materials Science and Processing*, vol. 114, no. 4, pp. 1145–1152, 2014.

[144] J. Xu and T. S. Fisher, "Enhancement of thermal interface materials with carbon nanotube arrays", *International Journal of Heat and Mass Transfer*, vol. 49, no. 9-10, pp. 1658–1666, 2006.

[145] K. Zhang, Y. Chai, M. M. F. Yuen, D. G. W. Xiao, and P. C. H. Chan, "Carbon nanotube thermal interface material for high-brightness light-emitting-diode cooling.", *Nanotechnology*, vol. 19, no. 21, p. 215 706, 2008.

[146] B. A. Cola, X. Xu, T. S. Fisher, M. A. Capano, and P. B. Amama, "Carbon Nanotube Array Thermal Interfaces for High-Temperature Silicon Carbide Devices", *Nanoscale and Microscale Thermophysical Engineering*, vol. 12, no. November, pp. 228–237, 2008.

[147] M. T. Barako, "Solder-Bonded Carbon Nanotube Thermal Interface Materials", *2012 13Th Ieee Intersociety Conference on Thermal and Thermomechanical Phenomena in Electronic Systems (Itherm)*, pp. 1225–1233, 2012.

[148] J. R. Wasniewski, D. H. Altman, S. L. Hodson, T. S. Fisher, A. Bulusu, S. Graham, and B. A. Cola, "Characterization of Metallically Bonded Carbon Nanotube-Based Thermal Interface Materials Using a High Accuracy 1D Steady-State Technique", *Journal of Electronic Packaging*, vol. 134, no. 2, p. 20 901, 2012.

[149] E. S. Polsen, D. Q. McNerny, B. Viswanath, S. W. Pattinson, and A. John Hart, "High-speed roll-to-roll manufacturing of graphene using a concentric tube CVD reactor.", *Scientific reports*, vol. 5, p. 10 257, 2015.

[150] M. R. Arcila-velez, J. Zhu, and A. Childress, "Roll-to-roll synthesis of vertically aligned carbon nanotube electrodes for electrical double layer capacitors", *Nano Energy*, vol. 8, pp. 9–16, 2014.

[151] R. Kempers, A. Robinson, and L. Alan, "Characterization of Metal Micro-Textured Thermal Interface Materials", *Thermal Investigations of ICs and Systems, 2009. THERMINIC 2009. 15th International Workshop*, no. November, 2009.

[152] R. Kempers, A. M. Lyons, and A. J. Robinson, "Modeling and Experimental Characterization of Metal Microtextured Thermal Interface Materials", *Journal of Heat Transfer*, vol. 136, no. 1, p. 011 301, 2013.

[153] R. Kempers and S. Kerslake, "In Situ Testing of Metal Micro-Textured Thermal Interface Materials in Telecommunications Applications", *Journal of Physics: Conference Series*, vol. 525, p. 012 016, 2014.

[154] B. Feng, F. Faruque, P. Bao, A.-T. Chien, S. Kumar, and G. P. Peterson, "Double-sided tin nanowire arrays for advanced thermal interface materials", *Applied Physics Letters*, vol. 102, no. 9, p. 093 105, 2013.

[155] M. T. Barako, S. Roy-Panzer, T. S. English, T. Kodama, M. Asheghi, T. W. Kenny, and K. E. Goodson, "Thermal Conduction in Vertically Aligned Copper Nanowire Arrays and Composites", *ACS Applied Materials & Interfaces*, vol. 7, no. 34, pp. 19 251–19 259, 2015.

[156] D. Shaddock, S. Weaver, I. Chasiotis, B. Shah, and D. Zhong, "Development of a Compliant Nanothermal Interface Material", in *ASME 2011 Pacific Rim Technical Conference and Exhibition on Packaging and Integration of Electronic and Photonic Systems, MEMS and NEMS: Volume 2*, 2011, pp. 13–17.

[157] S. Shen, A. Henry, J. Tong, R. Zheng, and G. Chen, "Polyethylene nanofibres with very high thermal conductivities", *Nature Nanotechnology*, vol. 5, no. 4, pp. 251–255, 2010.

[158] V. Singh, T. L. Bougher, A. Weathers, Y. Cai, K. Bi, M. T. Pettes, S. A. McMenamin, W. Lv, D. P. Resler, T. R. Gattuso, D. H. Altman, K. H. Sandhage, L. Shi, A. Henry, and B. A. Cola, "High thermal conductivity of chain-oriented amorphous polythiophene", *Nature Nanotechnology*, vol. 9, no. 5, pp. 384–390, 2014.

[159] X. Zhang, K. K. Yeung, Z. Gao, J. Li, H. Sun, H. Xu, K. Zhang, M. Zhang, Z. Chen, M. M. F. Yuen, and S. Yang, "Exceptional thermal interface properties of a three-dimensional graphene foam", *Carbon*, vol. 66, pp. 201–209, 2014.

[160] P. Lv, X.-W. Tan, K.-H. Yu, R.-L. Zheng, J.-J. Zheng, and W. Wei, "Super-elastic graphene/carbon nanotube aerogel: A novel thermal interface material with highly thermal transport properties", *Carbon*, vol. 99, pp. 222–228, 2016.

[161] Y. Zhang, H. Han, N. Wang, P. Zhang, Y. Fu, M. Murugesan, M. Edwards, K. Jeppson, S. Volz, and J. Liu, "Improved Heat Spreading Performance of Functionalized Graphene in Microelectronic Device Application", *Advanced Functional Materials*, vol. 25, no. 28, pp. 4430–4435, 2015.

[162] Q. Liang, X. Yao, W. Wang, Y. Liu, and C. P. Wong, "A three-dimensional vertically aligned functionalized multilayer graphene architecture: An approach for graphene-based thermal interfacial materials", *ACS Nano*, vol. 5, no. 3, pp. 2392–2401, 2011.

[163] N. Wang, S. Chen, A. Nkansah, Q. Wang, X. Wang, M. Chen, L. Ye, and J. Liu, "Vertically Aligned Graphene-based Thermal Interface Material with High Thermal Conductivity", *THERMINIC 2018 - 24th International Workshop on Thermal Investigations of ICs and Systems, Proceedings*, vol. 2018, no. September, pp. 1–4, 2018.

[164] X. Huang, C. Zhi, P. Jiang, D. Golberg, Y. Bando, and T. Tanaka, "Polyhedral oligosilsesquioxane-modified boron nitride nanotube based epoxy nanocomposites: An ideal dielectric material with high thermal conductivity", *Advanced Functional Materials*, vol. 23, no. 14, pp. 1824–1831, 2013.

[165] M. Loeblein, S. H. Tsang, Y. Han, X. Zhang, E. Hang, and T. Teo, "Heat Dissipation Enhancement of 2 . 5D Package with 3D Graphene & 3D Boron Nitride Networks as Thermal Interface Material (TIM)", in *2016 IEEE 66th Electronic Components and Technology Conference*, 2016, pp. 707–713.

[166] G. Yujun, L. Zhongliang, Z. Guangmeng, and L. Yanxia, "Effects of multi-walled carbon nanotubes addition on thermal properties of thermal grease", *International Journal of Heat and Mass Transfer*, vol. 74, pp. 358–367, 2014.

[167] H. Chen, M. Chen, J. Di, G. Xu, H. Li, and Q. Li, "Architecting three-dimensional networks in carbon nanotube buckypapers for thermal interface materials", *Journal of Physical Chemistry C*, vol. 116, no. 6, pp. 3903–3909, 2012.

[168] R. J. Warzoha, D. Zhang, G. Feng, and A. S. Fleischer, "Engineering interfaces in carbon nanostructured mats for the creation of energy efficient thermal interface materials", *Carbon*, vol. 61, pp. 441–457, 2013.

[169] K. Hu and D. D. L. Chung, "Flexible graphite modified by carbon black paste for use as a thermal interface material", *Carbon*, vol. 49, no. 4, pp. 1075–1086, 2011.

[170] Y. Aoyagi and D. D. L. Chung, "Antioxidant-based phase-change thermal interface materials with high thermal stability", *Journal of Electronic Materials*, vol. 37, no. 4, pp. 448–461, 2008.

[171] B. Carlberg, T. Wang, Y. Fu, J. Liu, and D. Shangguan, "Nanostructured Polymer-Metal Composite for Thermal Interface Material Applications", in *58th Electronic Components and Technology Conference (ECTC), 2008.*, 2008, pp. 191–197.

[172] X. Luo, Y. Zhang, C. Zandén, M. Murugesan, Y. Cao, L. Ye, and J. Liu, "Novel thermal interface materials: Boron nitride nanofiber and indium composites for electronics heat dissipation applications", *Journal of Materials Science: Materials in Electronics*, vol. 25, no. 5, pp. 2333–2338, 2014.

[173] B. Carlberg, T. Wang, J. Liu, and D. Shangguan, "Polymer-metal nano-composite films for thermal management", *Microelectronics International*, vol. 26, no. 2, pp. 28–36, 2009.

[174] C. Zandén, X. Luo, L. Ye, and J. Liu, "Fabrication and characterization of a metal matrix polymer fibre composite for thermal interface material applications", *19th International Workshop on Thermal Investigations of ICs and Systems (THERMINIC)*, vol. 2013, pp. 286–292, 2013.

[175] S. Sun, S. Chen, X. Luo, Y. Fu, L. Ye, and J. Liu, "Mechanical and thermal characterization of a novel nanocomposite thermal interface material for electronic packaging", *Microelectronics Reliability*, vol. 56, pp. 129–135, 2015.

[176] G. Kaptay, "The threshold pressure of infiltration into fibrous preforms normal to the fibers ' axes", *Composites Science and Technology*, vol. 68, pp. 228–237, 2008.

[177] C. Pradere, J. C. Batsale, J. M. Goyhénèche, R. Pailler, and S. Dilhaire, "Thermal properties of carbon fibers at very high temperature", *Carbon*, vol. 47, no. 3, pp. 737–743, 2009.

[178] Y. V. Naidich and G. A. Kolesnichenko, "Investigation of the wetting of diamond and graphite by molten metals and alloys V. Carbide-formation kinetics at the graphite/metallic melt interface", *Soviet Powder Metallurgy and Metal Ceramics*, vol. 7, no. 2, pp. 139–141, 1968.

[179] A. Hanss, E. Liu, M. Schmid, and G. Elger, "The influence of voids in solder joints on thermal performance and reliability investigated with transient thermal analysis", in *21st International Workshop on Thermal Investigations of ICs and Systems (THERMINIC)*, 2015, pp. 1–6.

[180] K. Seelig and K. Pigeon, "Overcoming the challenges of the QFN package", in *SMTA International Conference Proceedings*, 2011.

[181] K. C. Otiaba, M. I. Okereke, and R. S. Bhatti, "Numerical assessment of the effect of void morphology on thermo- mechanical performance of solder thermal interface material", *Applied Thermal Engineering*, vol. 64, no. 1-2, pp. 51–63, 2014.

[182] I. Corporation, *Thermal K Values List*.

[183] H. S. Kim and M. B. Bush, "The effects of grain size and porosity on the elastic modulus of nanocrystalline materials", vol. 11, no. 3, pp. 361–367, 1999.

[184] A. Shubert, H. Walter, R. Dudek, B. Michel, G. Lefranc, J. Otto, and G. Mitic, "Thermo- mechanical properties and creep deformation of lead-containing and lead-free solders", in *2001 International Symposium on Advanced Packaging Materials*, 2001, pp. 129–134.

[185] M. Klein, A. Hadrboletz, B. Weiss, and G. Khatibi, "The 'size effect' on the stress – strain, fatigue and fracture properties of thin metallic foils", *Materials Science and Engineering A*, vol. 321, pp. 924–928, 2001.

[186] Y. T. Zhu, "Microstructures and mechanical properties of ultrafine-grained Ti foil processed by equal-channel angular pressing and cold rolling", 2017.

[187] M. Song, X. Liu, and L. Liu, "Size Effect on Mechanical Properties and Texture of Pure Copper Foil by Cold Rolling", pp. 1–18, 2017.

[188] A. Diehl, U. Engel, and M. Geiger, "Mechanical properties and bending behaviour of metal foils", vol. 222, pp. 83–91, 2007.

[189] A. Bar-Cohen, K. Matin, and S. Narumanchi, "Nanothermal Interface Materials: Technology Review and Recent Results", *Journal of Electronic Packaging*, vol. 137, no. 4, p. 040 803, 2015.

[190] A. Moisala, A. G. Nasibulin, and E. I. Kauppinen, "The role of metal nanoparticles in the catalytic production of single-walled carbon nanotubes - A review", *Journal of Physics Condensed Matter*, vol. 15, no. 42, 2003.

[191] J. Standard *et al.*, "Temperature cycling", *JESD22-A104D, JEDEC Solid State Technology Association, Arlington, VA*, pp. 158–162, 2009.

[192] O. W. Käding, H. Skurk, and K. E. Goodson, "Thermal conduction in metallized silicon-dioxide layers on silicon", *Applied Physics Letters*, vol. 65, no. 13, pp. 1629–1631, 1994.

[193] J. Daon, S. Sun, D. Jiang, E. Leveugle, C. Galindo, S. Jus, A. Ziaei, L. Ye, Y. Fu, and J. Liu, "Chemically enhanced carbon nanotubes based thermal interface materials", in *2015 21st International Workshop on Thermal Investigations of ICs and Systems (THERMINIC)*, IEEE, 2015, pp. 1–4.

[194] T.-C. Lin, G. Seshadri, and J. A. Kelber, "A consistent method for quantitative xps peak analysis of thin oxide films on clean polycrystalline iron surfaces", *Applied Surface Science*, vol. 119, no. 1-2, pp. 83–92, 1997.

[195] H. I. Kim, M. Wang, S. K. Lee, J. Kang, J. D. Nam, L. Ci, and J. Suhr, "Tensile properties of millimeter-long multi-walled carbon nanotubes", *Scientific Reports*, vol. 7, no. 1, pp. 1–7, 2017.

[196] N. Wang, M. K. Samani, H. Li, L. Dong, Z. Zhang, P. Su, S. Chen, J. Chen, S. Huang, G. Yuan, X. Xu, B. Li, K. Leifer, L. Ye, and J. Liu, "Tailoring the Thermal and Mechanical Properties of Graphene Film by Structural Engineering", *Small*, vol. 14, no. 29, pp. 1–8, 2018.

[197] L. Wagner, "Overview of Energy Storage Technologies", in *Future Energy*, 2014, pp. 613–631.

[198] D. N. Futaba, K. Hata, T. Yamada, T. Hiraoka, Y. Hayamizu, Y. Kakudate, O. Tanaike, H. Hatori, M. Yumura, and S. Iijima, "Shape-engineerable and highly densely packed single-walled carbon nanotubes and their application as super-capacitor electrodes", *Nat Mater*, vol. 5, no. 12, pp. 987–94, 2006.

[199] R. Reit, J. Nguyen, and W. J. Ready, "Growth time performance dependence of vertically aligned carbon nanotube supercapacitors grown on aluminum substrates", *Electrochimica Acta*, vol. 91, pp. 96–100, 2013.

[200] B. Hsia, J. Marschewski, S. Wang, J. B. In, C. Carraro, D. Poulikakos, C. P. Grigoropoulos, and R. Maboudian, "Highly flexible, all solid-state micro-supercapacitors from vertically aligned carbon nanotubes", *Nanotechnology*, vol. 25, no. 5, p. 055 401, 2014.

[201] C. Zhang, Z. Peng, J. Lin, Y. Zhu, G. Ruan, C.-C. Hwang, W. Lu, R. H. Hauge, and J. M. Tour, "Splitting of a vertical multiwalled carbon nanotube carpet to a graphene nanoribbon carpet and its use in supercapacitors", *Acs Nano*, vol. 7, no. 6, pp. 5151–5159, 2013.

[202] M. G. Hahm, A. Leela Mohana Reddy, D. P. Cole, M. Rivera, J. A. Vento, J. Nam, H. Y. Jung, Y. L. Kim, N. T. Narayanan, D. P. Hashim, C. Galande, Y. J. Jung, M. Bundy, S. Karna, P. M. Ajayan, and R. Vajtai, "Carbon nanotube-nanocup hybrid structures for high power supercapacitor applications", *Nano Lett*, vol. 12, no. 11, pp. 5616–21, 2012.

[203] A. Ghosh, V. T. Le, J. J. Bae, and Y. H. Lee, "Tlm-psd model for optimization of energy and power density of vertically aligned carbon nanotube supercapacitor", *Sci Rep*, vol. 3, p. 2939, 2013.

[204] I. B. Dogru, M. B. Durukan, O. Turel, and H. E. Unalan, "Flexible supercapacitor electrodes with vertically aligned carbon nanotubes grown on aluminum foils", *Progress in Natural Science-Materials International*, vol. 26, no. 3, pp. 232–236, 2016.

[205] Y. Wang, Y. Song, and Y. Xia, "Electrochemical capacitors: Mechanism, materials, systems, characterization and applications", *Chemical Society Reviews*, vol. 45, no. 21, pp. 5925–5950, 2016.

[206] S. Sun, M. K. Samani, Y. Fu, T. Xu, L. Ye, M. Satwara, K. Jeppson, T. Nilsson, L. Sun, and J. Liu, "Improving Thermal Transport at Carbon Hybrid Interfaces by Covalent Bonds", *Advanced Materials Interfaces*, vol. 5, no. 15, pp. 1–9, 2018.

[207] C. L. Pint, N. T. Alvarez, and R. H. Hauge, "Odako growth of dense arrays of single-walled carbon nanotubes attached to carbon surfaces", *Nano Research*, vol. 2, no. 7, pp. 526–534, 2009.

[208] Y. J. Kang, H. Chung, C.-H. Han, and W. Kim, "All-solid-state flexible supercapacitors based on papers coated with carbon nanotubes and ionic-liquid-based gel electrolytes", *Nanotechnology*, vol. 23, no. 6, p. 065 401, 2012.

[209] P. Chen, H. Chen, J. Qiu, and C. Zhou, "Inkjet printing of single-walled carbon nanotube/ruo 2 nanowire supercapacitors on cloth fabrics and flexible substrates", *Nano Research*, vol. 3, no. 8, pp. 594–603, 2010.

[210] I. B. Dogru, M. B. Durukan, O. Turel, and H. E. Unalan, "Flexible supercapacitor electrodes with vertically aligned carbon nanotubes grown on aluminum foils", *Progress in Natural Science: Materials International*, vol. 26, no. 3, pp. 232–236, 2016.

[211] Y.-S. Kim, K. Kumar, F. T. Fisher, and E.-H. Yang, "Out-of-plane growth of cnts on graphene for supercapacitor applications", *Nanotechnology*, vol. 23, no. 1, p. 015 301, 2011.

[212] W. Qian, T. Liu, F. Wei, Z. Wang, G. Luo, H. Yu, and Z. Li, "The evaluation of the gross defects of carbon nanotubes in a continuous CVD process", *Carbon*, vol. 41, no. 13, pp. 2613–2617, 2003.

[213] R. Das, Z. Shahnavaz, M. E. Ali, M. M. Islam, and S. B. Abd Hamid, "Can We Optimize Arc Discharge and Laser Ablation for Well-Controlled Carbon Nanotube Synthesis?", *Nanoscale Research Letters*, vol. 11, no. 1, 2016.

[214] J. P. Salvetat, A. J. Kulik, J. M. Bonard, G. A. D. Briggs, T. Stöckli, K. Méténier, S. Bonnamy, F. Béguin, N. A. Burnham, and L. Forró, "Elastic modulus of ordered and disordered multiwalled carbon nanotubes", *Advanced Materials*, vol. 11, no. 2, pp. 161–165, 1999.

[215] M. Flygare and K. Svensson, "Quantifying crystallinity in carbon nanotubes and its influence on mechanical behaviour", *Materials Today Communications*, vol. 18, no. November 2018, pp. 39–45, 2019.

[216] L. A. Algharagholy, "Defects in Carbon Nanotubes and their Impact on the Electronic Transport Properties", *Journal of Electronic Materials*, vol. 48, no. 4, pp. 2301–2306, 2019.

[217] H. Dai, E. W. Wong, and C. M. Lieber, "Probing Electrical Transport in Nanomaterials: Conductivity of Individual Carbon Nanotubes", *Science*, vol. 272, no. 5261, pp. 523–526, 1996.

[218] Q. Zhou, F. Meng, Z. Liu, and S. Shi, "The thermal conductivity of carbon nanotubes with defects and intramolecular junctions", *Journal of Nanomaterials*, vol. 2013, no. Md, 2013.

[219] H. Jackman, P. Krakhmalev, and K. Svensson, "Large variations in the onset of rippling in concentric nanotubes", *Applied Physics Letters*, vol. 104, no. 2, 2014.

[220] W. Lin, K.-s. Moon, S. Zhang, Y. Ding, J. Shang, M. Chen, and C.-p. Wong, "Microwave Makes Carbon Nanotubes Less Defective", *ACS Nano*, vol. 4, no. 3, pp. 1716–1722, 2010.

[221] D. Mattia, M. P. Rossi, B. M. Kim, G. Korneva, H. H. Bau, and Y. Gogotsi, "Effect of Graphitization on the Wettability and Electrical Conductivity of CVD-Carbon Nanotubes and Films", *The Journal of Physical Chemistry B*, vol. 110, no. 20, pp. 9850–9855, 2006.

[222] K. Behler, S. Osswald, H. Ye, S. Dimovski, and Y. Gogotsi, "Effect of Thermal Treatment on the Structure of Multi-walled Carbon Nanotubes", *Journal of Nanoparticle Research*, vol. 8, no. 5, pp. 615–625, 2006.

[223] M. Kosaka, T. W. Ebbesen, H. Hiura, and K. Tanigaki, "Annealing effect on carbon nanotubes. An ESR study", *Chemical Physics Letters*, vol. 233, no. 1-2, pp. 47–51, 1995.

[224] J. T. Tsai and A. A. Tseng, "Defect reduction of multi-walled carbon nanotubes by rapid vacuum arc annealing", *Journal of Experimental Nanoscience*, vol. 4, no. 1, pp. 87–93, 2009.

[225] K. V. Elumeeva, V. L. Kuznetsov, A. V. Ischenko, R. Smajda, M. Spina, L. Forró, and A. Magrez, "Reinforcement of CVD grown multi-walled carbon nanotubes by high temperature annealing", *AIP Advances*, vol. 3, no. 11, p. 112 101, 2013.

[226] R. Jin, Z. X. Zhou, D. Mandrus, I. N. Ivanov, G. Eres, J. Y. Howe, A. A. Puretzky, and D. B. Geohegan, "The effect of annealing on the electrical and thermal transport properties of macroscopic bundles of long multi-wall carbon nanotubes", *Physica B: Condensed Matter*, vol. 388, no. 1-2, pp. 326–330, 2007.

[227] M. Dresselhaus, G. Dresselhaus, R. Saito, and A. Jorio, "Raman spectroscopy of carbon nanotubes", *Physics Reports*, vol. 409, no. 2, pp. 47–99, 2005.

[228] P. Tan, S. Zhang, K. T. Yue, F. Huang, Z. Shi, X. Zhou, and Z. Gu, "Comparative Raman Study of Carbon Nanotubes Prepared by D.C. Arc Discharge and Catalytic Methods", *Journal of Raman Spectroscopy*, vol. 28, no. 5, pp. 369–372, 1997.

[229] E. M. Baitinger, N. A. Vekesser, I. N. Kovalev, Y. I. Ryabkov, and V. V. Viktorov, "Defect structure of multiwalled carbon nanotubes studied by Raman spectroscopy", *Inorganic Materials*, vol. 47, no. 5, pp. 471–474, 2011.

[230] P. Mallet-Ladeira, P. Puech, C. Toulouse, M. Cazayous, N. Ratel-Ramond, P. Weisbecker, G. L. Vignoles, and M. Monthioux, "A Raman study to obtain crystallite size of carbon materials: A better alternative to the Tuinstra-Koenig law", *Carbon*, vol. 80, no. 1, pp. 629–639, 2014.

[231] O. V. Kharissova and B. I. Kharisov, "Variations of interlayer spacing in carbon nanotubes", *RSC Adv.*, vol. 4, no. 58, pp. 30 807–30 815, 2014.

[232] J.-C. Charlier, X. Gonze, and J.-P. Michenaud, "Graphite Interplanar Bonding: Electronic Delocalization and van der Waals Interaction", *Europhysics Letters (EPL)*, vol. 28, no. 6, pp. 403–408, 1994.

[233] Z. Q. Li, C. J. Lu, Z. P. Xia, Y. Zhou, and Z. Luo, "X-ray diffraction patterns of graphite and turbostratic carbon", *Carbon*, vol. 45, no. 8, pp. 1686–1695, 2007.

[234] J. Tao, Y. Jiao, Y. Mo, Z. H. Yang, J. X. Zhu, P. Hyldgaard, and J. P. Perdew, "First-principles study of the binding energy between nanostructures and its scaling with system size", *Physical Review B*, vol. 97, no. 15, pp. 1–13, 2018.

[235] M. Dion, H. Rydberg, E. Schröder, D. C. Langreth, and B. I. Lundqvist, "Van der Waals density functional for general geometries", *Physical Review Letters*, vol. 92, no. 24, pp. 22–25, 2004.

[236] K. Berland, C. A. Arter, V. R. Cooper, K. Lee, B. I. Lundqvist, E. Schröder, T. Thonhauser, and P. Hyldgaard, "Van der Waals density functionals built upon the electron-gas tradition: Facing the challenge of competing interactions", *Journal of Chemical Physics*, vol. 140, no. 18, 2014.

[237] K. Berland and P. Hyldgaard, "Exchange functional that tests the robustness of the plasmon description of the van der Waals density functional", *Physical Review B - Condensed Matter and Materials Physics*, vol. 89, no. 3, pp. 1–8, 2014.

[238] J. L. Figueiredo, M. F. Pereira, M. M. Freitas, and J. J. Órfão, "Modification of the surface chemistry of activated carbons", *Carbon*, 1999.

[239] H. Muckenhuber and H. Grothe, "The heterogeneous reaction between soot and NO2 at elevated temperature", *Carbon*, vol. 44, no. 3, pp. 546–559, 2006.

[240] K. Yang, J. He, Z. Su, J. B. Reppert, M. J. Skove, T. M. Tritt, and A. M. Rao, "Inter-tube bonding, graphene formation and anisotropic transport properties in spark plasma sintered multi-wall carbon nanotube arrays", *Carbon*, vol. 48, no. 3, pp. 756–762, 2010.

[241] T. Wang, S. Chen, D. Jiang, Y. Fu, K. Jeppson, L. Ye, and J. Liu, "Through-silicon vias filled with densified and transferred carbon nanotube forests", *IEEE Electron Device Letters*, vol. 33, no. 3, pp. 420–422, 2012.

[242] T. Wang, K. Jeppson, and J. Liu, "Dry densification of carbon nanotube bundles", *Carbon*, vol. 48, no. 13, pp. 3795–3801, 2010.

[243] D. Jiang, T. Wang, S. Chen, L. Ye, and J. Liu, "Paper-mediated controlled densification and low temperature transfer of carbon nanotube forests for electronic interconnect application", *Microelectronic Engineering*, vol. 103, pp. 177–180, 2013.

[244] T. Wang, D. Jiang, S. Chen, K. Jeppson, L. Ye, and J. Liu, "Formation of three-dimensional carbon nanotube structures by controllable vapor densification", *Materials Letters*, vol. 78, pp. 184–187, 2012.

[245] M. Wang, T. Li, Y. Yao, H. Lu, Q. Li, M. Chen, and Q. Li, "Wafer-Scale Transfer of Vertically Aligned Carbon Nanotube Arrays", *Journal of the American Chemical Society*, vol. 136, no. 52, pp. 18 156–18 162, 2014.

Papers I–VIII